DEVELOPING FLEXIBLE CAPACITIVE SYNTHETIC FABRIC FOR WEARABLE ELECTRONICS

HUI CHI YUEN

PhD

The Hong Kong Polytechnic University

2019

The Hong Kong Polytechnic University

Institute of Textiles & Clothing

Developing Flexible Capacitive Synthetic Fabric for Wearable Electronics

Hui Chi Yuen

A thesis submitted in partial fulfilment of the requirements

for the Degree of Doctor of Philosophy

December 2018

CERTIFICATE OF ORIGINALITY

I hereby declare that this thesis is my own work and that, to the best of my knowledge and belief, it reproduces no material previously published or written, nor material that has been accepted for the award of any other degree or diploma, except where due acknowledgement has been made in the text.

_____ (Signed)

HUI, Chi Yuen (Name of Student)

Abstract

In this study, polyester fabrics were metalized by electroless copper plating to become flexible metalized fabrics. PEO-based electrolytic material doped with different amount of $LiClO_4$ and different types of nanocarbons were solution casted on the fabric surface to form electrochemical double layer supercapacitors. The surface morphology, electrochemical properties, electrical performance and structural effects of these electrochemical systems were studied.

In the experiment of PEO-based supercapacitors doped with different amount of $LiClO_4$, the copper-plated polyester fabrics were solution casted with pure PEO solution, and PEO solution doped with 1 g/L of $LiClO_4$ in different PEO:Li ratio (1000:1, 667:1, 500:1, 400:1, 333:1 and 100:1). The specific capacitance of sample casted with PEO:Li ratio of 100:1 was 33.56 nF/cm^2 at 40 Hz, which is nearly 18 times higher than that of the sample casted with pure PEO. Besides, the maximum current density of the sample casted with PEO:Li ratio of 100:1 obtained under the scan rate of 100 mV/s was 1.84 $\mu A/cm^2$, which was 10 times more than that of the sample casted with pure PEO. It was suggested that the presence of Li^+ ions in PEO matrix could provide an enhancement of charge mobility in the electrolyte by providing sufficient ions to move between different active sites on the branches and backbones of the PEO matrix. Hence, the improvement of charge storage capability was then manifested.

In the experiment of PEO-based supercapacitors doped with different types of nanocarbons, the copper-plated polyester fabrics were solution casted with four types of nanocarbons included single-walled carbon nanotubes (SW-CNT), double-walled carbon nanotubes (DW-CNT), multi-walled carbon nanotubes (MW-CNT) and mesoporous carbon nanopowders to form four different types of supercapacitors. Among four types of nanocarbons, DW-CNT gave the highest value of specific capacitance at 32.798 nF/cm^2, which was 17 times more than that of the sample casted with only pure PEO. On the side of maximum current density, 10.51 $\mu A/cm^2$ was recorded from the sample doped with DW-CNT, which was nearly 60 times higher than that of sample with only pure PEO at 40 Hz

For the experiment of various layer combinations, PEO-based supercapacitors doped with DW-CNT and Li^+ ions under different layering combinations were fabricated and examined. The specific capacitance of sample with PEO:CNT active layers and PEO:Li spacer was 10.19 $\mu F/cm^2$, which was 5390 times more than that of the pure PEO sample. On the other hand, the maximum current density of sample with PEO:CNT:Li active layers and PEO:Li spacer was 49.75 $\mu A/cm^2$, which was 281 times than that of the pure PEO sample.

Comparing to the samples doped with single dopant, it is no doubt that CNT and Li^+ ions can enhance the charge storage capability of the electrochemical system, and improve the efficiency of current passing through the PEO matrix. Besides, it can be found that the charge storage capability of PEO-based supercapacitors

doped with both CNT and Li^+ ions were better than those samples have only doped either CNT or Li^+ ions.

By comparing all layering combinations, the sample with PEO and DW-CNT as active layers and PEO:Li as spacer gave the highest specific capacitance and highest number for charge-discharge cycles. It is suggested that the electrochemical system with PEO-based material can be enhanced by doping Li^+ ions and DW-CNT separately to achieve a better performance instead of mixing both dopants together.

Publications

[1] **Li, W.C., Mak, C.L., Kan, C.W. and Hui, C.Y.** "Microscopic study of polyethylene terephthalate metallization", *Current Microscopy Contributions to Advances in Science and Technology (A. Mendez-Vilas, Ed.),* Book series no. 5 (2012)

[2] **Li, W.C., Mak, C.L., Kan, C.W. and Hui, C.Y.** "Fabrication of Textile Based Capacitive Device", *European Materials Research Society 2014 Spring meeting, Lillie, France,* 26th-30th May, 2014.

[3] **Li, W.C., Mak, C.L., Kan, C.W. and Hui, C.Y.** "Enhancing the Capacitive Performance of Textile-Based CNT supercapacitor", *RCS Advances,* Vol.4, 64890-64900 (2014)

[4] **Liou, Y.D., Chau, K.H., Hui, C.Y., He, J.L., Lam, Y.L. and Kan, C.W.** "An Analysis of Effect of CO2 Laser Treatment on Carbon Fibre Fabric" *Coatings*, Vol.8, Issue 5, 178 (2018)

[5] **Hui, C.Y., Mak. C.L., Kan, C.W. and Chau K.H.** "Review on Electrochemical Double Layer Capacitor (EDLC) with polymeric electrolytes", *Polymer* (Under Preparation)

[6] **Hui, C.Y., Mak. C.L., Kan, C.W. and Chau K.H.** "A study of PEO-based Electrochemical Double Layer Capacitor (EDLC) with different dopants", *Composite B* (Under Preparation)

[7] **Hui, C.Y., Kan, C.W., Mak. C.L. and Chau K.H.** "PEO-based Electrochemical Double Layer Capacitor (EDLC) doped with $LiClO_4$ and double-walled CNT in different structures", *Composite B* (Under Preparation)

Acknowledgements

I would like to gratefully acknowledge my enthusiastic chief supervisor, Dr. C.W. Kan and co-supervisor, Dr C.L. Mak for their enlightening support and precious advice throughout the study of this research. Thanks are also due to Prof. X.M. Tao and Dr. Y.S. Szeto for their discussions and experience sharing. Dr. Patrick S.K. Pang, Ms. M.N. Sun and Mr. C.S. Lo are especially thanked also for their generous assistance.

I appreciate for all my friends Edward, Vincent, Matthew and Ivan for their continuous encouragement and support. Finally, I am indebted to my family for their understanding and endless patience while it is most required.

Table of Contents

List of Tables

List of Figures

Chapter 1

Introduction

1.1 Background

Over the past years, considerable effort has been devoted to the development of alternative energy storage/conversion devices with high power and energy densities because of the ever-increasing environmental problems and the up-coming depletion of fossil fuels. As an intermediate system between dielectric capacitors and batteries, supercapacitors have attracted a great deal of attention owing to their higher power densities relative to secondary batteries. Furthermore, they are maintenance-free, possess a longer life cycle, cope with a simple charging circuit, experience no memory effect, and are generally much safer. Physical rather than chemical energy storage is the crucial reason for their operational safety and exceptionally long life cycle. The most important is, supercapacitors can be charged and discharged at high rates **[1, 2, 3]**. Supercapacitors have two energy storage mechanisms: electrical double-layer (EDL) capacitance and pseudocapacitance. Currently, EDL capacitors contain activated carbon (AC) with high surface area as the electrode material, and the capacitance comes from the charge accumulated at the electrode/electrolyte interface. In contrast, a pseudocapacitor uses a conducting polymer or metal oxide as the electrode material, which undergoes reversible Faradic redox reactions. Conducting

polymers, such as polyanilines, have been shown to exhibit high pseudocapacitance **[4, 5, 6]**.

Besides, the conducting fibers, so called “electro-textiles (e-textile)”, have appeared as promising materials in wearable and flexible applications. Since it is lightweight, durable and bendable, it becomes popular and widely apply in textiles products like functional clothes with variable sensors in medical monitoring accessories. Recently, metal coating techniques on fabrics are conductive paints and lacquers, sputter coating, vacuum deposition, flame and arc spraying, and electroless plating. Among them, electroless plating is most likely the preferred way of producing metal-coated textile. This technique is preferred because of its coherent metal deposition, excellent conductivity, and applicability to complex-shaped materials or non-conductors so that it can be applied to almost all fiber substances. It can be performed at any step of textile production such as fiber, yarn, fabric and garment **[7]**.

1.2 Historical Development of supercapacitors

There are many types of methods and elements can perform energy storage, where capacitors are one of the fundamental electrical circuit elements to exhibit this function **[8]**. From the simplest electrostatic capacitor, developing to electrolytic capacitor, and then the supercapacitor, the capacitance has been largely increased from milli-Farad (mF) to hundreds or even thousands of Farads (F), and the efficiency and effectiveness of the capacitors have also been improved **[9]**.

The first supercapacitor was the Leyden jar, which was a double-layer supercapacitor made in 1746 at Leyden in the Netherlands, where it was discovered that electrical charges could be stored on the plates of a so-called condenser, that referred to as a capacitor recently, in the mechanism of electrostatics. Nevertheless, the first patent only dates back to 1957 where a capacitor based on high surface area carbon was described **[10]**.

Electrolytic capacitor was then developed and being large scale commercialized, it was a polarized capacitor, with a conductive electrolyte salt interact with metal electrodes. Practically, two metal foils coated with an insulating oxide layer were sandwiched with a electrolyte soaked paper spacer. The thin oxide layers on electrodes performed as dielectric, providing high capacitance per unit volume compared to those electrostatic capacitors. Aluminum , tantalum, niobium and niobium oxides were commonly used in manufacturing of electrolytic capacitors,

with relative permittivity varied from 9.6 to 41, and capacitance ranged from few μF to tens of mF, or even in some extreme case, up to hundreds of mF **[8, 11]**.

Compared with traditional capacitors, the specific energy of supercapacitors is several orders of magnitude higher than that of simple electrostatic capacitors and electrolytic capacitors. Besides, supercapacitors can provide a higher specific power that that of most batteries, where their specific energy is relatively lower than the batteries **[12]**.

Supercapacitors are said to be the key for bridging up the gap between the two energy storage devices, batteries and capacitors, to form fast charging energy-storage devices of intermediate specific energy. Due to their highly reversible charge-storage process, supercapacitor have a relative longer cycle-lives and can exhibit rapid responses in both charging and discharging process, resulting in a great interest in the application of consumer electronics, hybrid electric vehicles and industrial power management **[9, 12]**.

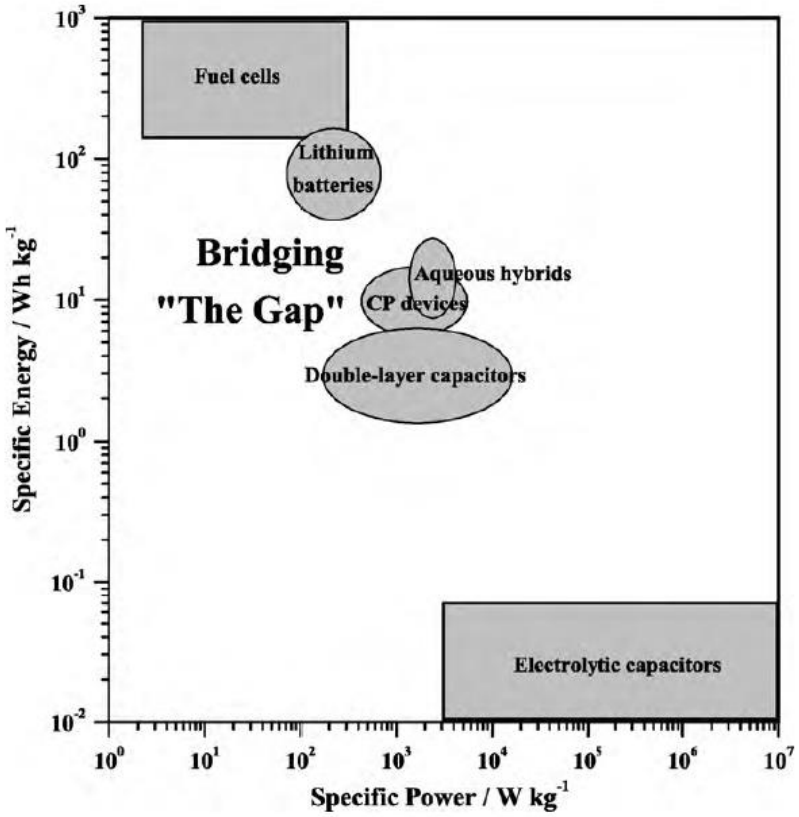

Figure 1.1 Ragone plots for different types of energy-storage devices; where CP is conducting polymer. ***[Reprinted from 9]***

Table 1.1 Comparison of typical capacitor and battery characteristics ***[12]***

Characteristics	*Electrolytic capacitor*	*Carbon supercapacitor*	*Battery*
Specific energy (Wh kg^{-1})	<0.1	1-10	10-100
Specific Power (W kg^{-1})	>>10000	500-10000	<1000
Discharging time	10-6 to 10-3 s	s to min	0.3-3 hrs
Charging time	10-6 to 10-3 s	s to min	1-5 hrs
Charge/discharge efficiency (%)	~100	85-98	70-85
Cycle-life (cycles)	Infinite	>500000	~1000
Max voltage (V_{max}) determinants	Dielectric thickness and strength	Electrode and electrolyte stability window	Thermodynamics of phase reactions
Charge stored determinants	Electrode area and dielectric	Electrode microstructure and electrolyte	Active mass and thermodynamics

1.3 Scope of The Study

In this project, to combine the benefits from supercapacitors and electro-textiles, a new structure of flexible capacitive fabric will be produced and examined. Different dopants will be doped and different combinations of functional layers will be applied to this new system, and the performances of this system will be investigated. To achieve the above target, some objectives are established and summarized below:

1) To examine the viability of electrical double layer capacitors (EDLCs) prepared by poly(ethylene oxide) (PEO) electrolyte with solution casting on the copper coated polyester fabrics.

2) To prepare and investigate the performance of PEO-casted EDLCs doped with different amount of lithium salt.

3) To prepare and investigate the performance of PEO-casted EDLCs doped with different type of nanocarbons.

4) To prepare and determine the performance of PEO-casted EDLCs with different structural combination of functional layers, where the materials applied for doping are based on the experimental results from the previous two objectives: the optimum amount of lithium salt and the type of nanocarbon.

1.4 The Overview of Thesis

In this thesis, the contents are divided into six chapters. Chapter 1 is the introduction, it explains about the background, the historical development of supercapacitors, the objectives and scope of the study. Chapter 2 is the literature review, contains explanations on various components in supercapacitors including mechanisms of charge trapping, electrode materials and electrolytic materials, the current development in textile-based flexible supercapacitors, and the background of theory characterization techniques. Chapter 3 explains the detail sample fabrications and characterization methods of various experiments. In Chapter 4, the experiment of PEO-based supercapacitors doped with different amounts of lithium salt and different types of nanocarbons will be introduced, the samples will be examined and the optimum concentration of lithium salt and type of nanocarbons to enhance the charge capability will be determined. Chapter 5 introduces the experiment of PEO-based supercapacitors with different structures of functional layers, where the amount of lithium salt and the type of nanocarbons doped are the optimum condition obtained in the previous chapter, the performances of samples with various structures are then investigated. Chapter 6 is a conclusion chapter that summarizes all the experimental results, and general conclusions of this research are drawn, besides some recommendations and future works are suggested.

Chapter 2

Literature Review

2.1 Nomenclature of Supercapacitors

Practically, supercapacitors are divided into three different categories as shown in Figure 2.1, which are classified in terms of their charging mechanism: (a) double layer capacitors, (b) pseudocapacitors and (c) hybrid capacitors.

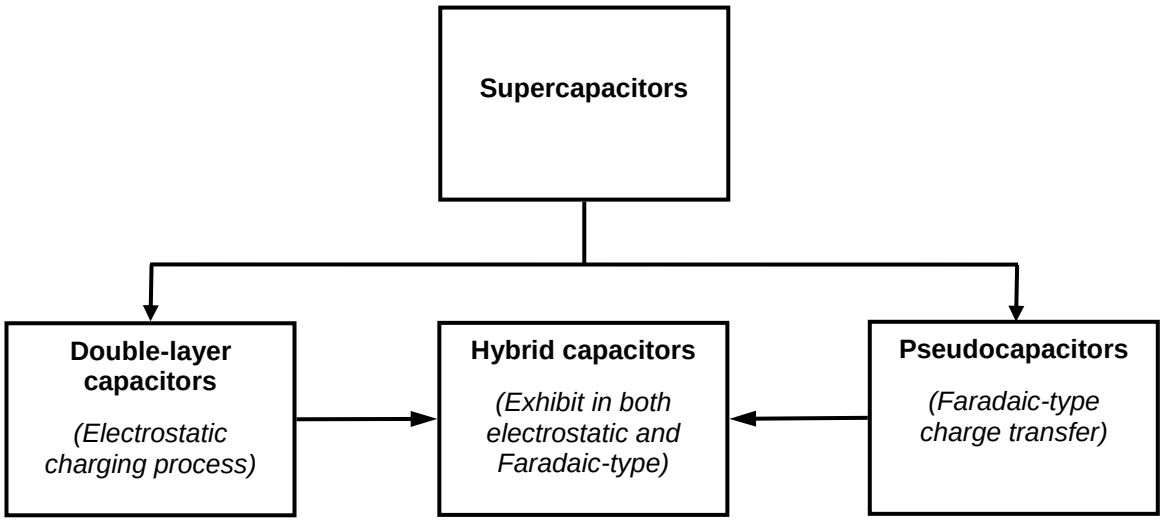

Figure 2.1 The classification of supercapacitors

For double layer capacitors, it is an energy storage system contains two layer of polarizing electrodes sandwiching with a separator and filled with electrolyte **[8]**. The energy can be stored in the form of electrostatic mechanism.

In pseudocapacitors, the energy is stored through the bulk of redox material in response to a redox reaction, where the fast chemical reaction acts like capacitance **[9]**.

For the hybrid capacitors, substances like active carbon, conducting polymers, or even transition metal oxides are doped or added to the electrodes, provided that the capacitors can be exhibited in both electrostatic responses and reversible Faradaic-type charge transfer, where lithium-ion capacitor is a typical example in this category.

2.2 Energy Storage Mechanism in Supercapacitors

Generally speaking, for supercapacitor, there are two different working principles for energy storage: (1) the double-layer capacitance, or so-called electrical / electrochemical double-layer capacitance (EDLC), and (2) the pseudocapacitance; their working mechanisms are described in the following.

2.2.1 Electrical Double-layer Capacitance (EDLC)

In double-layer capacitance, the energy is stored with the similar method as a traditional parallel capacitor, by means of charge separation. Nevertheless, it can store considerably more energy than a classical capacitor. Since the charge separation is taking place across a relatively small distance in the electrical double layer, which can set up the interphase between an electrode and the adjacent

electrolyte. Moreover, higher amount of charges can be stored on the highly extended electrode surface-area, which created by a large number of pores within a high surface area electrode material. This energy storage mechanism can respond rapidly because it just simply involves movement of ions that migrate to and from electrode surfaces at shown in Figure 2.2 **[9, 10, 12]**.

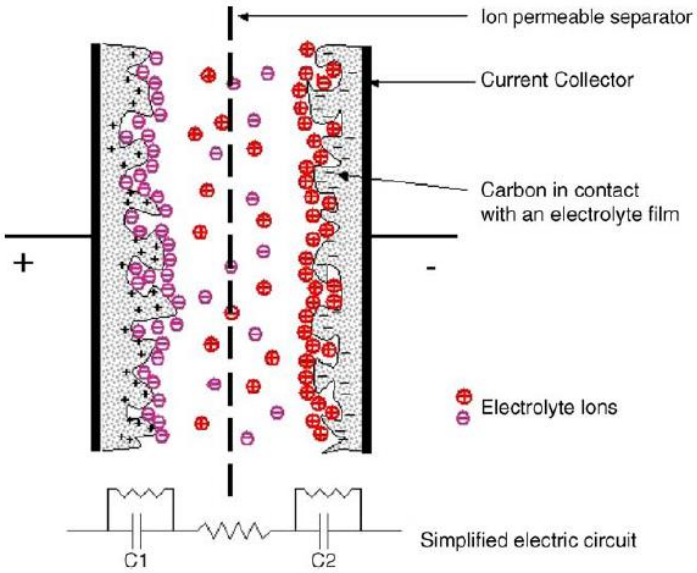

Figure 2.2 Representation of an electrochemical double layer capacitor (in its charged state) ***[Reprinted from 12]***

2.2.2 Pseudocapacitance

In pseudocapacitance, a relatively large capacitance under a non-electrostatic basis is found, which is due to a reversible Faradaic-type charge transfer being taken place. Hence, the capacitance is associated with an electrochemical charge-transfer process that occurs to an extent limited by a finite amount of active material or available surface. The most commonly investigated classes of pseudocapacitive materials are transition metal oxides (e.g. Manganese (II) oxide, MnO_2) and conducting polymers such as Polyaniline (PAni), Polypyrrole (Ppy) or derivatives of Polythiophene (PTh) (e.g. Poly(3,4-ethylenedioxythiophene), PEDOT). Since the charge storage in this type of supercapacitor is based on a redox process, and there is somewhat battery-like in its behavior, therefore pseudocapacitor is also referred to redox supercapacitor, a typical charge transferring process of Cl^- ions in a conducting polymer matrix is illustrated in Figure 2.3 **[9, 10, 12]**.

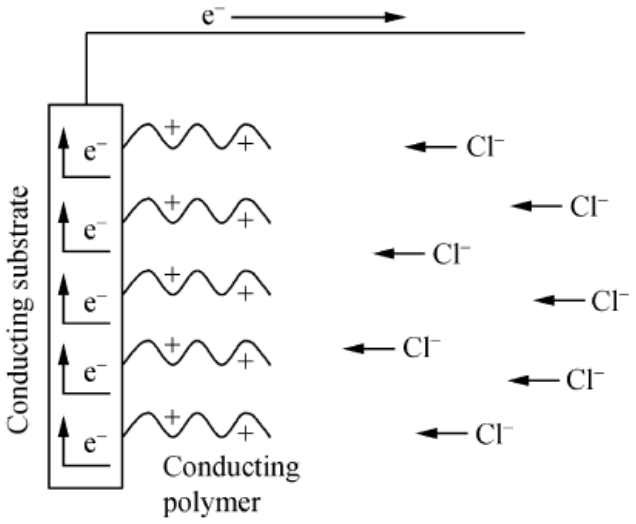

Figure 2.3 Illustration of pseudocapacitance in a conducting polymer ***[Reprinted from 10]***

2.3 Electrode materials

Supercapacitors can be fabricated from a wide range of materials, such as conducting polymers, carbon materials and metal oxides, where the selection is depending on the type of capacitance to be utilized. For double-layer capacitance, carbon materials are usually used and, for pseudocapacitance, metal oxides and conducting polymers are applied frequently. Hence, for those capacitors exhibit in both type of capacitances, the composites of carbon with either metal oxides or conducting polymers will be implemented.

2.3.1 Carbon materials

Carbon materials are usually used to prepare for supercapacitor electrodes due to its high conductivity and compatible in composite materials, with its controlled pore structure which can provide a high surface area range (~1 to >2000 m^2g^{-1}) **[12]**.

There are four crystalline allotropes in carbon: diamond (sp^3 bonding), graphite (sp^2), carbyne (sp^1) and fullerences (the so-called "distorted sp^2"), where graphite and diamond can be naturally found and the other two are synthetic. The allotrope typically used in fabrication of electrodes will be graphite. The carbon materials commonly used in supercapacitors were categorized based on their features, such as activated carbons, carbon fibers and carbon nanotubes (CNT).

Activated carbons like carbon blacks are a group of materials that are characterized by having near spherical carbon particles of colloidal size, which are produced by the partial combustion or thermal decomposition of hydrocarbons in the gas phase. The key properties of carbon blacks are considered to be fineness (primary particle size), structure (aggregate size/shape), porosity, and surface chemistry. The conductivity of carbon blacks typically ranges from 10^{-1} to 10^{2} (Ωcm^{-1}) and is influenced by the relative ability of electrons to jump the gap between closely-spaced aggregates (electron tunneling) and by graphitic conduction via touching aggregates **[12, 13]**.

Typically, the diameter of carbon fibers is about 10 μm and a very narrow pore-size distribution that is mainly microporous (<2 nm). Because of its limited dimensions, the porosity of carbon fibers is mainly situated at the surface of the fibers and thereby provides good accessibility to active sites. Therefore, the pore diameter and pore length can be more easily controlled in carbon fibres. These features make carbon fibers become a very attractive electrode material used in energy storage devices since both high adsorption capacities and adsorption rates are obtainable **[12]**.

To obtain the advantages from both activated carbons and carbon fibers, a new hybrid of these two materials – activated carbon fibers (ACFs) are produced. ACFs are porous carbons in fiber like structure, and its aspect ratio is higher than 10, which have a well-defined porous structure with high adsorption capacity. Generally, ACFs can be prepared from carbon fibers by a heat treatment to achieve

high porosity to fulfill requirement of specific applications. With this structure, an extremely large surface area at about 2000 m^2/g can be obtained. ACFs gain the benefits of high packing density and excellent volumetric capacity, which can present its importance and usefulness for adsorption application. For common activated carbons, due to its ladder-like structure, the adsorbate gas molecules have to pass through macropores in the beginning, and then mesopores before entering micropores. In ACFs, however, large amount of micropores can contact to adsorbate gas which are directly exposed to the surface of the fibers, so the adsorption mechanism can be largely improved **[14, 15]**.

The nanoscale tubular morphology of the CNT can offer a unique combination of low electrical resistivity and high porosity in a readily accessible structure. Single-walled (SWNT) and multi-walled nanotubes (MWNT) have been studied as electrode materials in both aqueous and non-aqueous electrolytes **[12, 13]**. The specific capacitance typically ranged from 15-80 Fg^{-1} with surface area varies from 120-400 m^2g^{-1}. The CNT surface area is mainly “mesoporous” and is coupled with the exterior of the tubes. By subsequent oxidative treatment which can alter the surface morphology of the CNT, additional surface will be produced and the specific capacitance can be raised to about 130 Fg^{-1}, which is capable of contributing to pseudocapacitance **[12]**.

2.3.2 Metal oxides

Transition metal oxides / hydroxides like ruthenium (Ru), cobalt (Co), manganese (Mn) and nickel (Ni) oxides / hydroxides are commonly used in supercapacitor applications. These conducting or semi-conducting transition metal oxides and perform redox active behaviors, provided that the pseudocapacitance occurred. Ruthenium oxide as a capacitive material has been studied widely since ruthenium dioxide (RuO_2) was first reported as a new electrode material in 1971 **[16]**. The application of RuO_2 in supercapacitors is based on its metallic type conductivity and reversible redox reactions in aqueous media (Ru^{2+}, Ru^{3+}, and Ru^{4+} couples). The oxide can provide relatively constant and appreciable capacitance larger than 1.4V with specific capacitance in the range from 600-1000 Fg^{-1}, which depends on various factors such as preparation procedure, measurement conditions, and use of support **[17]**. Another significant advantage is the ultra high stability or long life-cycle. Thermally formed RuO_2 films on titanium with its oxides derivatives (TiO_2 or Ti_2O_5) could be charged over 10^5 times between 0.02 - 1.2 V or even to as far as 1.4 V, with slightly degradation. However, the cost of using ruthenium oxide is relatively high, therefore these supercapacitor materials are mainly utilized in aerospace or military application **[18]**. Therefore, for commercially low cost applications, other metal oxides like Co_3O_4 **[19, 20]**, NiO **[21, 22]**, and MnO_2 **[23, 24]** have been synthesized and examined for further supercapacitor applications. As these metal oxides are much more cost effective, however, their specific capacitance is lower, typically within the range of 20-200 Fg^{-1}. Besides, other

electrical properties like potential window and conductivity are relatively low compared to ruthenium oxide **[10]**.

2.3.3 Conducting Polymers

Conducting polymers are suitable to prepare for supercapacitors because of their good electrical conductivity which can also provide large pseudocapacitance, with a relatively low cost, such as Polyaniline (PAni), Polypyrrole (Ppy) or derivatives of Polythiophene (PTh) (e.g. Poly(3,4-ethylenedioxythiophene), PEDOT). The electrical properties like electrochemical capacitance and charge storage are being studied by cyclic voltametry, electrochemical impedance spectroscopy and chronopotentiometry. Compared to ruthenium oxides, the specific capacitance of conducting polymer is compatible to the oxides with 775 Fg^{-1} for PAni, 480 Fg^{-1} for Ppy and 210 Fg^{-1} for PEDOT **[25, 26, 27]**. Nonetheless, the poor mechanical stability of conducting polymers due to repeated intercalation and depletion of ions during charging and discharging will be the weakness of these materials **[10]**. For those supercapacitors only consist of conducting polymers, they can be configured into the following three types: Type (I) which is symmetric by using the same *p*-dopable polymer for both electrodes; Type (II) which is asymmetric by using two different *p*-dopable polymers with a different range of electroactivity; and Type (III) which is symmetric by using the same polymer for both electrodes, with the *p*-doped form used as the positive electrode and the *n*-doped form used as the negative electrode **[28, 29, 30, 31, 32]**.

2.3.3.1 Polyaniline (PAni)

For PAni, it exhibits high electroactivity and a high doping level, with an excellent environmental stability and can provide a high specific capacitance. Moreover PAni has a controllable electrical conductivity (~ 0.1 Scm^{-1} in the doped state with a lithium dopant), and can be easily processed **[9]**. However, PAni needs a proton to be properly charged and discharged, therefore, a protic solvent, an acidic solution or a protic ionic liquid is required **[33]**.

PAni has been reported to have capacity in a range of 44-270 $mAhg^{-1}$ **[9]**. This variation in capacity may be due to synthetic route used, morphology of polymer, the amount and type of binders and additives, and the electrode thickness. It has the most variable specific capacitance of all conducting polymers, where the specific capacitance achievable is higher for electrodeposited than for chemically formed PAni **[9]**. Moreover, the life-cycle of PAni for a Li-doped positive electrode has been reported for over 5000 cycles, with a decrease of specific capacitance from 100 to 70 Fg^{-1}. From another studies, a decrease of specific capacitance from 107 to 84 Fg^{-1} when PAni is doped with $LiPF_6$ after 9000 cycles **[28, 34]**.

Reported by Park et al. **[35]**, a device with PAni as the positive electrode and carbon as the negative electrode has been made, which is so called hybrid electrochemical capacitor. This capacitor can provide similar or higher values than reported Type (III) supercapacitors made from PTh derivatives. A constant current charge-discharge test at 0.5 $mAcm^{-2}$ gives 380 Fg^{-1}, where the specific energy and

specific power at 20 $mAcm^{-2}$ gives 18 $Whkg^{-1}$ and 1.25 $kWkg^{-1}$ respectively. By cyclic voltammetry, a cycle-life of 4000 was observed, and the capacitor exhibits charge and discharge in the range of 1.25-1.5 V and 1.4-1.0 V respectively.

In PAni, the proton exchange sites are hindered by the methyl groups, therefore it can stabilize against chemical degradation and can provide more redox reaction. If PAni is coped with a lithium negative electrode, a capacity of 52 $mAhg^{-1}$ can be achieved **[9]**.

2.3.3.2 Polypyrrole (Ppy)

Ppy provides a larger degree of flexibility in electrochemical processing than many of conducting polymer, thus Ppy has been the subject of much research as a supercapacitor or battery electrode **[9]**. However, Ppy is not in favor of *n*-doped like those thiophene derivatives, so Ppy can only be found for use as a cathode material.

Since the density of Ppy is larger, it can provide a higher capacitance per unit volume (400-500 Fcm^{-3}) **[9]**. However, the aspect of the dense growth will lead to a limited access to the interior sites of the polymer for dopant ions. As a result, the capacitance per gram will be decreased, especially for those with thick coatings on electrodes **[36]**. Reported by Suematsu, Ppy is usually doped with single charged anions such as Cl^-, ClO_4^- and SO_3^-, but if it is doped with multiple-charged anions like SO_4^{2-}, physical cross-linking of the polymer will occur, where the cross-linked

materials have high diffusivity and high capacitance, probably due to the greater porosity of growth **[37]**.

Ppy can be applied as an electrode to prepare for Type (I) supercapacitor, and coped with poly(3-methyl thiophene) to form a Type (II) device **[30]**. The Type (I) supercapacitor provides a discharge capacitance of 8-15 $mFcm^{-2}$, which is similar to that for the Type (II) one. In Type (I), the voltage is ranged from 0.5-1.0 V, and being extended to 1.2 V for Type (II). Ppy can be utilized to make an all solid-state-supercapacitor with a PVA-based polymer electrolyte, provided that a stable capacitance of 84 Fg^{-1} after 1000 cycles and a specific energy of 12 $Whkg^{-1}$ can be obtained **[38]**.

2.3.3.3 Thiophene-based conducting polymer

Polythiophene (PTh) is not a good candidate for making an electrode in supercapacitor because of its poor stability, in *n*-doped state at very low potentials (below -2.0 V with $Ag|Ag^{+}$) **[39, 40]**, it has low stability to oxygen and water, and also lower conductivity than that in the *p*-doped state **[41]**. Besides, it has high self-discharge and low cycle-life in devices, in other words, it is easily oxidized back to neutral form.

To improve the material stability and functionality, Pth derivatives with a lower band-gap, which the *n*-doped at less negative potentials can be prepared **[29, 30, 42]**. By replacing at the 3 position of the thiophene ring with phenyl, ethyl and

alkoxy groups stability to oxygen and water can be further improved **[43]**, therefore, most PTh derivatives are stable in air and moisture in both the *p*-doped and undoped forms **[44]**, and one of the common used Pth derivatives is poly(3,4-ethylenedioxythiophene) (PEDOT). *n*-doped Pth derivations are seldom reported to be applied as supercapacitor materials due to intrinsic difficulties in the *n*-doping process **[45]**, which causes a strong dependence of the behavior on the size of the counter ion and on the solvent. Another method to improve the stability of *n*-doped PTh is to use active carbon as the negative electrode in an symmetric configuration, with positive electrode made with *p*-doped polymer. By this configuration, a supercapacitor with higher specific power, compared with the carbon-carbon supercapacitor can be produced and can be cycled for more than 10000 times **[41]**.

PEDOT is highly conductive, compared to other PTh derivatives, and can be *p*-doped and *n*-doped. It has a higher potential range of 1.4 V, but the smallest specific capacitance due to combination of the large molecular weight of the monomer unit and the low doping level **[46]**. Besides, it is electron rich and consequently has a low oxidation potential **[47]** together with a wide potential window over which the capacitance is high (1.2-1.5 V wide) **[29, 36, 48]**. Moreover, the band-gap of PEDOT is relatively low at 1-3 eV, which is highly conducting in the p-doped state (300-500 Scm^{-1}) **[44]**, provided that a good thermally and chemically stable, and a high charge mobility which provide with fast electrochemical kinetics **[42, 44, 48, 49]**. With a high surface area coupled with high conductivity, PEDOT can exhibit a very rapid kinetics. In addition, it has good

film-forming properties and can be switched rapidly within a minimum of side reactions leading to a long life cycle **[47, 48, 49]**.

On the other hand, due to its large molecular weight and a doping level at about 0.33, the specific capacitance is relatively low at about 90 Fg^{-1} **[44, 46]**. Since the monomer of PEDOT cannot be dissolved in aqueous solvents, therefore, volatile and toxic organic solvents like acetonitrile are to be used for material deposition.

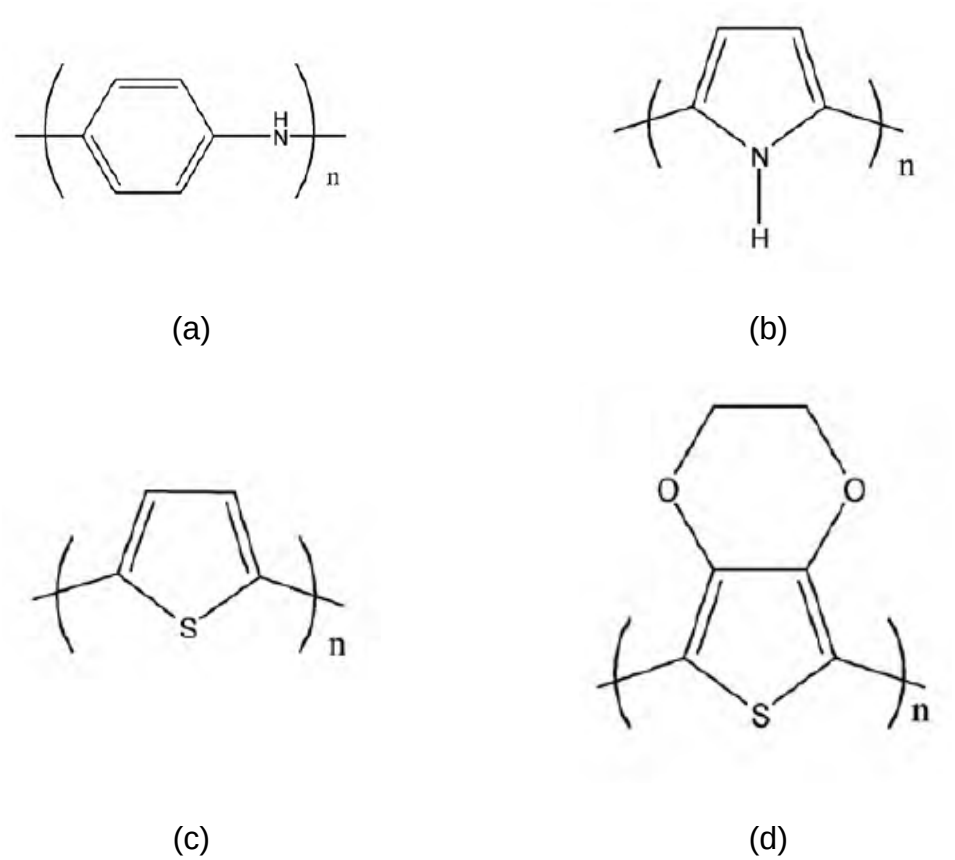

(a) (b)

(c) (d)

Figure 2.4 Structure of various conducting polymers: (a) PAni, (b) Ppy, (c) PTh and (d) PEDOT.

2.4 Electrolytic materials

2.4.1 Electrolytes in EDLC

For many of commercial EDLCs, they use non-aqueous electrolyte solutions to achieve high terminal voltage *V*. The capacitor energy *E* can be expressed by:

$$E = \frac{CV^2}{2} \,\&\, P_{\max} = \frac{V^2}{4R} \qquad (2.1)$$

Where P_{max}, *C*, *R* are the maximum power, cell capacitance in F and internal resistance in Ω, respectively. Besides non-aqueous electrolyte, aqueous electrolyte solution can also be found in the market. For the aqueous one, they are potentially beneficial to large installations for storage of large amount of power and unsteady electricity generated by natural energy resources, due to its low cost, longer lifetime, low internal resistance therefore more safer.

In EDLCs, the sizes of cation and anion of the electrolyte are important factors in relation to the surface area, effective for the adsorption of the ions, of the electrode carbons. For non-aqueous electrolyte solutions, there are various combinations of electrolytes, either organic or inorganic, with solvents are possible **[13]**. As the solvent will also affect the capacitance **[50, 51]** and some of the combination is not always optimum for all carbon materials. If the EDLC applies electrolytes containing lithium ions, the intercalation of Li^+ ions was pointed out to occur together with its adsorption on to the surface of the carbon electrodes **[52]** and also implemented in hybrid capacitors. In some ionic liquid doped with carbon, like 1-

ethyl-3-methyl-imidazolium (EMI^+) or N-butyl-N-methylpyrrolidnium ($PyR14^+$) with anion of bis(trifluoromethane-sulfonyl) imide ($TSFI^-$), and polymer gel like poly(ethylene oxide) (PEO), poly(methyl methacrylate) (PMMA) and polyacrylonitrile (PAN), were proposed to be solvent-free electrolytes because these materials can provide a large potential window but a high viscosity **[53, 54, 55, 56]**.

On the other hand, various aqueous electrolyte solutions are frequently used, such as sulphric acid (H_2SO_4), sodium sulphate (Na_2SO_4) and potassium hydroxide (KOH) for acidic, neutral and alkaline solutions, respectively. Potassium sulphate (K_2SO_4) and sodium hydroxide (NaOH) are also used but chloride salts are not frequently used because of specific adsorption and reducible nature of chloride ion. Aqueous solution must be deaerated before and during electrochemical measurements to eliminate dissolved oxygen **[9]**.

2.4.2 Electrolytes in pseudocapacitors

In redox supercapacitors, many of them which are based on liquid electrolytes have been reported, like acetonitrile composites ACN-$ME_4NCF_3SO_3$, ACN-Et_4NBF_4, ACN-Bu_4NPF_6 **[57]**, ACN-$LiClO_4$ **[58]**, and propylene carbonate composite (PC)-$LiClO_4$, PC-Et_4NBF_4. However, there are some drawbacks coming from these aqueous electrolytes, like corrosion, self-discharge, low energy density and bulky design **[38]**. On the other hand, some solid state redox capacitors based on polymeric gel electrolytes have also been reported, including polyethylene oxide

composites PEO-PC-Et_4NBF_4, polyethylene glycol composites PEG-Et_4NBF_4 **[59]**, PEO-PEG-$LiCF_3SO_3$ **[60, 61]**, polymethyl methacrylate composites PMMA-PC-EC-$LiClO_4$ **[62]**. All solid-state redox supercapacitors are in the early stage of development and need various improvements in their performance characteristics **[30]**.

2.4.3 Polymer electrolytes

Polymer electrolytes are well known as a promising material in the research and development of electrochemical systems. In the past two decades, massive researches related to polymer electrolyte have been done to achieve the systems with a good conductivity and electrochemical stability. According to the basis of materials, the polymer electrolytes have been classified as different categories: (a) dry solid polymer electrolytes, (b) plasticized polymer electrolytes, (c) gel polymer electrolytes, and (d) composite polymer electrolytes.

2.4.3.1 Dry solid polymer electrolytes (Polymer-salt complex electrolytes)

Practically, a solid polymer electrolyte is prepared by dissolving inorganic salts into a polar functional polymer, after drying, an ion conducting solid electrolyte is formed. With the interactions between metal ions and polar groups of polymers, electrostatic forces will occur due to the formation of coordinating bonds. Factors like the nature of functional groups attached to the polymer backbone, compositions and distance between functional groups, molecular weight, degree

of branching, nature and charge of metal cation, and the counter ions may affect the polymer-metal ion interactions in the electrolyte. Because of the weak coordinate of cations to sites along the polymer chain, when an electric field is applied, the cations may move from one coordinated site to another one **[63, 64]**. There is a wide range of polymers can be used to form dry solid polymer electrolytes, such as poly(ethylene oxide) (PEO), poly(methyl methacrylate) (PMMA), polycarbonate (PC) and poly(vinyl alcohol) (PVA). For metal ions, various soluble compounds such as salts containing lithium (Li), sodium (Na) and potassium (K) are commonly used **[65]**.

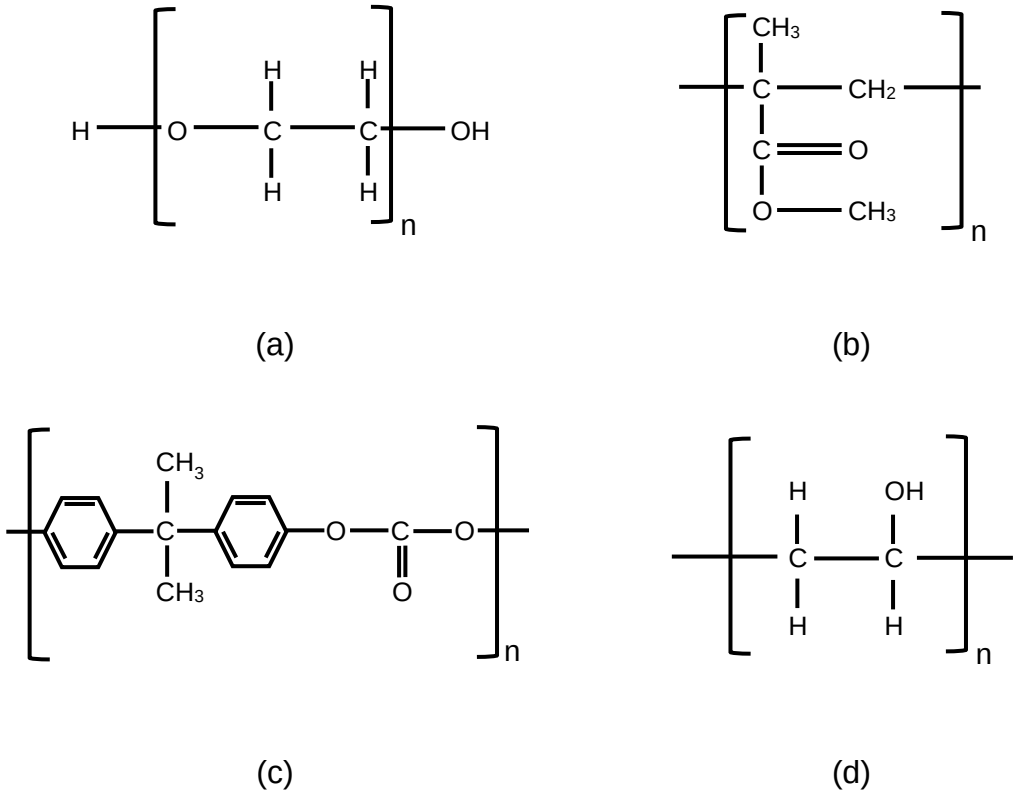

Figure 2.5 Structure of various host polymers: (a) PEO, (b) PMMA, (c) PC and (d) PVA.

In the mid-1970s, Wright et al. discovered the ionic conductivity in PEO doped with salts containing different alkali metal included Na and K. After few years, Armand reported the ionic conductivity to amorphous phases of the PEO:salt systems, by suppression of crystallinity, the increase of these domains in the bulk materials can be enhanced. In 1980s and early 1990s, the application of Li ion and raising of electrolyte conductivity were focused, researches about sufficient electrochemical stability and the prevention of excessive dendrite growth of Li ion were reported **[65]**.

For solid polymer electrolyte, the PEO-based matrix doped with Li ion is highly concerned. PEO is a typical semi-crystalline polymer due to the coupling effect between Li ion and the ether oxygen atoms of the PEO matrix **[66]**. The glass transition temperature (T_g) of PEO is relatively low (-60 °C) and its dielectric constant is low ($\varepsilon_r \approx 5$) compared to other host polymers, however, it exhibits a very good complexing agent for Li ion **[65, 67]**. Alkali metals are well known as effective dopants for electrolytic materials due to their low standard potentials and densities, where lithium is the most attractive candidate because it has the lowest standard potential in all elements. Besides, lithium is the lightest metallic element in the periodic table; its cation is so small that can make the cation to diffuse in solids rapidly and easily **[68]**. Lithium salt like lithium perchlorate ($LiClO_4$), lithium hexafluoroarsenate(V) ($LiAsF_6$), lithium tetrafluoroborate ($LiBF_4$) and lithium hexafluorophosphate ($LiPF_6$) are commonly used to dope into the PEO matrix to form a solid electrolyte.

Since the Li ions are dissolved in solid PEO matrix, compared to other aqueous electrolytes, the electrochemical system is more stable with very low volatility, as a result, the reliability and safety is improved. Moreover, the possibility of destructive decomposition at electrodes and leakage can be limited.

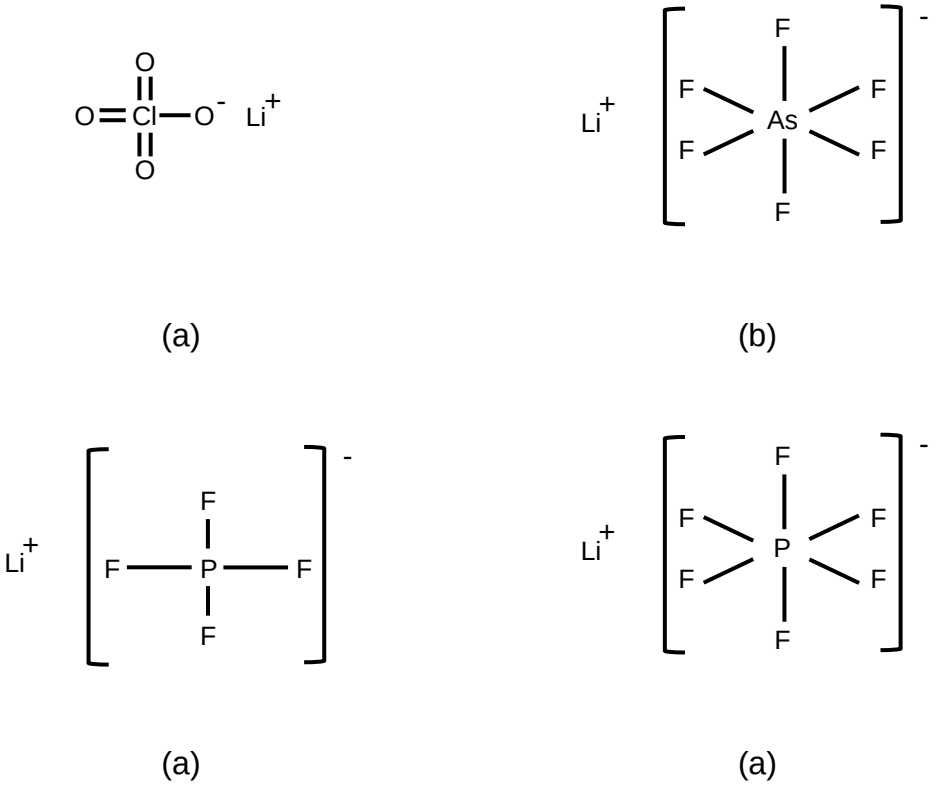

Figure 2.6 Structure of various lithium salts: (a) $LiClO_4$, (b) $LiAsF_6$, (c) $LiBF_4$ and (d) $LiPF_6$.

2.4.3.2 Plasticized polymer electrolytes

To prepare plasticized polymer electrolytes, a host polymer with low molecular weight like ethylene carbonate, propylene carbonate and poly(ethylene glycol) (PEG) will be used. With the application of plasticizers, the number of active centers in the host polymer can be reduced and hence weaken the intermolecular and intramolecular forces between the polymer chains. As a result, the rigidity of polymer structure will be decreased, and the mechanical and thermomechanical properties of the polymer will be changed. Hence, the glass transition temperature of polymer electrolyte system will be decreased due to the addition of low molecular weight plasticizers. Consequently, the increase of salt dissociation capability and the reduction of crystallinity can be achieved, resulting in the enhancement of charge carrier transport. Nevertheless, the mechanical strength of the polymer electrolyte will be weakened **[63, 64]**.

2.4.3.3 Gel polymer electrolytes

Gel polymer electrolytes have attracted researchers' focus because it can combine the advantages of high ionic conductivity like liquid-based electrolytes, and high stability like solid-based electrolytes. For gel polymer electrolytes, the host polymer matrix has been employed to trap the liquid constituents, so it is safer to use compared to liquid-based electrolytes, especially the matrix is doped with lithium ion. During gel polymer electrolyte preparation, a large amount of organic solvents or plasticizers will be added into the host polymer, a wide network will be formed

with these plasticizers molecules, hence the ion conduction will then take place along with the host polymer, which can provide structural support to the matrix **[63, 64]**.

2.4.3.4 Composite polymer electrolytes

Usually, the dielectric constant (***ε***) of host polymers in electrolyte matrix are relatively small, it is related to the presence of ion-pairs (or ion-association) and ion triplets, resulting in poor ionic conductivity **[63, 69]**. By doping different types and amounts of inorganic inert fillers with higher dielectric constant into the polymer matrix, the electrical properties of polymer electrolytes can be improved. Ceramic materials are one of the commonly used inorganic dopant, which is fragile with low dielectric strength. On the other hand, polymers are having relatively low permittivity but can endure high electric field. Combining the inorganic dopants with polymers, the new type composite electrolytic material with higher relative permittivity can be produced. Since these composite electrolytes consist of ceramic particles, these electrolytes can be regarded as heterogeneously disordered systems, which the electrical properties are highly dependent on the relative permittivity and the conductivity of the dopants. Moreover, the electrical performances of these composite electrolytic materials are affected by the volume fraction, size and shape of the dopants **[63, 64]**.

2.5 Current Development in Textile-based Flexible Supercapacitors

Due to the highly flexible structure of textile materials, researchers like to take this advantage and apply it into the preparation of supercapacitor in various applications. These textile materials can be produced by fibers in natural or synthetic, such as cotton and polyester, respectively, or even carbon fibers, in different production methods like pressing, weaving, knitting or felting **[70, 71, 72]**.

To facilitate a better electrical conduction on various non-conducting fabric surfaces, usually a layer of conducting material will be coated on yarn or fiber surfaces. This conducting layer can be prepared by Chemical Vapour Deposition (CVD), Physical Vapour Deposition (PVD), electro-sputtering, electro-spinning, electroless metal deposition, dip-coating, or simply screen-printing. Besides, various materials can be applied to prepare this conducting layer, like bulk metals or metal solutions containing copper, nickel, silver or gold. Other than metal, solutions and pastes containing various types of carbon materials like active carbons and carbon nanotubes can also be used **[7, 73, 74, 75, 76, 77, 78, 79]**.

Various types of textile materials including cotton, polyester, polyamide, Spendex and carbon cloths are widely applied to produce supercapacitors and fruitful researches have been reported **[80, 81, 82, 83]**. To achieve a greater charge trapping efficiency, usually fabrics with microfibers or nanofibers will be used as substrates to prepare for the supercapacitor **[70, 72]**. For microfiber, it is a fine synthetic fiber with diameter less than 10 μm. For nanofiber, the fiber is even finer

and the diameter is down to nanoscale. Since the fiber diameter is smaller than those usual fibers used in common fabrics, therefore it can provide greater specific surface area per unit volume of fabrics, and hence the increase of surface area can enhance the charge trapping capability of the supercapacitor. Besides, various carbon materials like activated carbon, carbon fibers and carbon nanotube (CNT) will be added on the fiber surface by solution-casting, dip-coating and spraying to further improve the charge trapping capability of the textile-based supercapacitors **[84, 85, 86, 87, 88, 89]**.

2.6 Characterization techniques for supercapacitors

As the electrical properties of supercapacitors are the most concerned for researchers, various techniques have been developed to help researchers to study the properties and behaviours of these charge storage devices, for example: Cyclic Voltammetry, Electrochemical Impedance Spectroscopy and Cyclic Charge-discharge Measurement.

2.6.1 Cyclic Voltammetry (CV)

Cyclic voltammetry is one of the most common and useful electroanalytical technique for studying electrochemical properties in supercapacitors. Usually, CV is the first experiment to perform in the electrochemical study of a material or an electrode surface, as it can rapidly observing the electrical properties and redox behaviours over a broad potential range. The voltammogram result is comparable to a conventional spectrum in that it can present information as a function of energy scan **[90]**.

To perform CV, different electrodes will be made to connect to the testing sample or solution for different voltage-current measuring functions, the major two electrodes are (a) working electrode and (b) reference electrode. For working electrode, it will connect to side of the sample or solution that the desired reactions will occur. Usually the current change will be measured through this electrode. For

reference electrode, it will connect to the opposite side of reaction occurred. The potential between working and reference electrodes are controlled. This controlled potential that applied between these two electrodes can be said as the excitation signal. The excitation signal for measurement in CV is a linear potential scanning with a waveform of triangular shape shown in Figure 2.7. To investigate the charge transfer efficiency and other electrical properties with temporal dependence, different rate of change of potential, or in other words, the scan rate can be applied.

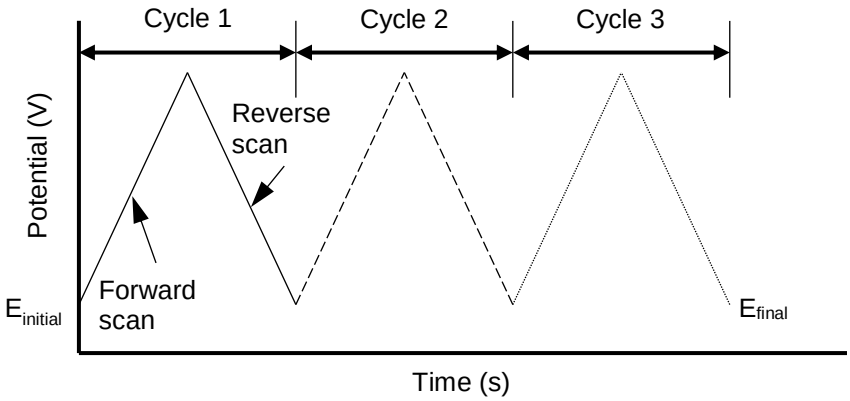

Figure 2.7 Typical excitation signal for cyclic voltammetry with a triangular potential waveform.

In CV, the variation of current at the working electrode will be measured during the potential scan. With the change of current at working electrode and the controlled potential scan, a voltammogram can be obtained and a typical cyclic voltammogram is shown in Figure 2.8.

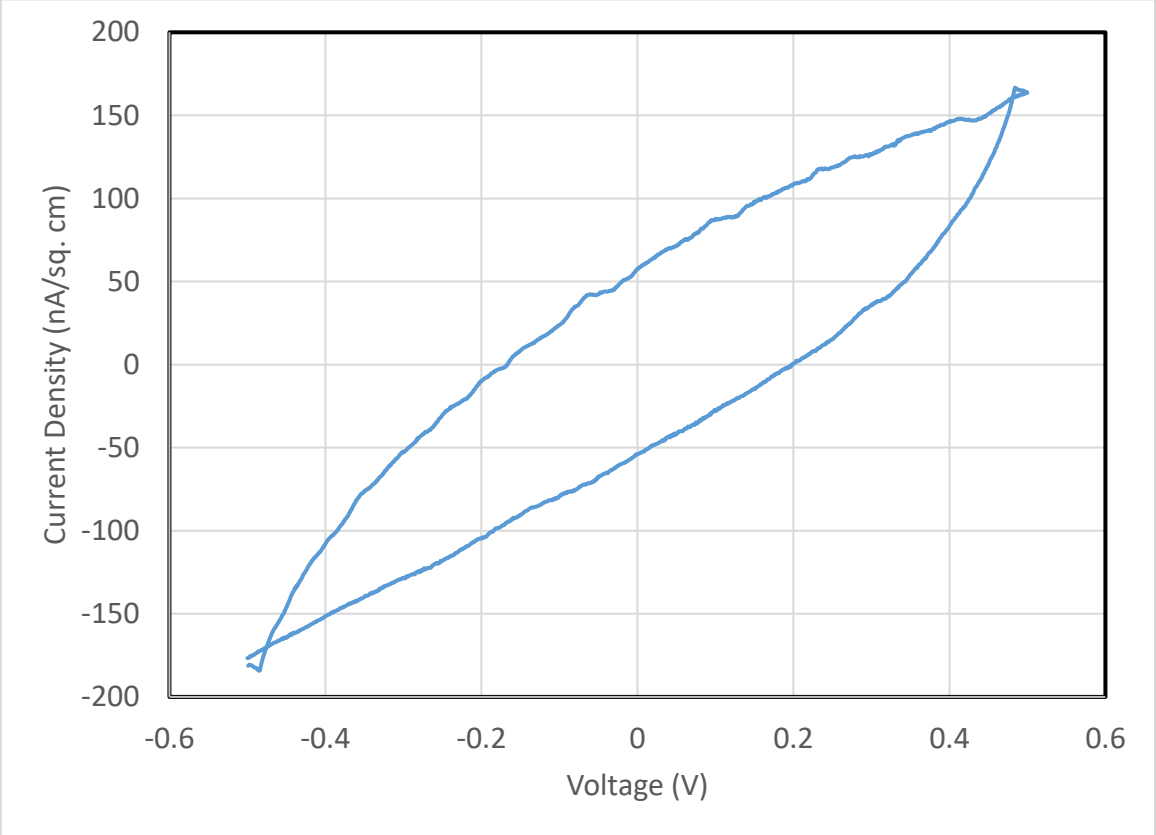

Figure 2.8 Typical cyclic voltammogram of pure PEO electrolyte on copper coated polyester fabric.

In modern instrumentation, two more electrodes: (a) sense electrode and (b) counter / auxiliary electrode, are introduced in CV to cater various types of sample and solution characterization. For sense electrode, it is usually connected to the working electrode, which is a component of differential amplifier that measures the voltage between the reference electrode and itself. For counter /auxiliary electrode, it can either connect to the side opposite to the working electrode, or acting as the third electrode, to control the power output / signals from the instrument.

Since more electrodes are involved in the measurement, different configurations of electrode connection like two-electrode connection and three-electrode connection have been applied, and these configurations are shown in Figure 2.9.

For two-electrode connection, working electrode and sense electrode are connected to one side of the sample, where reference electrode and counter / auxiliary electrode are attached to another side of the sample. Usually, this connection can be used with batteries, capacitors, fuel cells and some sensors which are rigidly formed and 2 significant poles can be recognized for measurement.

In three-electrode connection, it is commonly used in general aqueous electrochemistry. The working electrode and sense electrode are connected together as a single electrode, where reference electrode and counter / auxiliary electrode are independently connected to the sample solution. A controlled potential is applied between working electrode and reference electrode by the

potentiostat, where electrolysis will be taken place at the working electrode. Counter /auxiliary electrode will then provide the current required to support the electrolysis at the working electrode. By this arrangement, large current can be prevented from passing through the reference electrode, which may change the potential in the measuring system **[90, 91, 92]**.

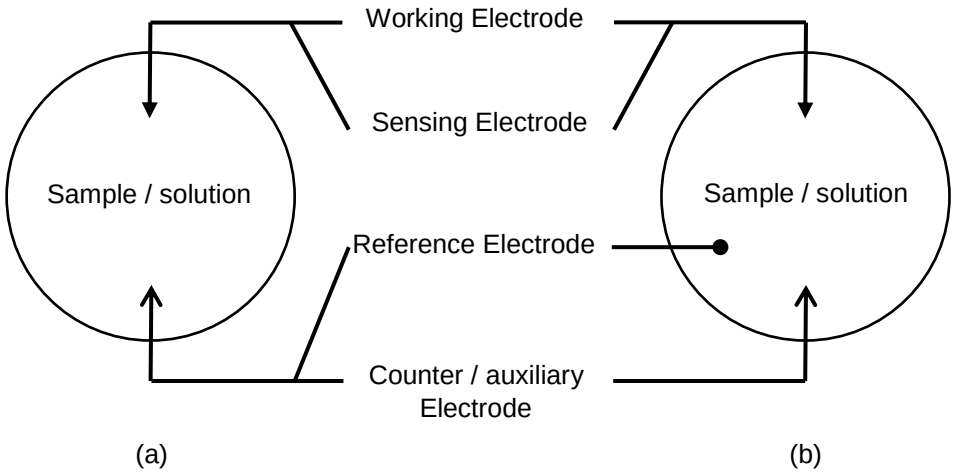

Figure 2.9 Different connecting configurations in cyclic voltammetry (a) two-electrode connection and (b) three-electrode connection.

2.6.2 Electrochemical Impedance Spectroscopy (EIS)

Electrochemical Impedance Spectroscopy is one of the commonly used analytical technique to examine the properties of double layer electrochemical system. It can reveal various information from processes occurring in the active layer, or electrolyte like polymer matrix when it is doped by different dopants. Besides, EIS can investigate the kinetic of doping processes and parameters of the ion diffusion into the polymers **[93, 94, 95]**.

In EIS, a small sinusoidal potential $V(\omega,t) = V_o \sin \omega t$ with an amplitude of V_o and variable frequency f ($f = \omega/2\pi$, where ω is the angular frequency) is applied to the sample under measurement, and the corresponding current $I(\omega,t)$ is measured at the same frequencies. Therefore, the corresponding impedance $Z(\omega,t)$ related to the measured sample can be deduced from the ohm's law as:

$$\mathrm{Z}(\omega, t) = \frac{\mathrm{V}(\omega,t)}{\mathrm{I}(\omega,t)} \qquad (2.2)$$

From the particular angular frequency ω, the current measured from sample can appear in-phase or out-of-phase to the corresponding sinusoidal potential applied, provided that the current can be expressed in the form of $I(\omega,t) = I_o \sin(\omega t-\theta)$, where I_o is the current amplitude and θ is the phase angle between potential and current. By the expression of complex number notation, this AC potential and current signal can be rewritten as $V(\omega,t) = V_o e^{j\omega t}$ and $I(\omega,t) = I_o e^{j(\omega t-\theta)}$ respectively,

where j is the imaginary unit. With this transformation, Equation (2.2) can be expressed as:

$$\mathrm{Z}(\omega,t) = \frac{\mathrm{V}(\omega,t)}{\mathrm{I}(\omega,t)} = \frac{V_o}{I_o} e^{j\theta} = |Z(\omega)|e^{j\theta} \qquad (2.3)$$

where $|Z|$ is the impedance modulus and θ is the impedance phase angle. By applying Euler's formula, Equation (2.3) can be further transformed into:

$$\mathrm{Z}(\omega,t) = |Z(\omega)|(\cos\theta + j\sin\theta) = Z'(\omega) + jZ''(\omega) \qquad (2.4)$$

where $Z' = |Z| \cos\theta$ and $Z'' = |Z| \sin\theta$ are the real and imaginary part of the impedance respectively. From Equation (2.4), the modulus and the phase angle of impedance can be found by:

$$|Z(\omega)| = \sqrt{Z'^2(\omega) + Z''^2(\omega)} \qquad (2.5)$$

$$\theta(\omega) = \tan^{-1}[Z''(\omega)/Z'(\omega)] \qquad (2.6)$$

With the about relations, the measured impedance along different frequencies can be plotted into the Nyquist Plot and Bode Plot **[96]**.

2.6.2.1 *The Nyquist Plot*

The Nyquist Plot plots the imaginary impedance component *Z''* against the real impedance component *Z'* at each excitation frequency. The plot in Figure 2.10 shows the expected response of the corresponding equivalent circuit.

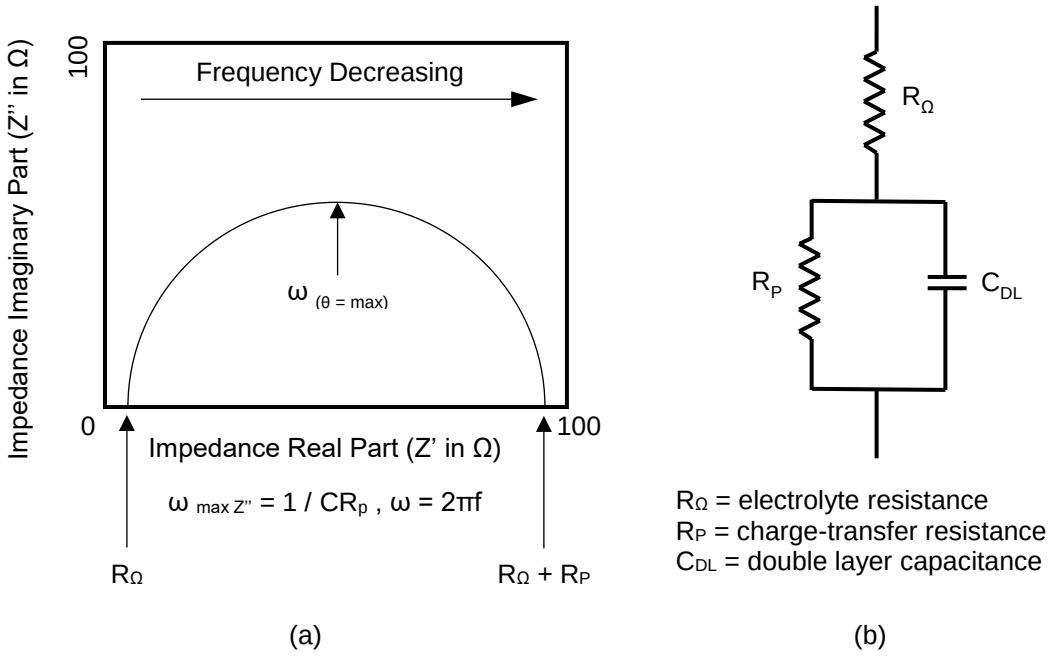

Figure 2.10 (a) The Nyquist Plot for a simple electrochemical system and (b) its corresponding equivalent circuit.

For the equivalent circuit, the resistance in series with Voigt elements is applied to model the electrochemical impedance of an interface and can fit for many chemical systems. The electrolyte resistance (R_Ω) is connected to a parallel connection of the charge-transfer resistance (R_P) and double layer capacitance (C_{DL}) in a serial configuration. R_Ω is an ohmic resistance of the electrolyte measured between the working electrode and reference electrode. R_P is another

ohmic resistance occurred at the electrode/electrolyte interface, and C_{DL} is the double layer capacitance at the testing interface, which is a frequency dependent element. When the frequency increases, the impedance of the capacitor, or in other words, the capacitive reactance will decrease and R_P is frequency independent element that will remain unchanged. At a certain level of high frequency, the capacitive reactance of C_{DL} will become very small and even negligible. This phenomenon can be said as short circuit at C_{DL}, and therefore R_Ω will dominate the resistance of the electrochemical system. Vice versa, at low frequency or even at a constant potential (i.e. D.C.), the capacitive reactance of C_{DL} will largely increase to become an open circuit status, in this situation, the impedance of equivalent circuit will highly depend on the two frequency independent elements, R_Ω and R_P. In the Nyquist plot at Figure 2.10, during both high and low frequency situation, the capacitive reactance of C_{DL} will be considered as short circuit and open circuit, respectively. So the electrochemical system will mostly behave as resistor, with negligible effect from the capacitive element, the imaginary component is very small and the plot will nearly touch the X-axis and the lowest and highest end of frequencies. However, at intermediate frequencies, the capacitive reactance of C_{DL} will begin to affect the total impedance of the equivalent circuit, and the cell will become a capacitive component. In the plot, the imaginary component will become significant, the phase angle θ will increase and approach to 90 degrees.

2.6.2.2 The Bode Plot

The Bode Plot plots the absolute impedance |*Z*| along the change of frequencies, where the magnitude of |*Z*| consists of *Z'* and *Z''* according to the equation (2.5) at particular frequency. The plot can also show the relation of phase angle (θ) between the real and imaginary part of impedance, against the change of frequencies, for investigating the changes between these two impedances at different frequencies **[97, 98]**.

In Figure 2.10, the total impedance of the equivalent circuit $Z(\omega)$ can be rewritten as:

$$Z(\omega) = Z_R(\omega) + Z_v(\omega) \tag{2.7}$$

where $Z_R(\omega)$ is the impedance of resistive element in series and $Z_v(\omega)$ is the impedance of Voigt element. Since the electrolyte resistance (R_Ω) is a frequency independent element, therefore, $Z_R(\omega)$ is directly equal to R_Ω and

$$Z_R(\omega) = R_\Omega \tag{2.8}$$

For the Voigt element, it consists of a parallel connection of a resistive element and a capacitive element, Therefore, the total impedance of Voigt element is

$$Z_v(\omega) = \left[{}^{1}/_{R_P} + {}^{1}/_{X_C}\right]^{-1} \tag{2.9}$$

where R_P is the charge-transfer resistance and X_C is the capacitive reactance of the double layer capacitor (C_{DL}). In case of a sinusoidal potential is applied to the system, the corresponding current will be out-of-phase with respect to the potential

($\theta = -\pi/2$). The capacitive reactance of double layer capacitor can be determined by:

$$X_C(\omega) = \frac{V(\omega)}{I(\omega)} = \frac{V_0}{I_0} e^{j\theta} = \frac{1}{\omega C} e^{-j\pi/2} = \frac{1}{j\omega C} \quad (2.10)$$

With the relation of equation (2.9) and R_P, equation (2.8) can be rewritten as:

$$Z_v(\omega) = \left[{}^{1}\!/_{R_P} + {}^{1}\!/_{\frac{1}{j\omega C}} \right]^{-1} = {}^{R_P}\!/_{(1 + j\omega R_P C)} \quad (2.11)$$

and the $Z(\omega)$ can be evaluated by substituting equation (2.8) and (2.11) into equation (2.7):

$$Z(\omega) = R_\Omega + \left[{}^{R_P}\!/_{(1 + j\omega R_P C)} \right] \quad (2.12)$$

In Figure 2.11, there is a Bode plot of the electrochemical system with PEO electrolyte mixed with DW-CNT. The absolute impedance $|Z|$ of the electrochemical system increases at the lower frequency limit from 10 mHz and reaches the maximum about 1Hz. When the frequency increases, the X_C increases and the electrochemical system becomes capacitive, the total impedance increases correspondingly, until it reaches the higher frequency limit, X_C becomes smaller and tends to short circuit, the capacitive element becomes diminished and the total impedance becomes dominant again by resistive element.

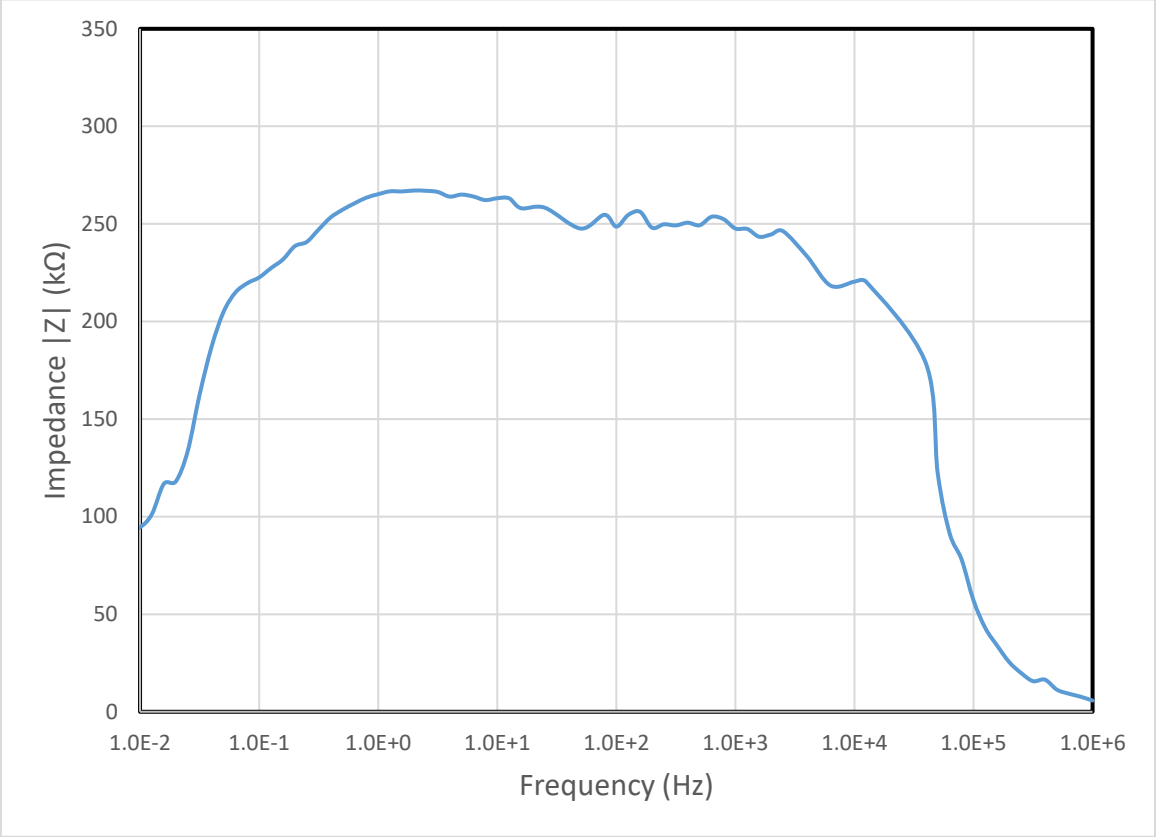

Figure 2.11 The Bode Plot for the electrochemical system with PEO electrolyte mixed with DW-CNT along different frequencies.

2.6.3 Cyclic Charge-discharge Measurement

Usually in electrochemical analysis, to study the performance and life cycle of a double layer electrochemical system, a repeating loop of charging and discharging measurement will be introduced. During the measurement, a constant level of current will be applied to the electrochemical system, a certain level of voltage has been reached, and the time consumed will be recorded. For another measuring method, the period for charging and discharging is fixed; the voltage change during charge-discharge cycle will then be obtained. Practically, the latter method is commonly used for multicycle measurement, because the performance of electrochemical system can be easily investigated and studied by repeating a constant period. This type of analytic technique is called the cyclic chronopotentiometry, or specifically, the cyclic galvanostatic charge-discharge measurement **[99, 100, 101, 102]**.

In constant current chronopotentiometry (galvanostatic charge-discharge measurement), the constant anodic or cathodic current will be applied to the double layer electrochemical system, which activates the electroactive species to be oxidized or reduced at a constant rate.

As the concentration ratio of reactant to product will change at the electrode surface of the system, the electrode potential will then change according to time. In some cases, this process is used for titrating the reactant around the electrode, thus a potential titration curve can be obtained. At the electrode surface, when the

concentration of the reactant has been dropped to zero, the reactant may be failed to supply to the electrode surface to accept all of the electrons being forced by the application of a constant current. As a result, the electrode potential will dramatically increase to anodic or cathodic. The shape of the curve is highly dependent on the reversibility of the electrode reaction **[99, 103, 104]**.

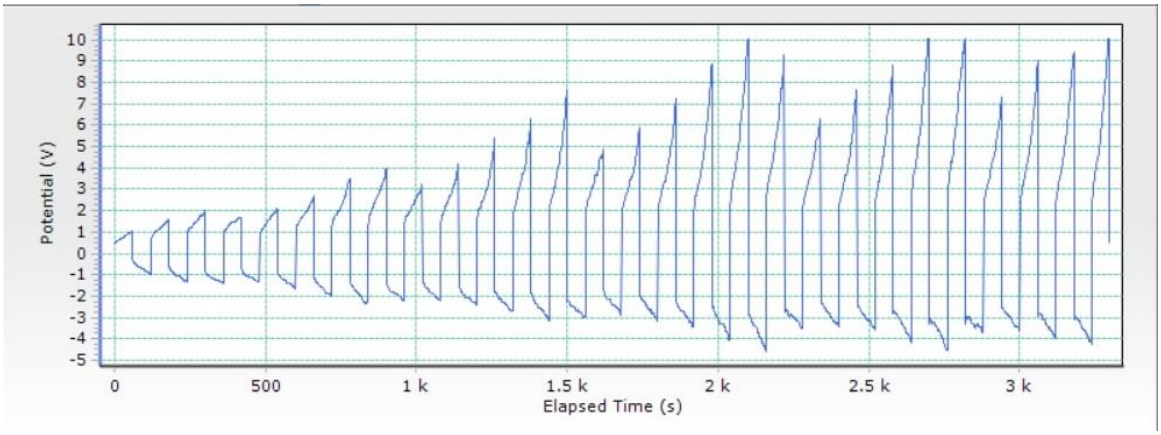

Figure 2.12 The chronopotentiogram of a double layer electrochemical system with DW-CNT and lithium ion doped in PEO electrolyte under cyclic chronopotentiometry.

To conclude, the modern development of supercapacitor is rapid and promising. From the first supercapacitor, the bulky Leyden jar made in 1746, the size has been largely reduced to nowadays in micron scale. Moreover, the charge storage capability has been enhanced from milli-Farads to thousands of Farads, by using solid or gel polymeric electrolytes. Polymeric electrolytes like PEO, PVA and PMMA are safe and more reliable to be used in the supercapacitor, instead of using aqueous electrolytes such as H_2SO_4, Na_2SO_4 and KOH, which are corrosive and unstable to handle.

Besides, by doping alkaline metal salts such as $LiClO_4$ into the electrolyte to increase the charge mobility, and applying nanocarbons like double-walled carbon nanotubes to the electrode to increase the charge accumulation capability in the supercapacitor, the efficiency of energy harvesting in the supercapacitor has been enhanced and therefore, the performance of supercapacitor becomes more favorable.

With various non-destructive electrochemical testing methods such as cyclic voltammetry, electrochemical impedance spectroscopy and cyclic charge-discharge measurement, the electrochemical properties including voltage-current response during charge-discharge cycles, impedance of the electrolytic materials and the life cycle of the electrochemical system can be characterized.

Chapter 3

Sample Preparation & Characterizations

3.1 Fabrication of conducting fabric

In this research, commercial polyester fabric samples (mainly contain poly(ethylene terephthalate), PET; 75 x 75 threads per sq. inch, Lai Tak Enterprises Ltd.) were metallized by 2 steps: (a) electroless nickel (Ni) plating and (b) electroless copper (Cu) plating to become conducting fabric samples for further experiment **[7, 73, 74, 75, 76, 77, 105]**.

3.1.1 Metallization with electroless nickel plating on polyester fabric

3.1.1.1 Preparation of polyester fabric samples

Before the metallization, 15 x 15 cm plain polyester fabric samples were washed with 2% non-ionic detergent (Diadavin EWN 200%, Bayer AG) at pH 7 for 30 minutes under 30°C to degrease and clean up the polyester fabric surface for further chemical adhesion reaction. After washing the fabric samples thoroughly to remove the remaining detergent, the pre-washed fabric samples were then rinsed by de-ionized water (DI water) to eliminate the remaining ions on the samples.

3.1.1.2 *Alkaline etching on sample surfaces*

To activate the sample surfaces for further metallization, the samples were immersed into a 4M sodium hydroxide (NaOH) at 50°C for 20 minutes. By alkaline etching, the polymer bonding and functional groups of polyester will be opened to provide a better surface roughness and increased surface area for metal ion adhesion during palladium (Pd) coating and eventually nickel coating processes (*Figure 3.1*). NaOH acts as nucleophilic agent and carries out the hydrolysis of polyester, which hydrolysis increases the number of hydrophilic group. The carboxylate groups of polyester are feasible to form metal complex with palladium and tin ions (Pd/Sn^{2+}). After etching, the samples were rinsed by DI water to neutralize the sample surface and the excess water on sample surfaces have to be removed to prevent contamination on the following procedures.

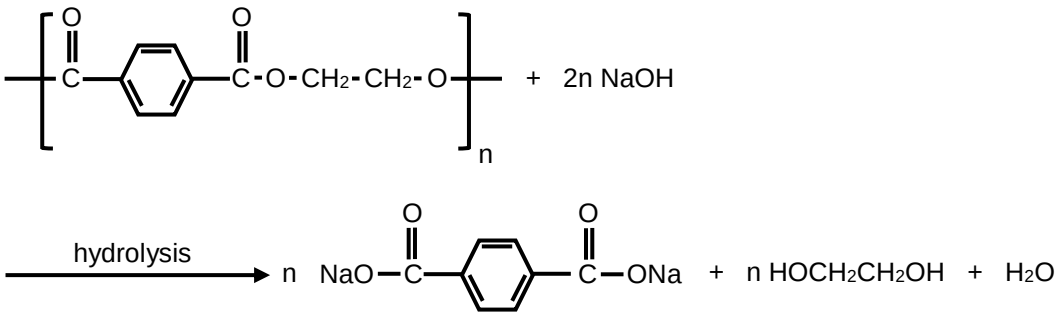

Figure 3.1 Hydrolysis of PET (Polyester) in alkaline etching.

3.1.1.3 Acidification of sample surface

To provide an acidic environment of the sample surfaces for further palladium coating process, the samples were immersed into 1% hydrochloric acid (HCl) at room temperature for 30 s. After acidification, the samples should not be rinsed by any solvents to maintain its acidic state for further coating process.

3.1.1.4 Palladium coating

To metalize the sample surfaces, a nucleation with catalytic treatment was taken place to adhere the palladium atoms on the sensitized surface. The polyester samples were immersed into an acidic bath with 37% HCl, DI water, Macuplex® 78 Sensitizer (MacDermid) and Macuplex® activate D-34C (MacDermid) with volume percent of 21.57% : 75.88% : 1.96% : 0.59% at room temperature for 3 minutes. Since Macuplex® 78 Sensitizer contains Potassium iodine (KI) and potassium iodate (KIO_3), which can be used to maintain the divalent tin (Sn^{2+}) in the acidic bath, and Macuplex® activate D-34C is an activating solution based on colloidal suspension of palladium (Pd) particles in a stannous chloride ($SnCl_2$) medium. By this bath, the polyester surfaces can be activated and sensitized, tin (Sn) ions would transform from Sn^{2+} to Sn^{4+} and react with the negatively charged carboxylate functional group while palladium ions would adhere on the tin ions and work as a catalyst due to its high metal ion adsorption ability. After coating, the samples were rinsed by DI water to neutralize and clean the sample surfaces.

3.1.1.5 Removal of excess ions

For removal of excess tin ions on the sample surfaces and those surrounding palladium ions, the samples were immersed into a 50 g/L sulphuric acid (H_2SO_4) bath at 50°C for 1 minute. After the acid dipping, samples were rinsed by DI water to neutralize the surfaces.

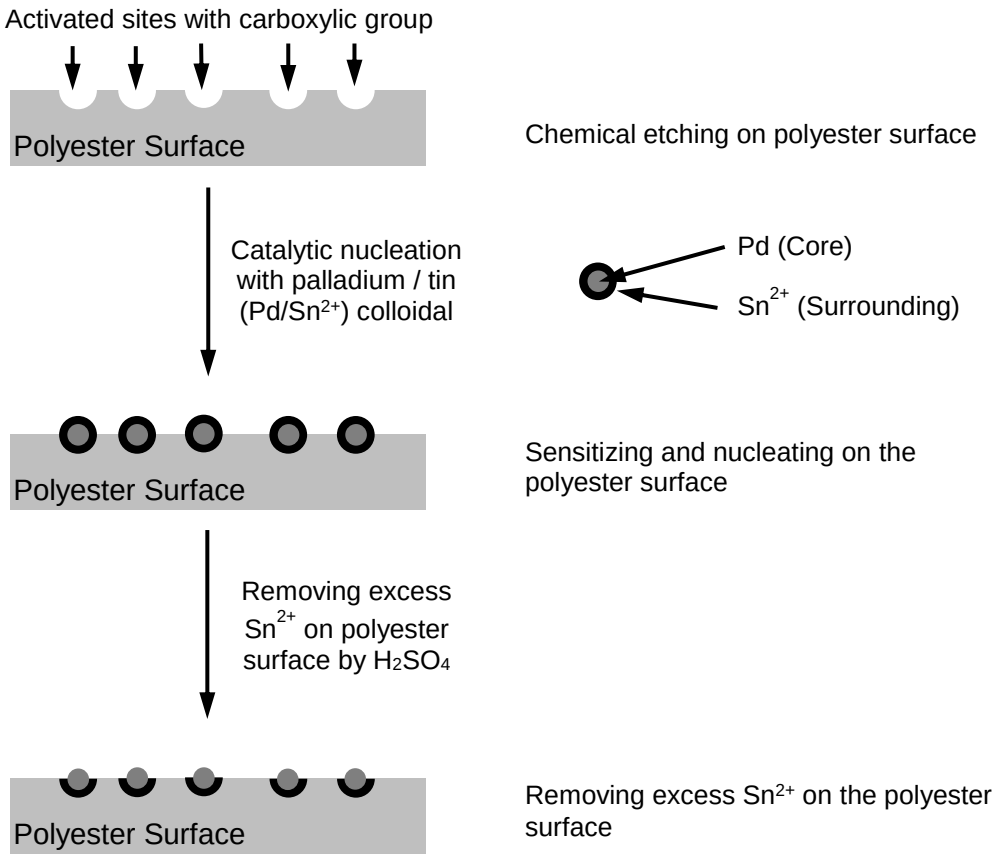

Figure 3.2 Schematic diagram showing the surface activation process on the polyester fabrics.

3.1.1.6 Electroless nickel plating

For further copper plating process on the polyester fabrics, a layer of nickel will be plated on the sample surface. The samples were immersed into a nickel bath with 28% ammonium hydroxide (NH_4OH), DI water, Macuplex® J-60 (MacDermid) and Macuplex® J-61 (MacDermid) with volume percent of 0.5% : 86.5% : 10.0% : 3.0% at 35°C for 3 minutes. Macuplex® J-60 mainly contains nickel chloride ($NiCl_2$) and Macuplex® J-61 is a nickel-containing reducing agent. In the nickel-rich solution mixture, nickel ions were adhered on the polyester surface with the palladium ions by recombining with electrons, and a layer of conducting nickel was formed.

Formation of nickel: $Ni^{2+} + 2\,e^- \rightarrow Ni$

After plating, the samples were rinsed by DI water to remove the remaining solution and to terminate the reaction. Finally the samples were dried in the oven at 50°C for 6 hours.

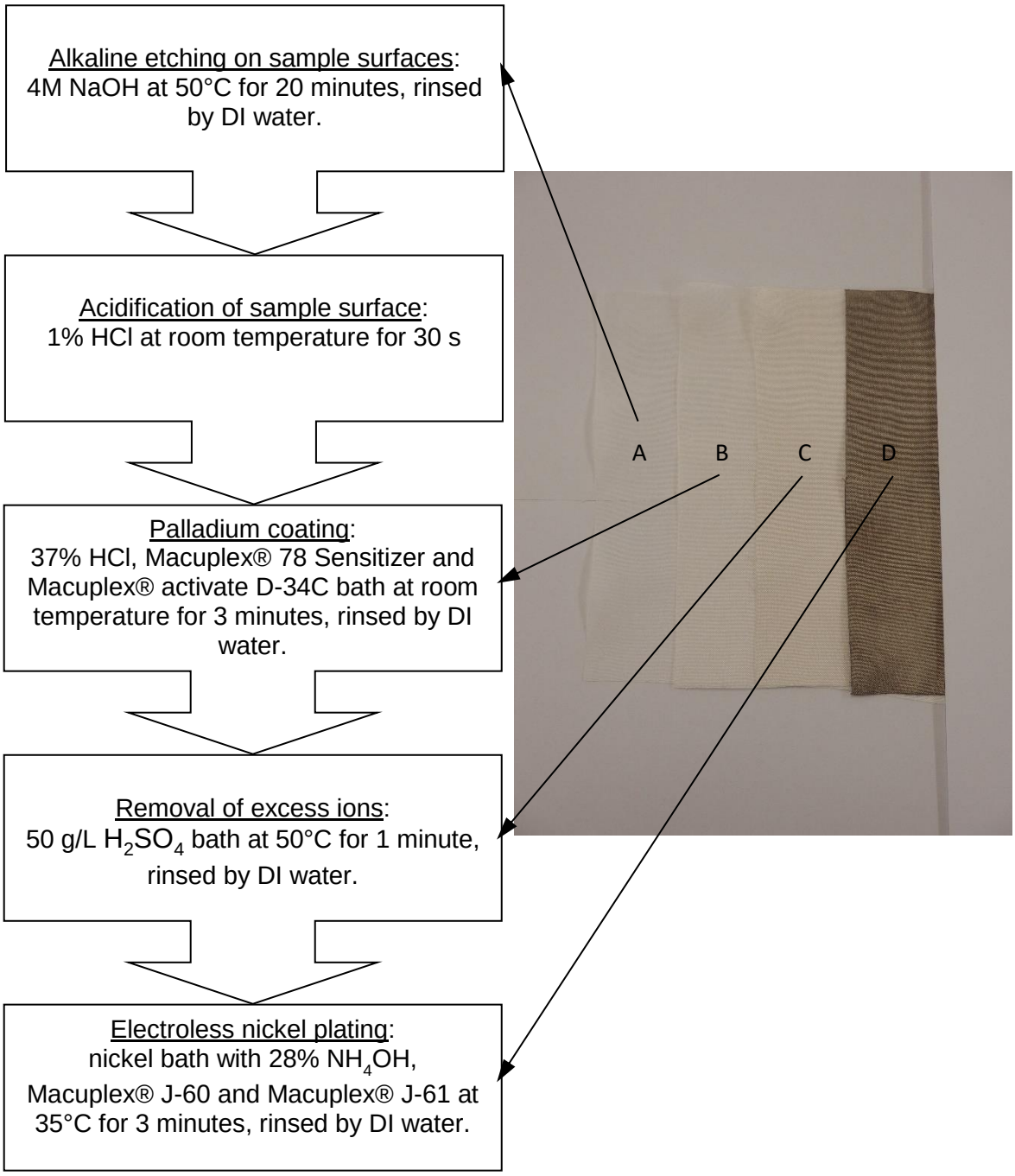

Figure 3.3 The metallization process of polyester fabric sample (Left) and the change of sample surface after corresponding treatments (Right). A is an alkaline etched sample with no significant colour changes. B is a palladium-tin complex coated sample with a slightly yellowish colour on surface. C is a palladium-tin complex coated sample treated by H_2SO_4 to remove excess ions on sample surface, and a pale yellow colour appeared. D is an electroless nickel-plated sample with a shiny dark grey surface.

3.1.2 Metallization with electroless copper plating on nickel plated polyester fabric surface

To facilitate a uniform and better conducting surface, a copper layer will be coated on the polyester samples to provide a good conducting layer for current collection. Traditionally copper coating can be prepared by acid copper plating method, coping with chemicals containing cyanide. However, the processes are highly toxic and the quality of copper layer plated on the sample surface will not be satisfactory, as this method is beneficial in smoothening the material surface by bulk of copper instead of producing a fine conducting layer on the woven fabric surface. Therefore, non-cyanide alkaline copper strike process has been implemented to produce a fine conducting copper layer with several microns in thickness on the delicate woven polyester surface.

In the experiment, the Ni-plated polyester samples were immersed into electrolytic bath for degreasing, where the metalized samples were connected to the cathode by applying a current density of 3 ASD (ASD: Current per square decimeter, A/dm^2) at 50 °C for 1 minute. After degreasing, the samples were rinsed by DI water for further processing. The samples were then dipped into sulphuric acid bath at 50°C for 30 s to remove the traces of oxide film and to activate the surface of substrate, followed by rinsing with DI water. Finally, the polyester samples were coated with copper by non-cyanide alkaline copper strike using 2 ASD at 50°C for 6 minutes as shown in Figure 3.4, followed by DI water rinsing and dried by oven at 50°C for 30 minutes. Figure 3.5 shows the final metallized PET fabric.

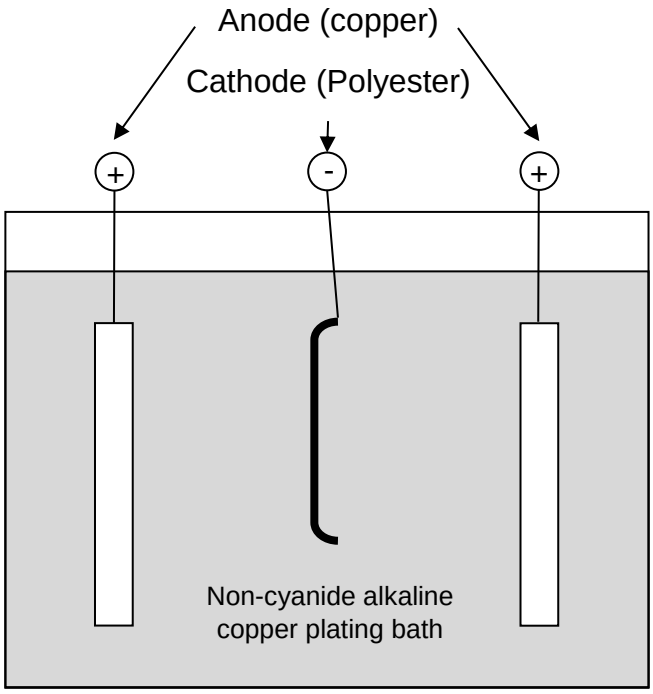

Figure 3.4 The electrode configuration of non-cyanide electroless copper plating.

Figure 3.5 The polyester fabric electroless plated with non-cyanide alkaline copper strike process.

3.2 Fabrication of electrochemical double layer capacitors

There are many methods can be applied to obtain a uniform, effective and thin capacitive coating layer on the conductive fabric surface for further charge storage. However, for a woven fabric, deposition like chemical vapour deposition (CVD) and spin coating may not be viable methods to do so because of the fabric surface morphology. As woven fabrics are woven from numbers of weft and warp yarns to produce a large surface, microscopically, the fabric surface is consisted of continuous peak-and-trough, and even some pits between the junction of yarns. These porous surfaces usually deteriorate the quality of uniform capacitive layer formation as the materials deposited may not fill up the pits and yarn surface thoroughly. It may cause discontinue of layer, which will degrade the effectiveness and efficiency of charge/discharge processes **[78, 106, 107, 108, 109]**. Therefore, in this research, PEO with solution casting has been implemented to prepare a continuous capacitive layer on the copper-plated polyester fabric surface.

3.2.1 Preparation of current collecting substrate

As a current collecting substrate in an electrochemical system, the copper-plated polyester fabrics were cut into small pieces with the dimension of 7.5 x 20 mm. Then the polyester pieces were flatly aligned and fixed on the 5 mm thick, 100 x 100mm poly(tetrafluoroethylene) sheet (PTFE, provided by Goodfellow) for further solution casting of PEO active layer shown in Figure 3.6.

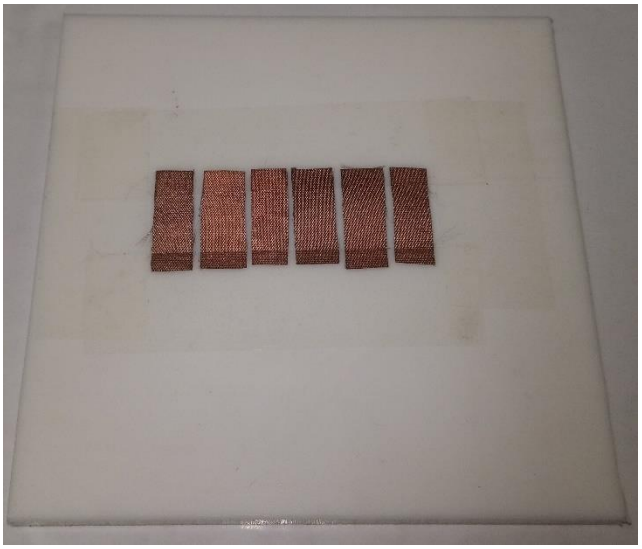

Figure 3.6 The copper-plated polyester fabrics aligned and fixed on PTFE sheet for further solution casting.

3.2.2 Preparation of pure PEO dielectric spacer

As a dielectric material to separate the two electrodes in an electrochemical system, a PEO spacer was inserted between the electrodes and lithium doped PEO active layers. 1 g PEO powder (average molecular weight (M_v) 600000, Sigma Aldrich) was dissolved into 50 ml of deionized water. The solutions were stirred thoroughly without heating to ensure PEO powder can be completely dissolved in the solution without thermal degradation. Then the solution was poured on a 330 x330 mm glass slide and dried in the ambient for 24 hours. Once the solution was dried, a layer of PEO with thickness of 15 μm was formed. The PEO was peeled off from the glass slide and was cut into a square of 10 x 10 mm for further use.

3.2.3 Preparation of PEO-based electrochemical cell with various amount of $LiClO_4$

In this experiment, the electrical properties of PEO-based electrochemical double layer capacitor with various amount of $LiClO_4$ were determined. Therefore, PEO solutions with different amount of $LiClO_4$ were prepared for further sample fabrication.

A stock solution of $LiClO_4$ was prepared by dissolving 250 mg of $LiClO_4$ (99.99% trace metals basis, Sigma Aldrich) into 250 ml of deionized water. For each PEO:Li^+ solution, 1 g PEO powder (average molecular weight (M_v) 600000, Sigma Aldrich) was dissolved into 50 ml of deionized water. Then different amount of $LiClO_4$ solution was added into various PEO solutions according to Table 3.1 as shown below:

Table 3.1 The amount of PEO and LiClO4 in various PEO:Li+ solutions.

Solution	**Amount of PEO (in mg)**	**Amount of $LiClO_4$ (in mg)**	**Amount of $LiClO_4$ (in ml)**	**PEO : Li^+ ratio in weight**
R	1 g	N/A	N/A	Control solution
A	1 g	1.0 mg	1.0 ml	1000:1
B	1 g	1.5 mg	1.5 ml	~ 667:1
C	1 g	2.0 mg	2.0 ml	500:1
D	1 g	2.5 mg	2.5 ml	400:1
E	1 g	3.0 mg	3.0 ml	~ 333:1
F	1 g	10.0 mg	10.0 ml	100:1

The solutions were stirred thoroughly without heating to ensure PEO powder and $LiClO_4$ could be completely dissolved in the solution without thermal degradation. Afterwards, solutions were poured on the fixed polyester pieces as shown in Figure 3.7. To ensure the casted PEO layer can formed uniformly, samples were put in a box connected to a low throughput ventilation system with a negative pressure to dry for 24 hours. This process was repeated for three times to ensure a continuous uniform PEO layer can be casted on the polyester surface with a good adhesion and a workable thickness.

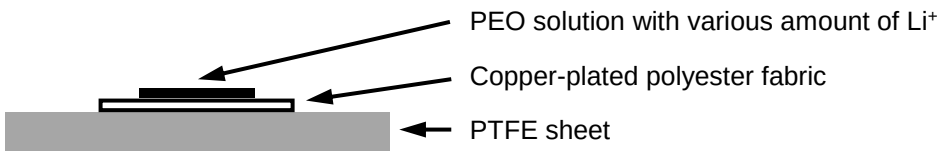

Figure 3.7 The schematic diagram shown the PEO-based electrolytic material solution casted on the polyester fabric.

After the PEO layer casted on the polyester, two casted pieces were laminated together with a 10 x 10 mm PEO spacer as shown in Figure 3.8 to form an electrochemical double layer capacitor. The overlapping area of two casted pieces was the effective area for capacitive effect taken place. The laminated PEO-based electrochemical double layer capacitor with connecting wires for further measurement was illustrated in Figure 3.9.

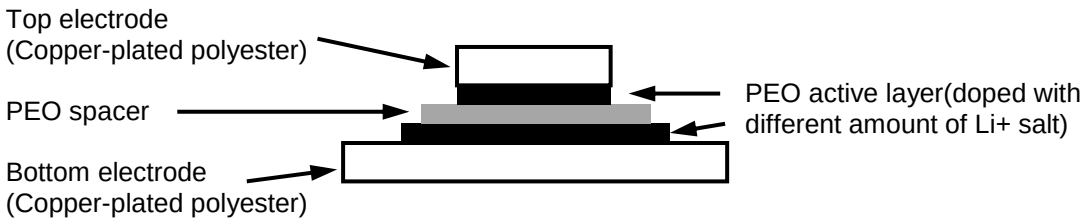

Figure 3.8 The schematic diagram shown the structure of PEO-based electrochemical double layer capacitor.

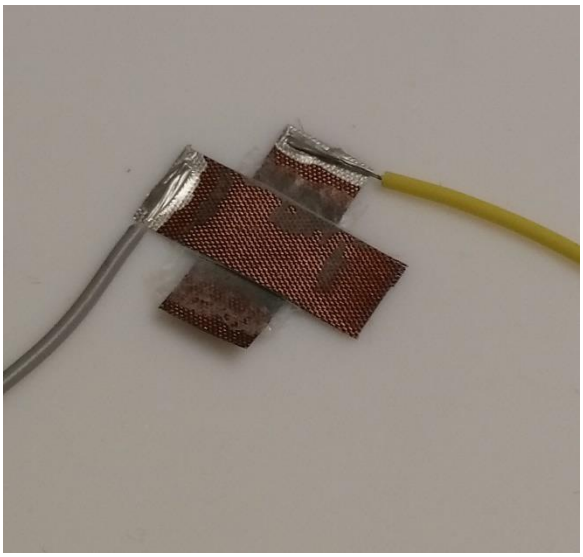

Figure 3.9 The PEO-based electrochemical double layer capacitor.

3.2.4 Preparation of PEO-based electrochemical cell with various types of nanocarbon

In this experiment, the electrical properties of PEO-based electrochemical double layer capacitor with various types of nanocarbon were investigated. Hence, PEO solutions with different types of nanocarbon were prepared for further sample fabrication.

For various PEO:Nanocarbon solutions, each type of nanocarbon with 40 mg was dissolved into 10 ml of deionized water, including: (a) Single-walled carbon nanotube (SW-CNT, Sigma Aldrich), (b) Double-walled carbon nanotube (DW-CNT, Sigma Aldrich), (c) Multi-Walled carbon nanotube (MW-CNT, Sigma Aldrich) and (d) Mesoporous carbon nanopowder (Meso-C, Sigma Aldrich). The specification of these nanocarbons are listed in Table 3.2. These nanocarbon solutions were then sonicated by ultrasound for 2 hours to ensure the nanocarbon can well disperse in the solution without forming aggregates.

Table 3.2 The specification of various nanocarbons used in the experiment.

Item	Dimension	Density at 25°C (g/cm^3)
SW-CNT	Diameter: 0.7 – 1.3 nm	1.7 – 1.9
DW-CNT	5 nm x 1.3 – 2.0 nm x 50 μm (O.D. x I.D. x Length)	1.7 – 2.1
MW-CNT	6 – 13 nm x 2.5 – 20 μm (O.D. x Length)	2.1
Mesoporous Carbon	< 500 nm particle size	1.887

After sonication, 200 mg PEO powder (average molecular weight (M_v) 600000, Sigma Aldrich) was added into various PEO:nanocarbon solutions and the ratio of PEO:nanocarbon was 5:1. The solutions were stirred thoroughly without heating to ensure PEO powder and nanocarbons could be completely dissolved in the solution without thermal degradation. Afterwards, solutions were poured on polyester pieces which were fixed on PTFE sheet as shown in Figure 3.10. The samples were then put in a box connected to a low throughput ventilation system with a negative pressure to dry for 24 hours.

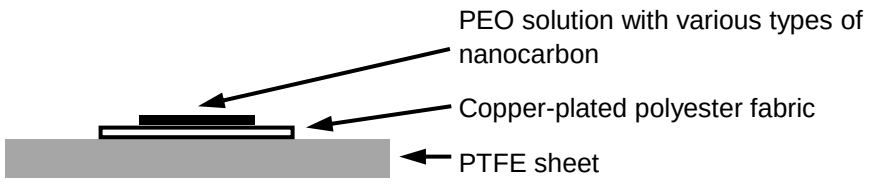

Figure 3.10 The schematic diagram shown the PEO:nanocarbon electrolytic material solution casted on the polyester fabric.

This process was repeated for three times to ensure a continuous uniform PEO layer can be casted on the polyester surface with a good adhesion and a workable thickness as shown in Figure 3.11.

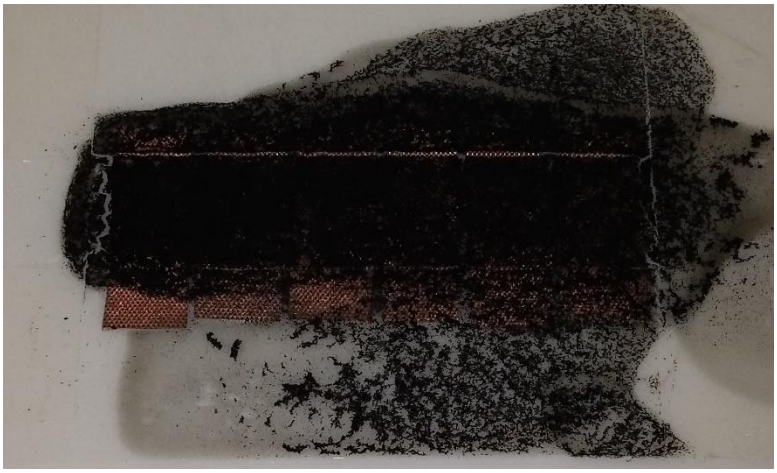

Figure 3.11 The solution casted PEO:nanocarbon electrolytic material on polyester fabric pieces.

After the PEO active layer casted on the polyester, two casted pieces were laminated together with a 10 x 10 mm PEO spacer to form an electrochemical double layer capacitor. The overlapping area of two casted pieces was the effective area for capacitive effect taken place.

3.2.5 Preparation of PEO-based electrochemical cell with various structures

In this study, the electrical properties of PEO-based electrochemical double layer capacitor with different combination of active layers were investigated. The amount of $LiClO_4$ and the type of nanocarbon selected to apply in this section were depended on the experimental results concluded from Sections 3.2.3 and 3.2.4.

3.2.5.1 Preparation of PEO-based dielectric materials

Two different types of PEO spacers were prepared for further experiment. In each PEO spacer solution, 1 g PEO powder (average molecular weight (M_v) 600000, Sigma Aldrich) was dissolved into 50 ml of deionized water. Then 10 ml of $LiClO_4$ solution prepared in section 3.2.3 was added into one of these solutions to form a PEO:Li solution. The solutions were stirred thoroughly without heating to ensure PEO powder could be completely dissolved in the solution without thermal degradation. The details of the solutions were listed in Table 3.3.

Table 3.3 The amount of PEO and $LiClO_4$ in spacer solutions.

Solution	**Amount of PEO (in mg)**	**Amount of $LiClO_4$ (in mg)**	**Amount of $LiClO_4$ (in ml)**	**Ratio of PEO : Li^+**
F1	1 g	N/A	N/A	N/A
Q2	1 g	10.0 mg	10.0 ml	100:1

Each solution was then poured on a 330 x330 mm glass slide and dried in the ambient for 24 hours. Once the solutions were dried, a pure PEO layer and a PEO:Li layer with thickness of 15 μm was formed. These PEO layers were peeled off from the glass slide and were cut into a square of 10 x 10 mm for further use.

3.2.5.2 Preparation of PEO-based active layers with different dopants

In this study, two different type of PEO-based electrolytic solutions were prepared for further experiment on the study of capacitor structure.

In each solution, 40 mg of double-walled carbon nanotube (DW-CNT) was dissolved into 10 ml of deionized water. The DW-CNT solutions were then sonicated by ultrasound for 2 hours to ensure the DW-CNT can well disperse in the solution without forming aggregates.

After sonication, 200 mg PEO powder (average molecular weight (M_v) 600000, Sigma Aldrich) was added into each PEO:DW-CNT solutions and the ratio of PEO:DW-CNT was 5:1.Then 2 ml of $LiClO_4$ solution prepared in section 3.2.3 was added into one of these solution to form a PEO:DW-CNT:Li solution. Both solutions were stirred thoroughly without heating to ensure PEO powder could be completely dissolved in the solution without thermal degradation. The details of the solutions are listed in Table 3.4.

Table 3.4 The amount of PEO, DW-CNT and $LiClO_4$ in electrolytic solutions.

Solution	Amount of PEO (in mg)	Amount of CNT (in mg)	Amount of $LiClO_4$ (in mg)	Ratio of PEO:CNT:Li^+
W1	200 mg	40 mg	N/A	5:1
W2	200 mg	40 mg	2 mg	100:20:1

Afterwards, solutions were poured on the fixed polyester pieces and dried in the ambient with negative pressure for 24 hours. This process was repeated for three times to ensure a continuous uniform PEO layer can be casted on the polyester surface with a good adhesion and a workable thickness.

After the PEO active layer casted on the polyester, two casted pieces with same type of electrolytic materials were laminated together with either a pure PEO spacer or a PEO:Li spacer prepared before to form an electrochemical double layer capacitor. The overlapping area of two casted pieces was the effective area for capacitive effect taken place. The combination of the PEO-based electrolytic materials and spacers are listed in Table 3.5.

Table 3.5 The combination of active layers and spacers of various PEO-based electrochemical double layer capacitors.

Sample combination [active layer // spacer // active layer]	Type of active layer	Type of spacer
PC // P // PC	PC	P
PC // P:Li // PC	PC	P:Li
PCL // P // PCL	PCL	P
PCL // P:Li // PCL	PCL	P:Li
Remark: PC = PEO+DW-CNT P = Pure PEO	PCL = PEO+DW-CNT+Li P:Li = PEO:Li	

3.3 Material Characterization

Throughout the fabrication of capacitive fabric, the characteristics of different functional layers including the electrodes and active layers were investigated to understand the working mechanism of charge storage capability. The surface and structural characterization were performed by using different instrumental and analytical techniques, including the investigation of surface topography, physical, chemical, electrical and mechanical properties.

3.3.1 Surface morphology of different functional layers in EDLC

3.3.1.1 Scanning electron microscopy (SEM)

The surface morphology of different functional layers on the capacitive fabric has been studied by SEM. The surface and topological structure of the coated fabric can be observed with a sub-micron resolution using SEM. Moreover, the uniformity of different functional layer deposition, layer structure and surface morphology can be determined **[7, 63, 64, 65, 66, 67]**. In this study, the surface morphology of polyester fabrics treated in different stages, starting from metallization to PEO casting were being investigated by a scanning electron microscope (SEM) (Hitachi, TM3000).

3.3.1.2 Laser triangulation

To examine the PEO casted polyester fabric, the non-contacting laser triangulation method was introduced to investigate the surface change, hence to estimate the thickness of PEO electrolyte layer. The surface scanning was taken place by laser surface profiler (MTI instruments, Mircotrak™ 3), with laser diode of 670 nm wavelength. The cross section of the plated and casted PET was scanned along the base plate to polyester fabric surface, towards to the PEO-based active layer as shown in Figure 3.12.

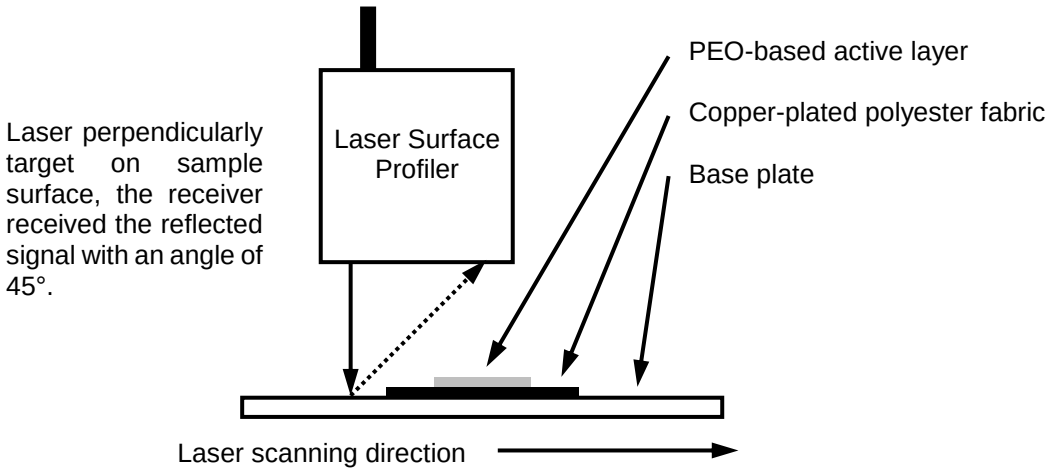

Figure 3.12 Schematic diagram shown the laser surface profiler scanning on copper-plated polyester fabrics casted with PEO-based active layer by laser triangulation.

3.3.2 Investigation of dielectric properties on PEO-based electrochemical double layer capacitor

After fabricating various PEO-based electrochemical double layer capacitors, the electrical properties of these capacitors such as charge storage capability, impedance and endurance of cyclic charge-discharge process were determined and their performances were compared.

In the double layer electrochemical system, the relative permittivity (ε_r) or dielectric constant of a polymeric material can be determined by measuring the ratio of the total charge stored between the separation of two electrodes, subjected to a given voltage and the charge that would be accumulated by identical electrodes separated by a vacuum at the same voltage. The relative permittivity of a dielectric can be expressed as below

$$\varepsilon_r = \frac{Cd}{\varepsilon_0 A} \qquad (3.1)$$

where *C* is the capacitance of parallel plate electrodes of a sample, *d* is the distance between electrodes, ε_0 is the dielectric permittivity of vacuum which is equal to 8.85×10^{-12} F/m and *A* is the area of the electrode.

For ac measurement, the complex frequency-dependent relative permittivity $\varepsilon_r(\omega)$ of the dielectric can be expressed as

$$\varepsilon_r(\omega) = \varepsilon'(\omega) - j\varepsilon''(\omega) \quad (3.2)$$

where ***ε'(ω)*** is the real part of the relative permittivity while ***ε"(ω)*** is the imaginary part. The dielectric loss (***ε"***) is related to the dissipation factor (*tan δ*) that can be calculated by

$$\varepsilon'' = \varepsilon' \tan \delta \quad (3.3)$$

In the experiment, the capacitance and the loss factor were measured simultaneously from 40 Hz to 1 MHz by an impedance analyzer (HP, 4294A Precision Impedance analyzer). Besides, the relation between the resistance (*R*) and the frequency-depending element – reactance (*X*) were also determined.

3.3.3 Investigation of electrochemical properties on PEO-based electrochemical double layer capacitor

There are different categories of measurements can be done in order to investigate the electrochemical properties of the supercapacitors. In this study, the Cyclic voltammetry (CV), Electrochemical Impedance Spectroscopy (EIS), and Galvanostatic Charge-discharge Measurement will be applied to determine the performance of various electrochemical systems. To measure these electrochemical properties, the samples were connected to the electrochemical system (Princeton Applied Research, VersaSTAT 3) with a sample holder in the following two-electrode configuration as shown in Figure 3.13.

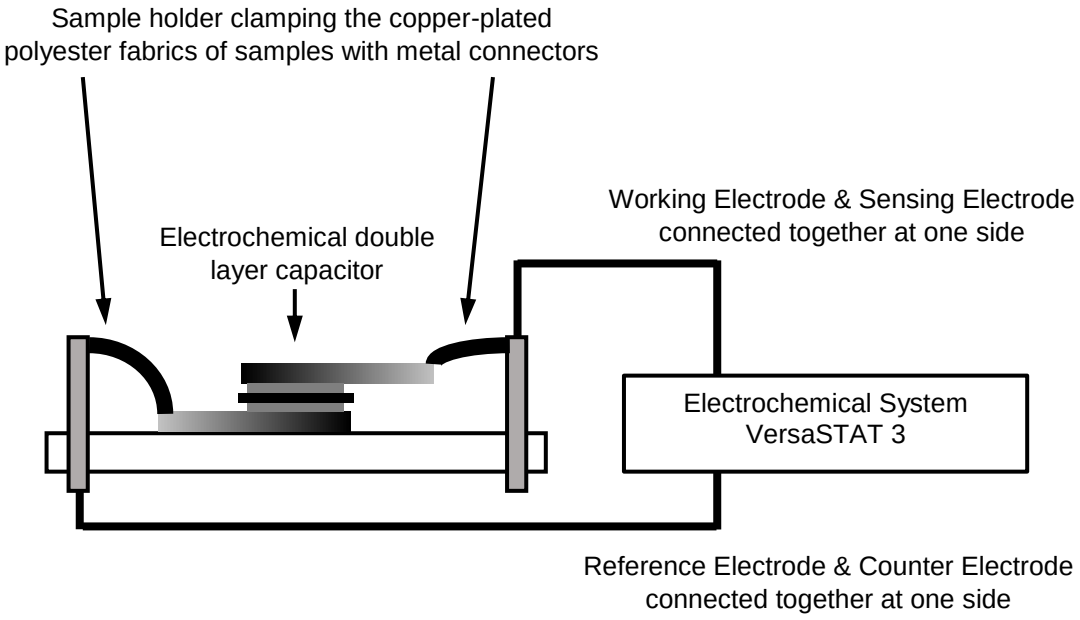

Figure 3.13 Schematic diagram shown the connection of the sample capacitor to the electrochemical system for electrochemical properties measurement.

3.3.3.1 Cyclic voltammetry (CV)

For CV, when the capacitance is only generated from EDL, the CV curve is almost rectangular and the capacitance, *C*, can be estimated from the current density, *I*, at the mid-point of the potential range measured and the potential scan rate, *r*, where $C = I / r$. The potential range, ΔV, is dependent on the type of electrolyte. When pseudocapacitance is existed in the measurement, the point of potential for capacitance calculation is needed to be carefully chosen as the CV curve will no longer in rectangular. When the potential scan rate increases, the CV curve will be distorted and even asymmetric, which is a phenomenon showing the existence of pseudocapacitance. Moreover, the total electric charge, *Q*, can be calculated by integrating the CV curve, which $Q = C (2 \Delta V)$. The value of *C* will be decreased with increasing *r*, therefore the value of *r* should be sufficiently low to obtain high performance. The value of *Q* can be obtained also from a current decay curve by potentiostatic polarization **[9, 13]**. In the experiment, the samples were measured with various scan rates including 10, 20, 50 and 100 mV/s under a potential ranged between -0.5 V and +0.5 V.

3.3.3.2 *Electrochemical Impedance Spectroscopy (EIS)*

For capacitor electrodes, EIS is carried out at the open-circuit potential by applying small amplitude of alternative potential (e.g. ±5 to ±10 mV) over a wide range of frequency, *f* (e.g. 1 mHz to 1 MHz). With absolute impedance |*Z*|, the capacitance is given by $C = 1 / (2\pi f|Z|)$ using a linear portion of *log* |*Z*| versus *log f* curve, which is so called Bode plot **[9, 13]**. In this study, the electrochemical samples were examined with the frequencies ranged from 1 mHz to 1 MHz in logarithmic scale, and a amplitude of 10 mV_{rms}.

3.3.3.3 *Galvanostatic Charge-discharge Measurement*

In galvanostatic charge-discharge measurement, adsorption (charge) and desorption (discharge) processes are usually included in each slope, as anion is adsorbed at more than the open-circuit voltage and cation is adsorbed at less than the open-circuit voltage in each slopes. By applying this method, capacitances of anion and cation are determined separately, when potential ranges of the slope are selected for calculation **[9, 13]**. In the experiment, a current density of 17.78 $\mu A/cm^2$ was applied to various samples to determine their charge-discharge performances.

Chapter 4

Effects of Dopants on PEO-based Supercapacitors

4.1 Surface Morphology of Metalized Polyester Fabrics

The surface morphology of polyester fabrics treated in different stages, starting from metallization to PEO casting was investigated by a scanning electron microscope (SEM). In Figure 4.1, a clean and uniform woven surface is observed on the untreated polyester fabric, from the SEM photo, the diameter of each polyester fiber is about 15 μm.

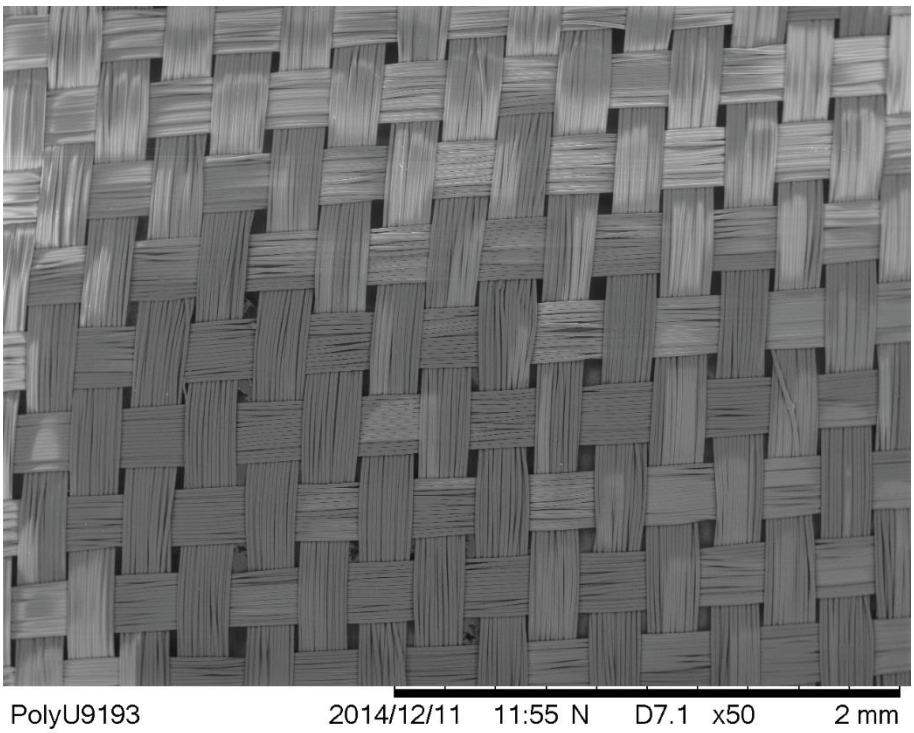

Figure 4.1 SEM photo of the untreated polyester fabric (with 50x).

Figure 4.2 shows the polyester fabric after being coated by palladium under the metallization process. In this palladium plating process, a uniform layer of palladium / tin mixture is coated on the fiber surface, the diameter of palladium coated polyester fiber is observed slightly larger than the untreated fiber at about 15 μm.

After the nickel-plating process taken place, a layer of nickel is plated on the fabric surface and the fiber surface becomes metallic shiny and the fiber diameter is increased to about 17 μm as shown in Figure 4.3. Estimated from the higher magnification SEM photo, the thickness of the nickel plating is under the sub-micron range (with few hundred nm).

Once the polyester fabric is electroless plated with copper, a shiny metal layer can be observed on the fabric surface. A layer of copper is coated surrounding the polyester fiber as shown in Figure 4.4, and the diameter of the copper plated polyester fiber is about 20 μm and the thickness of copper was about 1 μm.

Table 4.1 Summary of the fiber diameter changes after different plating processes taken place.

Treatment on polyester fabric	Diameter of the fiber
Untreated	15 μm
Palladium coated	15 μm
Nickel coated	17 μm
Copper coated	20 μm

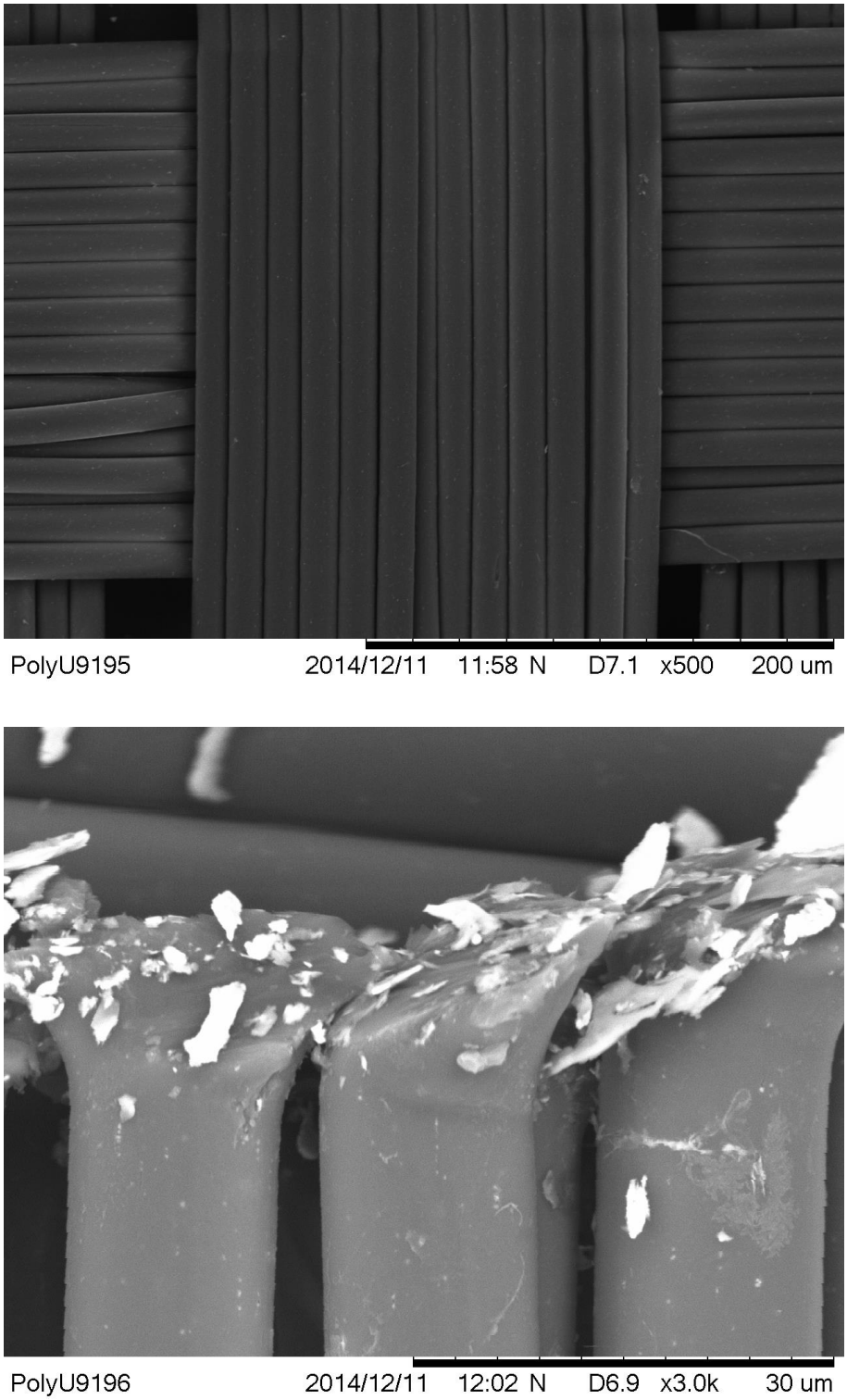

Figure 4.2 SEM photos of the palladium coated polyester fabric (upper with 500x and lower with 3000x).

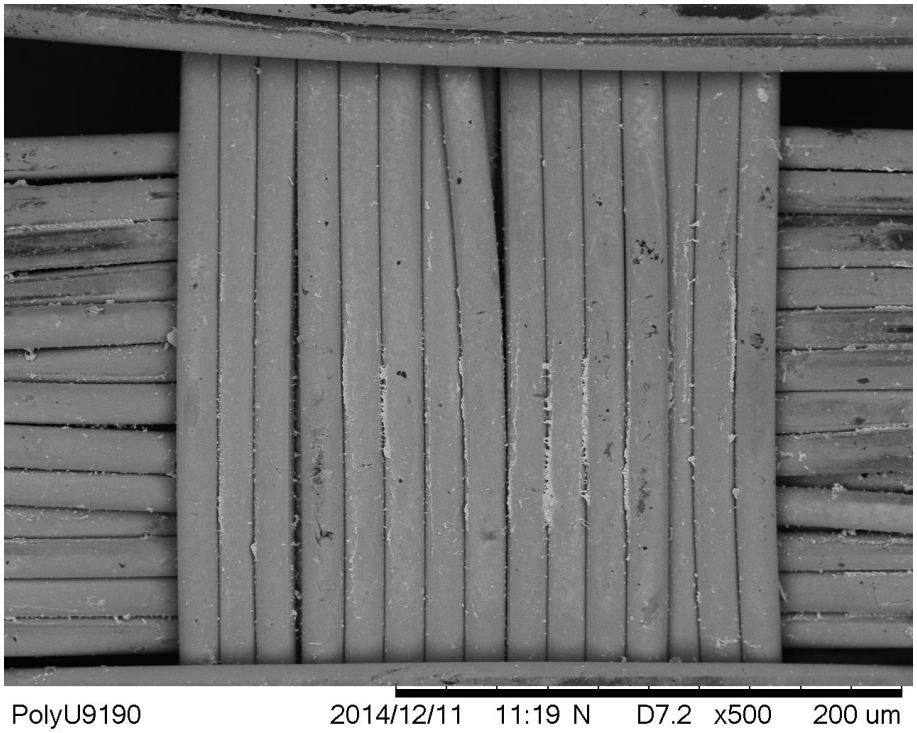

Figure 4.3 SEM photos of the nickel coated polyester fabric (upper with 500x and lower with 3000x).

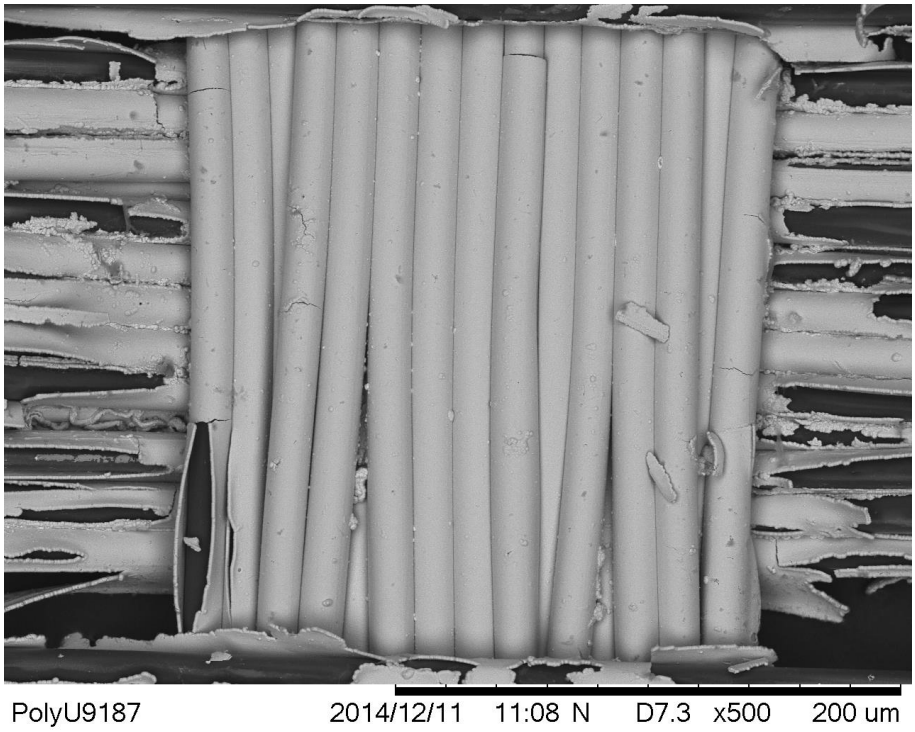

Figure 4.4 SEM photos of the copper coated polyester fabric (upper with 500x and lower with 3000x).

After fabric metallization process, a layer of PEO has been casted on the fabric surface. In Figure 4.5, a layer of pure PEO without any dopants is solution casted on the fabric surface. White particles are observed in the PEO layer, these particles are crystallized PEO, which can combine with ionic dopants such as Li^+ and Na^+ in further experiment, and can provide effective charging/discharging response in the sample.

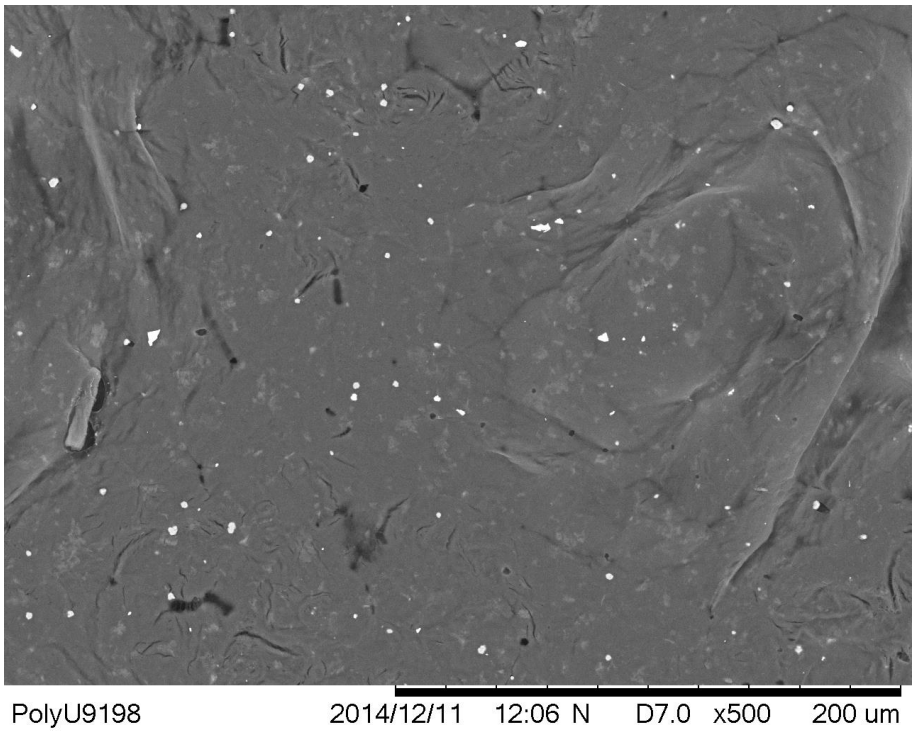

Figure 4.5 SEM photo of the PEO casted polyester fabric (with 500x).

Generally speaking, ion transport in solid polymers is related to the hopping of ions between various adjacent sites. Ions in the polymer electrolyte move in a dynamic environment created by the polymer chain motion in the amorphous phase above the glass transition temperature. A crankshaft-like motion related to short

segments of the polymer chains will randomly generate suitable coordination sites adjacent to ions, and therefore, those ions can free hop. This kind of segmental modes, consist of the motion of groups of atoms on the polymer chains are usually slow, which limits the hopping rate and therefore, it affects the material conductivity. With the increase of crystallinity, this mechanism will become less effective **[110, 111, 112]**.

However, in some linear polymers like PEO, the presence of crystallized sites exhibits an enhancement in the presence of ionic dopants, which can largely increase the effectiveness of ion transport in the polymer matrix. These two mechanisms are simultaneously presented in the PEO matrix and competing. As a result, the conductivity of PEO matrix will no longer dominate by the amorphous phase of the material **[113, 114]**.

4.2 Surface profile of PEO casted polyester fabric

As PEO is a soft and elastic polymer, traditional mechanical contacting method may not be the best way to measure its thickness, especially in micron scale. Therefore, the non-contacting laser triangulation method is introduced in this study to measure various type of PEO-based electrolytic layer and spacer. The thickness on these electrolytic layers and spacers are tabulated in Table 4.2.

Table 4.2 The summary of thickness on various type of electrolytic layers and spacers.

Type of electrolytic layers or spacers	Average Thickness (μm)
Copper plated polyester fabrics	65
Pure PEO spacer	25
PEO:Li spacer	25
Pure PEO and PEO with various amounts of Li casted on polyester fabrics	20
PEO with various types of nanocarbons casted on polyester fabrics	50

4.3 Capacitance of PEO-based supercapacitors with different amount of $LiClO_4$

Besides the surface morphology, the electrical properties of the PEO-casted samples are being investigated. The PEO-casted samples are connected to the impedance analyzer to determine their electrical properties in the frequency range between 40 Hz and 110 MHz, including series capacitance (C_s), dissipation factor (D), series resistance (R), series reactance (X), absolute impedance ($|Z|$) and the phase difference between the resistance and reactance (θ).

The specific capacitances of various PEO-based supercapacitors are estimated from the series capacitance measured by the impedance analyzer, and their values at 40 Hz, 1 KHz, 100 KHz and 100 MHz are summarized in Table 4.3 and the change of specific capacitance is shown in Figure 4.6. In low frequency range, the specific capacitance of PEO-based supercapacitors increased with the increase of the amount of Li^+ ions. At 40 Hz, the sample without Li^+ ion gave 1.89 nF/cm^2, and drastically increased for 263% to 6.86 nF/cm^2 with 1.0 ml of $LiClO_4$ was added into the PEO solution, and finally reached to 33.56 nF/cm^2 when the amount of $LiClO_4$ raised to 10.0 ml. At another testing frequency 1 kHz, the specific capacitance increased from 0.05 to 0.12 and reached to 2.00 nF/cm^2 when the amount of $LiClO_4$ has been raised from null to 1.0 ml and 10.0 ml, respectively. However, when the testing frequency has been increased to 100 kHz or even higher, the change of specific capacitance in various samples with different amount of $LiClO_4$ became less significant and remained in the level of 0.05 nF/cm^2 in average.

Table 4.3 Summary of specific capacitance at various frequencies for PEO-based supercapacitors with different amount of $LiClO_4$ added.

Sample	@ 40 Hz	@ 1 kHz	@ 100 kHz	@ 100 MHz
PEO with no Li^+	1.89 (0%)	0.05	0.02	0.03
PEO + 1.0 ml Li^+	6.86 (+363.0%)	0.12	0.03	0.05
PEO + 1.5 ml Li^+	17.32 (+916.4%)	0.44	0.02	0.03
PEO + 2.0 ml Li^+	27.92 (+1477.2%)	0.64	0.03	0.06
PEO + 2.5 ml Li^+	24.23 (+1282.0%)	0.77	0.02	0.02
PEO + 3.0 ml Li^+	29.67 (+1569.8%)	1.02	0.04	0.05
PEO + 10.0 ml Li^+	33.56 (+1775.7%)	2.00	0.04	0.02

*all units are in nF/cm^2

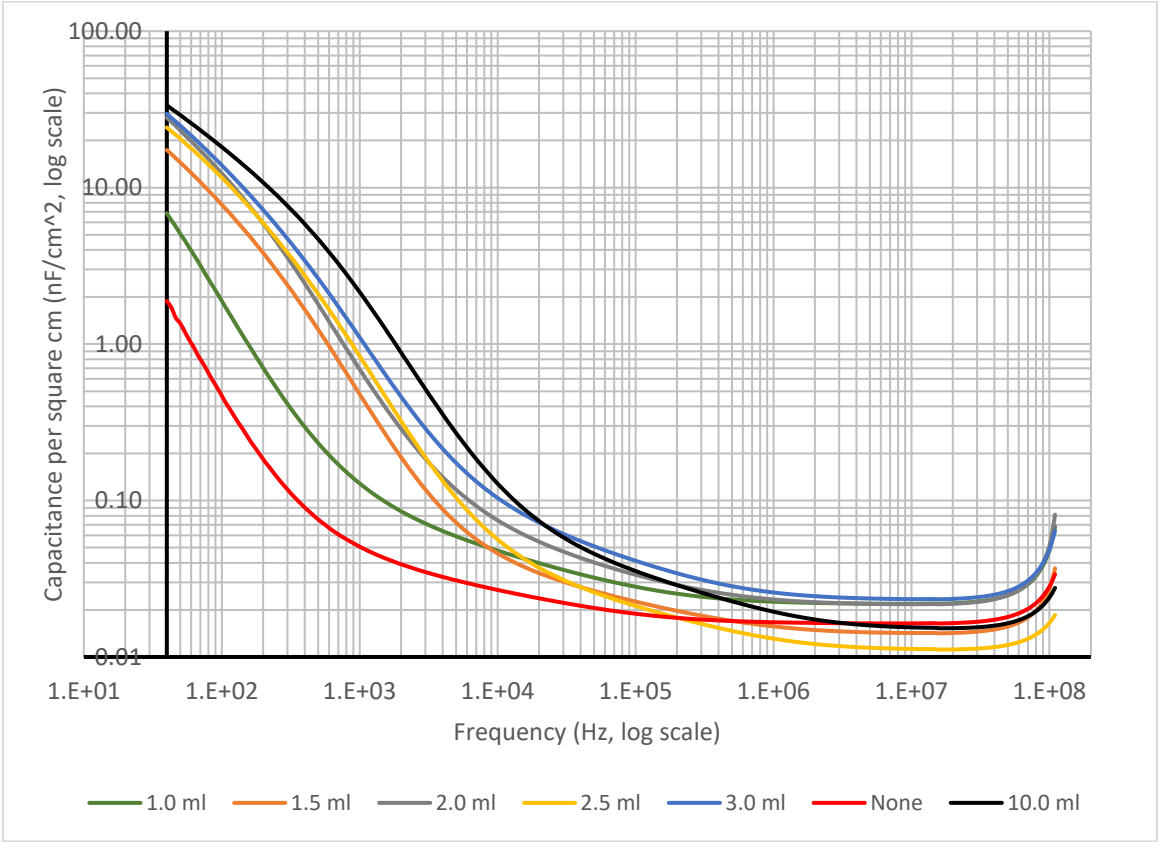

Figure 4.6 The specific capacitances of PEO-based supercapacitors at various frequencies with different amount of $LiClO_4$ added.

As oligoethers are good candidates for alkali salts to dissolve due to their moieties as constitutive units, which can be found in their main chain or side chains. The degree of dissociation of Li^+ salt dissolved in the PEO matrix is dependent on the total concentration of Li^+ in the matrix. In general, the degree of dissociation will decrease with the increase in salt concentration. In some recent reports, the researchers suggested an optimal salt concentration is around $Li^+ / O \approx 0.04$ (the molar ratio of Li^+ salt over oxygen (of ethylene oxide units)). For linear oligo(ethylene oxide)s like PEO, it will form complexes with the Li^+ ions. Besides, from other studies on molecular dynamics simulations, Li^+ ions in the PEO matrix will form complexes with approximately five ether oxygen of a PEO chain, and this complexation may cause the decrease of cations mobility. As a result, the motions of these Li^+ containing complexing segments of PEO chains will highly affect the mobility of Li^+ ions. The motion of Li^+ ions between those complexation sites is supported by the segmental motion of PEO matrix shown in Figure 4.7 **[67]**.

In the experiment, the presence of Li^+ ions in PEO matrix gave a significant increase of charge storage capability at low frequency range. Since the increase of Li^+ ions in concentration (from 0.001 to 0.01) can provide more cations and anions in the matrix to contribute to the ion conductivity, which can enhance the charge storage capability of the electrochemical system, thus the capacitance of the capacitor can be increased.

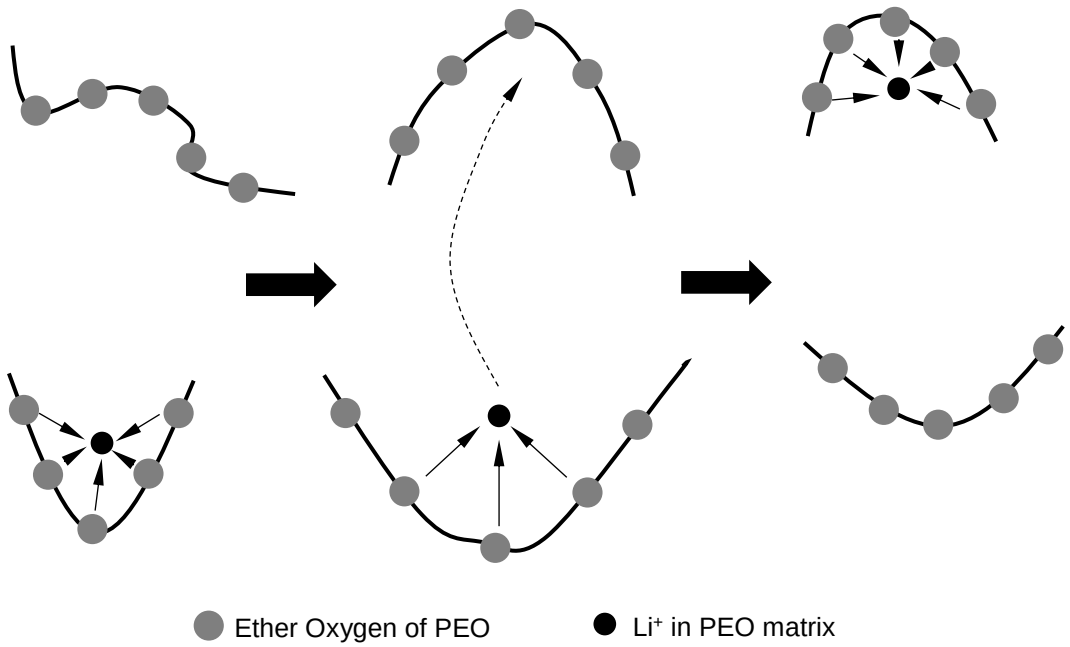

Figure 4.7 Schematic diagram shown the segmental motion assisted diffusion of Li^+ ions in the PEO matrix.

However, when the applied frequency increases to intermediate range (i.e. 1 kHz to 100 kHz), the capacitive reactance of electrolytic material increases which decreases the charge mobility in the materials. Consequently, the total capacitance of the capacitor decreased. Until the frequency has been increased to 100 MHz, the reactive elements become open-circuit, and resistive elements in the electrochemical system dominate the total impedance again, and the capacitance of the PEO-based capacitor increases.

For Dissipation factor (D) of the capacitor, it can be expressed into:

$$D = \frac{ESR}{|X_c|} \quad (4.1)$$

where *ESR* and X_c are the equivalent resistance and the capacitive reactance of the electrochemical system, respectively. ESR represents the loss in capacitor, which is a derived quantity with physical origins in both the dielectric's conduction electrons and dipole relaxation phenomena. The relation can be expressed as:

$$ESR = \frac{\sigma}{\varepsilon\omega^2 C} \quad (4.2)$$

where σ, ε, ω and C are the dielectric material's conductivity, the lossless permittivity of the dielectric, the angular frequency of the signal applied to the dielectric material and the lossless capacitance of the dielectric material, respectively. Since X_c is equal to

$$X_c = \frac{1}{2\pi f C} = \frac{1}{\omega C} \quad (4.3)$$

where *f* is the frequency applied to the sample. By substituting Equation (4.2) and (4.3) into Equation (4.1), dissipation factor can be rewritten as:

$$D = \frac{\sigma}{\varepsilon\omega} \quad (4.4)$$

From Equation (4.4), the dissipation factor is a frequency dependent value.

The dissipation factor of various PEO-based supercapacitors measured at 40 Hz, 1 KHz, 100 KHz and 100 MHz are summarized in Table 4.4 and the change of specific capacitance is shown in Figure 4.8. For all capacitors with different amount of PEO:Li, the values of *D* decrease from 3.87 – 6.69 at 40 Hz to 0.03 – 0.22 when the frequency reaches 100 MHz.

Table 4.4 Summary of dissipation factor at various frequencies for PEO-based supercapacitors with different amount of $LiClO_4$ added.

Sample	@ 40 Hz	@ 1 kHz	@ 100 kHz	@ 100 MHz
PEO with no Li^+	3.87 (0%)	0.52	0.15	0.03
PEO + 1.0 ml Li^+	5.86 (+151.4%)	0.89	0.24	0.22
PEO + 1.5 ml Li^+	6.54 (+169.0%)	2.19	0.27	0.11
PEO + 2.0 ml Li^+	6.69 (+172.9%)	1.73	0.31	0.18
PEO + 2.5 ml Li^+	5.40 (+139.5%)	2.34	0.28	0.10
PEO + 3.0 ml Li^+	6.49 (+167.7%)	2.04	0.37	0.09
PEO + 10.0 ml Li^+	6.05 (+156.3%)	3.00	0.39	0.14

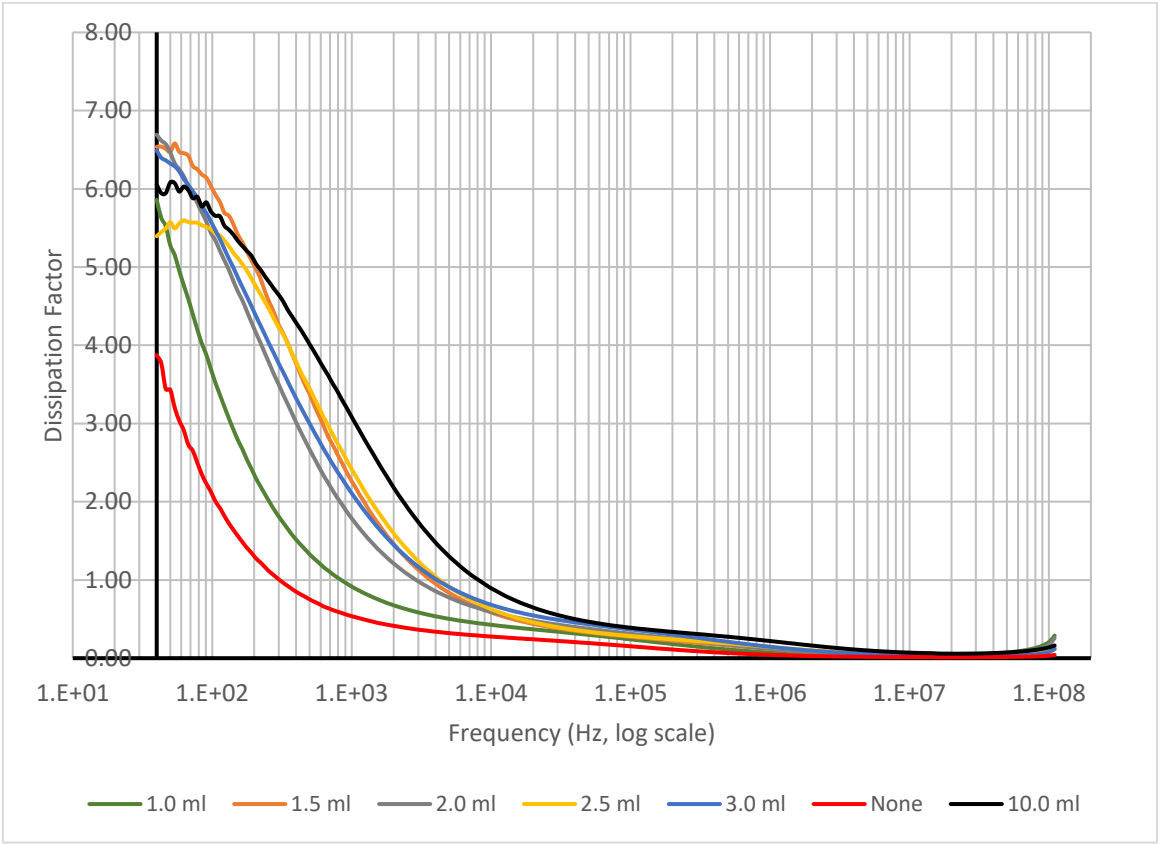

Figure 4.8 The dissipation factor (D) of PEO-based supercapacitors at various frequencies with different amount of $LiClO_4$ added.

In the measurement of electrical properties of capacitor, the value of series resistance and reactance, measured from various PEO:Li samples at 40 Hz, 1 kHz, 100 kHz and 100 MHz are tabulated in Tables 4.5 to 4.6. Besides, their frequency responds in the range of 40 Hz to 100 MHz are shown in Figures 4.9 to 4.10.

In the experiment, the total impedance measured from the sample consisted of two components: the resistive element and reactive element, which are the real part and imaginary part of the impedance, respectively. When the frequency increases, the resistance (*R*) of PEO sample without Li^+ ions drops from 46 MΩ at 40 Hz to few Ω at 100 MHz. For those samples doped with Li^+ ions, the resistance decreases from the range of kΩ at 40 Hz to less than 20 Ω at 100 MHz. On the side of reactance (*X*), the PEO sample without Li^+ ions drops from -31 MΩ at 40 Hz to about 110 Ω at 100 MHz. For those samples doped with Li^+ ions, the reactance increases from 40 Hz and reaches the maximum at about 1 kHz. Then it drops to less than 200 Ω at 100 MHz. The negative value of *X* indicates it is mainly influenced by the capacitive element (i.e. capacitive reactance).

Table 4.5 Summary of resistance (R) at various frequencies for PEO-based supercapacitors with different amount of $LiClO_4$ added.

Sample	@ 40 Hz	@ 1 kHz	@ 100 kHz	@ 100 MHz
PEO with no Li^+	46373.67 (0%)	2712.78	23.18	0.00
PEO + 1.0 ml Li^+	10099.36 (-78.2%)	2054.68	25.06	0.01
PEO + 1.5 ml Li^+	10156.82 (-78.1%)	5105.76	39.65	0.02
PEO + 2.0 ml Li^+	7110.52 (-84.7%)	1620.95	27.25	0.01
PEO + 2.5 ml Li^+	2346.95 (-94.9%)	1442.97	28.81	0.01
PEO + 3.0 ml Li^+	3387.20 (-92.7%)	1377.66	26.02	0.00
PEO + 10.0 ml Li^+	7070.60 (-84.8%)	3303.59	34.84	0.02

*all units are in kΩ

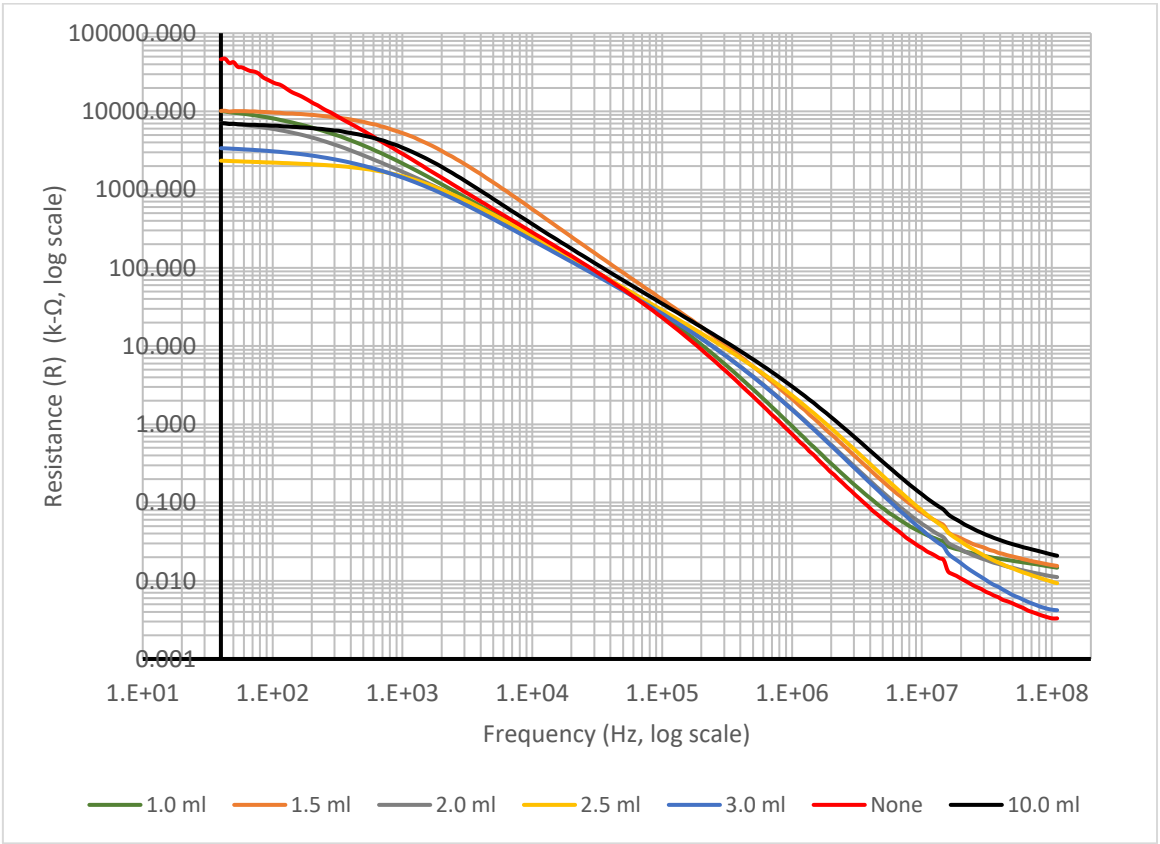

Figure 4.9 The resistance (R) of PEO-based supercapacitors at various frequencies with different amount of $LiClO_4$ added.

Table 4.6 Summary of reactance (X) at various frequencies for PEO-based supercapacitors with different amount of $LiClO_4$ added. (The negative values represent the capacitive properties of the reactance)

Sample	@ 40 Hz	@ 1 kHz	@ 100 kHz	@ 100 MHz
PEO with no Li^+	-31325.38 (0%)	-6471.99	-152.31	-0.11
PEO + 1.0 ml Li^+	-2581.87 (-91.8%)	-2608.91	-105.89	-0.07
PEO + 1.5 ml Li^+	-1849.45 (-94.1%)	-3888.73	-210.13	-0.20
PEO + 2.0 ml Li^+	-1569.23 (-95.0%)	-1842.49	-93.09	-0.07
PEO + 2.5 ml Li^+	-316.90 (-99.0%)	-812.02	-83.64	-0.10
PEO + 3.0 ml Li^+	-522.57 (-98.2%)	-1084.45	-78.46	-0.06
PEO + 10.0 ml Li^+	-850.10 (-97.3%)	-2692.39	-138.93	-0.15

*all units are in kΩ

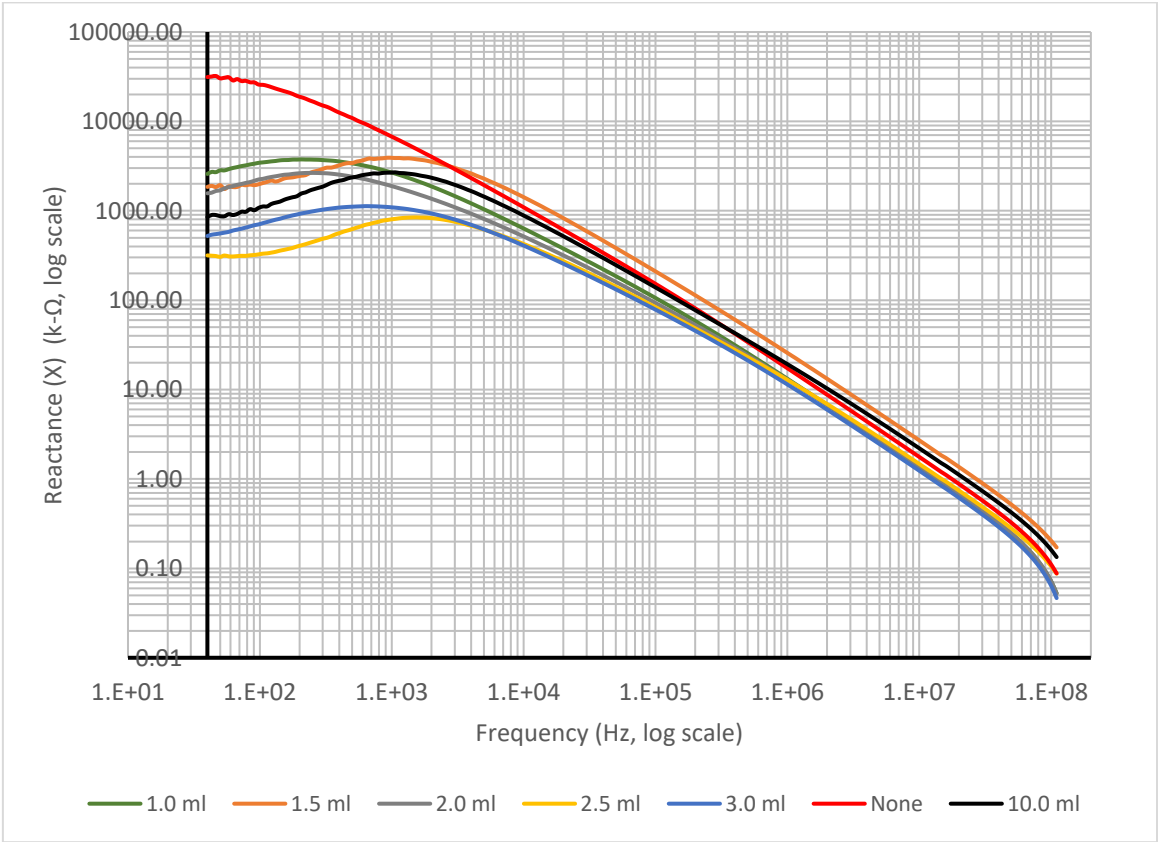

Figure 4.10 The reactance (X) of PEO-based supercapacitors at various frequencies with different amount of $LiClO_4$ added.

With the relation of Equations (2.5) and (2.6) in Chapter 2, we know the relationship between *R* and *X* of the electrochemical system, to the absolute impedance *(|Z|)* and the phase angle (*θ*) between the resistive and reactive elements obtained from the measurement. The absolute impedance and the corresponding phase angle measured from various PEO:Li samples at 40 Hz, 1 kHz, 100 kHz and 100 MHz are tabulated in Tables 4.7 and 4.8. Besides, their frequency responds in the frequency range of 40 Hz to 100 MHz are shown in Figures 4.11 and 4.12.

At low frequency range (e.g. 40 Hz), the magnitude of |*Z*| and *R* are in the same order, where the magnitude of *X* is different from that of |*Z*|. Besides, the values of *θ* in various PEO:Li samples are varying between -6.15° to -23.11°, where the negative value shows the reactance is capacitive. This represents the electrochemical system is mainly dominated by the resistive elements instead of reactive elements.

When the frequency increases to 1 kHz, the effect from reactive element becomes significant. The value of |*Z*| is attributed to both *R* and *X*, and the value of phase angle has been raised. After the frequency has been increased to 100 MHz, the magnitude of |*Z*| is mainly dominated by *X*, and the phase angle has been increased to more than -45°, which represents the dominance of capacitive reactance.

Table 4.7 Summary of absolute impedance (|Z|) at various frequencies for PEO-based supercapacitors with different amount of $LiClO_4$ added.

Sample	@ 40 Hz	@ 1 kHz	@ 100 kHz	@ 100 MHz
PEO with no Li^+	56727.70 (0%)	7149.97	154.26	0.11
PEO + 1.0 ml Li^+	10384.77 (-81.7%)	3341.51	108.60	0.07
PEO + 1.5 ml Li^+	10328.40 (-81.8%)	6454.05	215.02	0.20
PEO + 2.0 ml Li^+	7318.01 (-87.1%)	2543.76	97.63	0.07
PEO + 2.5 ml Li^+	2368.53 (-95.8%)	1669.78	88.93	0.10
PEO + 3.0 ml Li^+	3428.50 (-94.0%)	1783.19	82.95	0.06
PEO + 10.0 ml Li^+	7124.34 (-87.4%)	4294.57	144.79	0.16

*all units are in kΩ

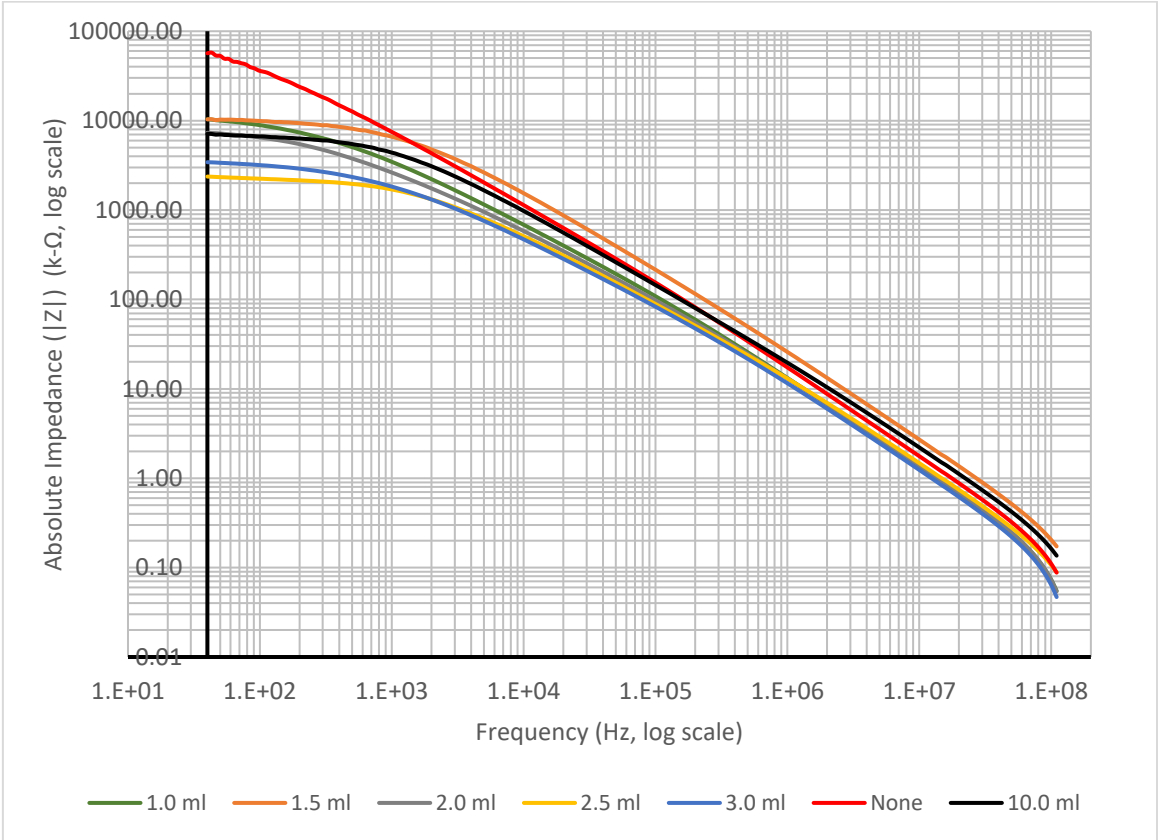

Figure 4.11 The absolute impedance (|Z|) of PEO-based supercapacitors at various frequencies with different amount of $LiClO_4$ added.

Table 4.8 Summary of phase angle (θ) between the resistance and capacitive reactance at various frequencies for PEO-based supercapacitors with different amount of $LiClO_4$ added.

Sample	@ 40 Hz	@ 1 kHz	@ 100 kHz	@ 100 MHz
PEO with no Li^+	-23.11	-63.55	-81.34	-88.06
PEO + 1.0 ml Li^+	-11.40	-50.26	-76.78	-77.80
PEO + 1.5 ml Li^+	-9.15	-29.15	-74.81	-83.89
PEO + 2.0 ml Li^+	-10.07	-39.51	-72.84	-79.77
PEO + 2.5 ml Li^+	-6.15	-16.49	-52.12	-62.10
PEO + 3.0 ml Li^+	-9.31	-31.57	-70.06	-85.13
PEO + 10.0 ml Li^+	-10.54	-24.92	-69.39	-81.99

*all units are in degree

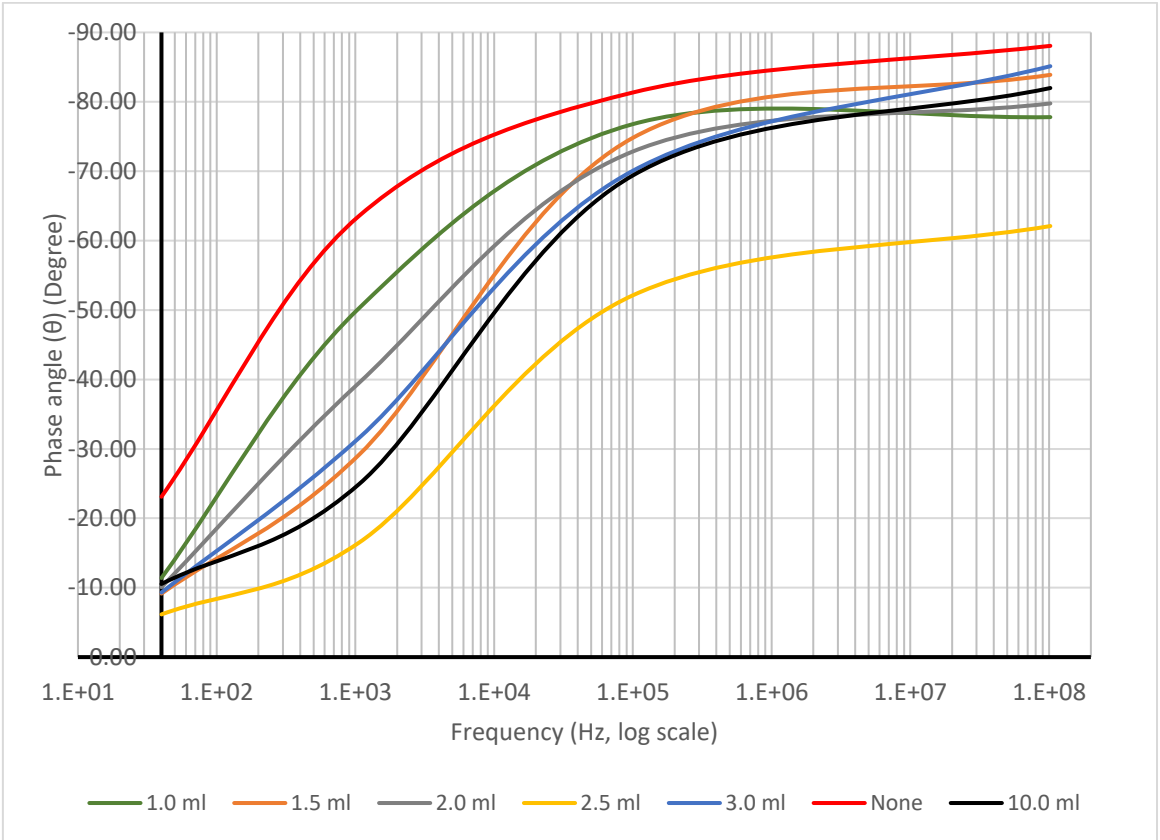

Figure 4.12 The phase angle (θ) between the resistance and capacitive reactance of PEO-based supercapacitors at various frequencies with different amount of $LiClO_4$ added.

It can be observed that the values of *R*, *X*, and |*Z*| in various PEO:Li samples are dramatically decreased to less than 25% of the pure PEO sample at low frequency range. This phenomenon shows the presence of Li^+ ions in PEO matrix that could provide an enhancement of charge mobility in the electrolyte, and manifests the improvement of charge storage capability. Besides, the presence of Li^+ ions would introduce a certain effect on reactance at the frequency around 1 kHz.

4.4 Voltage-current responses of PEO-based supercapacitors with different amount of $LiClO_4$

In an ideal double layer capacitor, its charge/discharge behavior can be expressed in the rectangular form of voltammetry characteristics as shown in Figure 4.13. The direction of current is reversed instantly with the reversal of the potential sweep. The charge storage mechanism occurs in the system is mainly electrostatic and the current is usually independent on the potential. If the electrodes contain materials with pseudocapacitance properties, the shape of voltammetry curve will be altered and in some cases, the redox peaks related to pseudofaradaic reactions will be observed. In this case, the charge accumulated in the capacitor is highly dependent on the electrode potential. Since a kinetically slow process is comprised in the charging of pseudocapacitance, a delay of potential change during the reverse of potential is observed **[115]**.

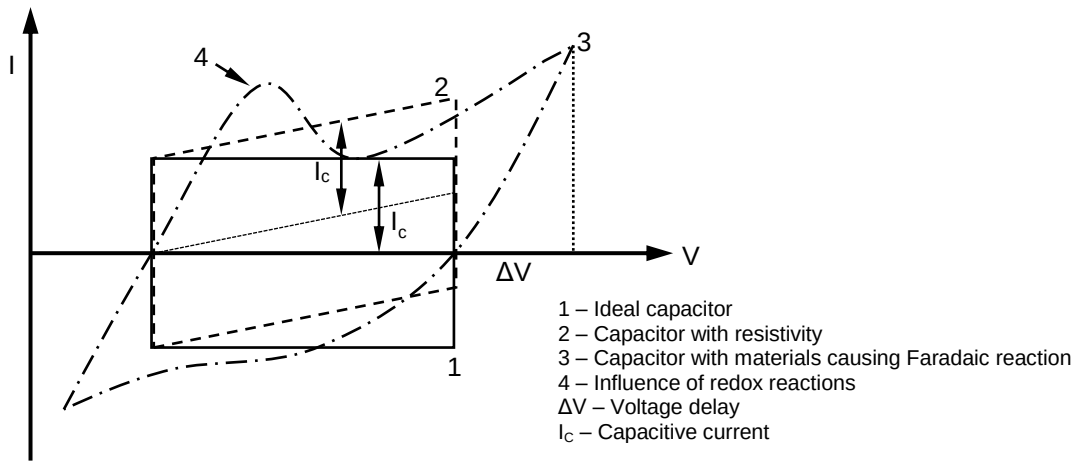

Figure 4.13 Typical cyclic voltammetry of an electrochemical capacitor

In this study, the maximum current density of various scan rates are tabulated in Table 4.9.

Table 4.9 Summary of maximum current density measured from PEO-based supercapacitors with different amount of $LiClO_4$ added, by cyclic voltammetry between -0.5 V and +0.5 V under different scan rates.

Sample	100 mV/s	50 mV /s	20 mV/s	10 mV/s
PEO with no Li^+	177 (0%)	172	87	71
PEO + 1.0 ml Li^+	243 (+137.3%)	191	136	102
PEO + 1.5 ml Li^+	351 (+198.3%)	279	205	189
PEO + 2.0 ml Li^+	562 (+317.5)	475	347	186
PEO + 2.5 ml Li^+	883 (+498.9%)	538	385	377
PEO + 3.0 ml Li^+	924 (+522.0%)	695	510	313
PEO + 10.0 ml Li^+	1844 (+1041.8%)	1304	876	330

*all units are in nA/cm^2

Generally, voltammograms of pure PEO and all PEO:Li samples exhibit in an olive shape, with maximum values of current density observed at ±0.5V with the corresponding positive and negative sign. In each sample, the fastest scan rate (100 mV/s) would provide the highest value of current density and the maximum current density will decrease with the increase of scan rate.

For the cyclic voltammogram in each sample, the cyclic voltage-current density responses for different scan rates present in quite similar shape, where the current density increases with the increasing of scan rate. It can be explained in the size of diffusion layer and the time taken to record the scan.

As the testing voltage is sweeping from low to high potential, the current rises correspondingly from its initial value as the equilibrium position is shifted further to the positive side, therefore more reactant in the electrolyte will be converted, and the diffusion layer has grown sufficiently above the electrode (i.e. copper-plated polyester fabrics).

Practically, a slower scan rate needs a longer time for voltage sweeping, thus the size of diffusion layer above the electrode surface will be different depending upon the scan rate applied. The establishment of diffusion layer is highly related to the efficiency of charges in the PEO matrix migrating from one active site to another. In the case of slower scan rate, the period for voltage applied to the electrochemical system is longer, the diffusion layer will grow much further from the electrode to the electrolyte compared to the faster scan rate, causing an inefficient charge transfer in the electrolyte. Moreover, the flux passing through the electrode surface is relatively smaller at slower scan rate than that of faster one. Since the current density is proportional to the flux towards the electrode, lower flux value will cause the magnitude of current density becomes smaller at slow scan rates. This rapid process is usually referred as a reversible electron transfer reaction. The voltage-current responses of PEO:Li samples with different amount of Li^+ and scan rates are presented in the form of cyclic voltammetry in Figures 4.14 to 4.20.

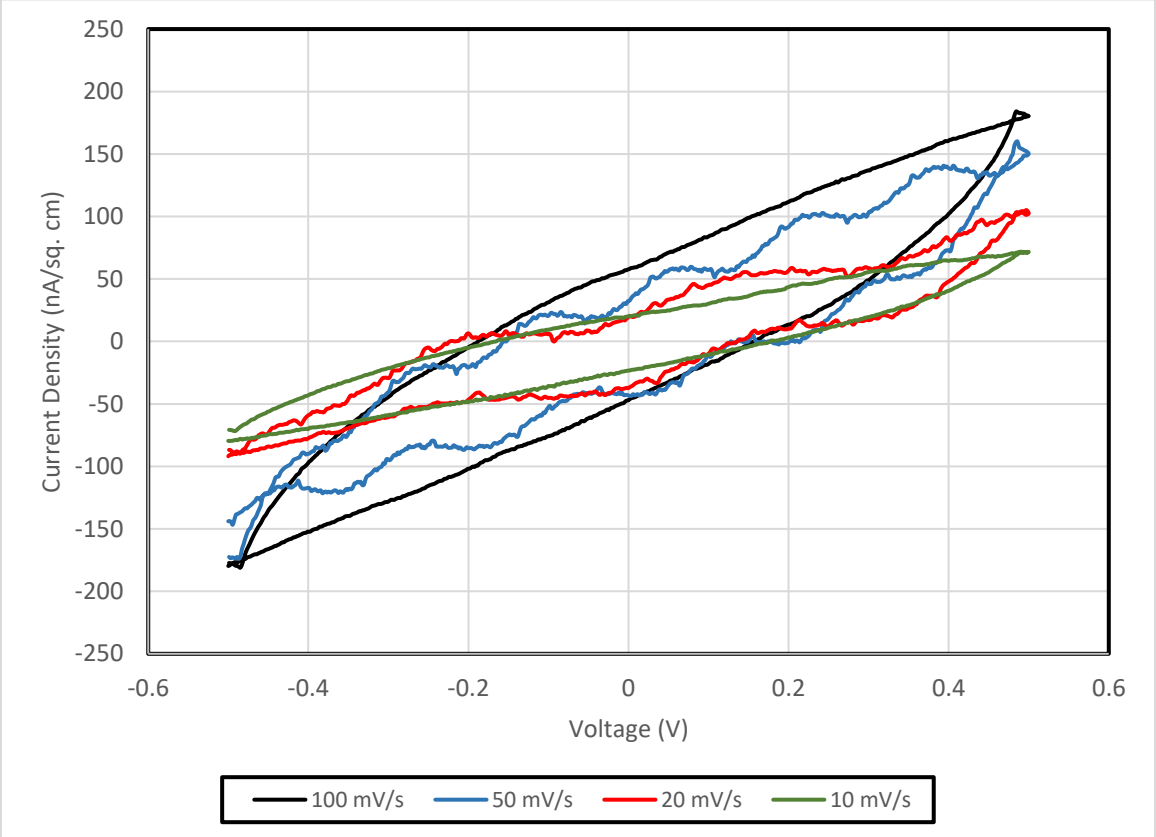

Figure 4.14 Cyclic voltammogram of PEO active layer without Li^+ ion at different scanning rates.

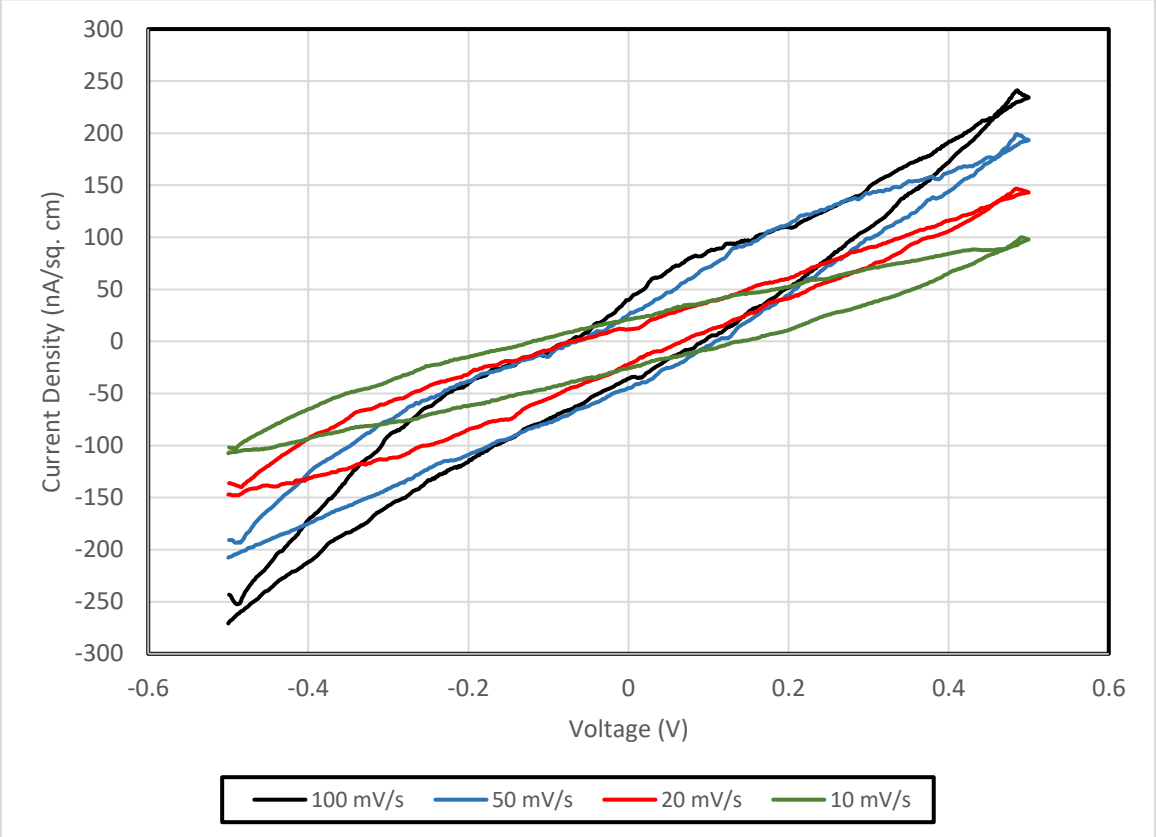

Figure 4.15 Cyclic voltammogram of PEO active layer added with 1.0 ml $LiClO_4$ at different scan rates.

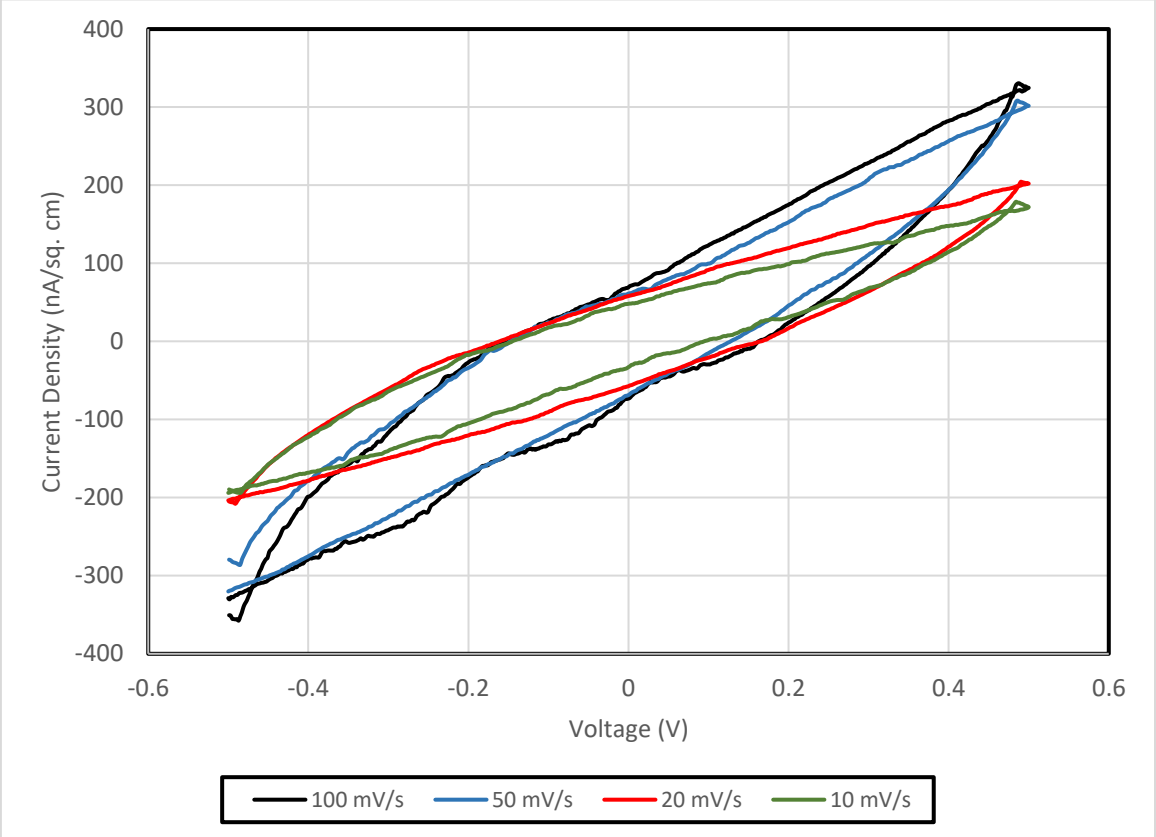

Figure 4.16 Cyclic voltammogram of PEO active layer added with 1.5 ml $LiClO_4$ at different scan rates.

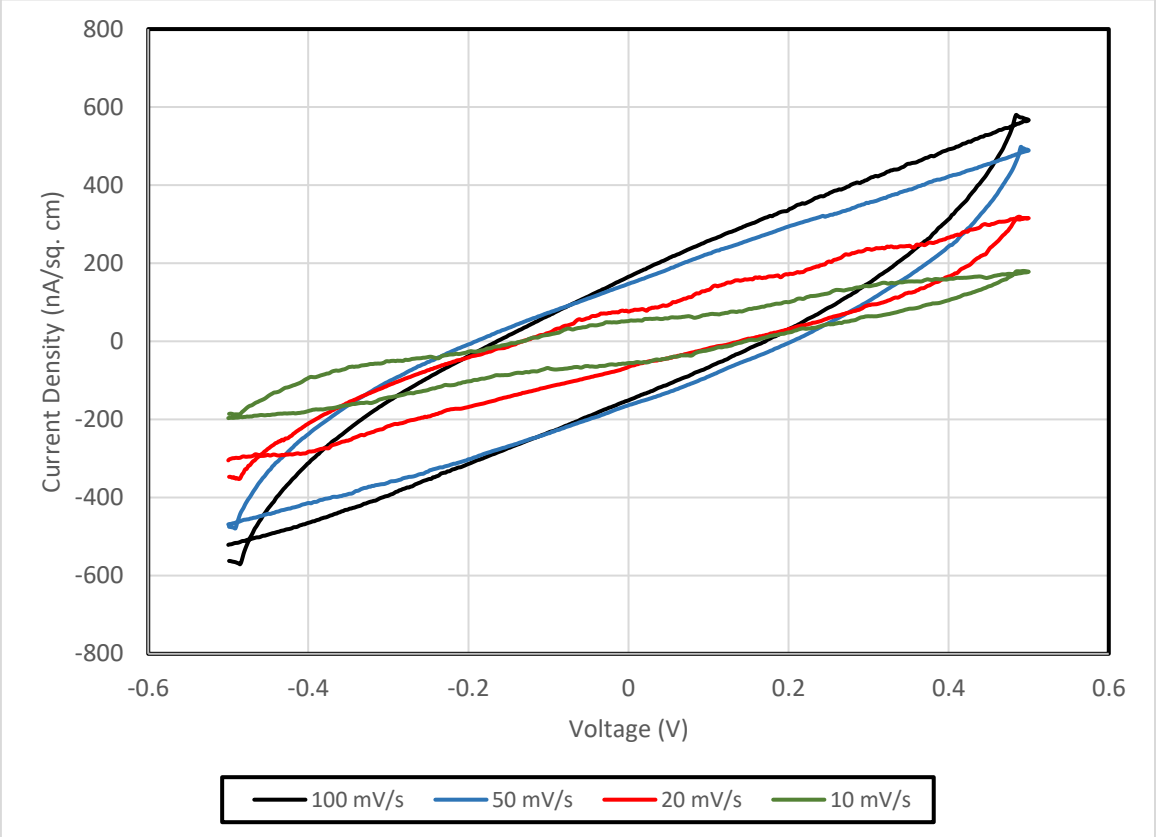

Figure 4.17 Cyclic voltammogram of PEO active layer added with 2.0 ml $LiClO_4$ at different scan rates.

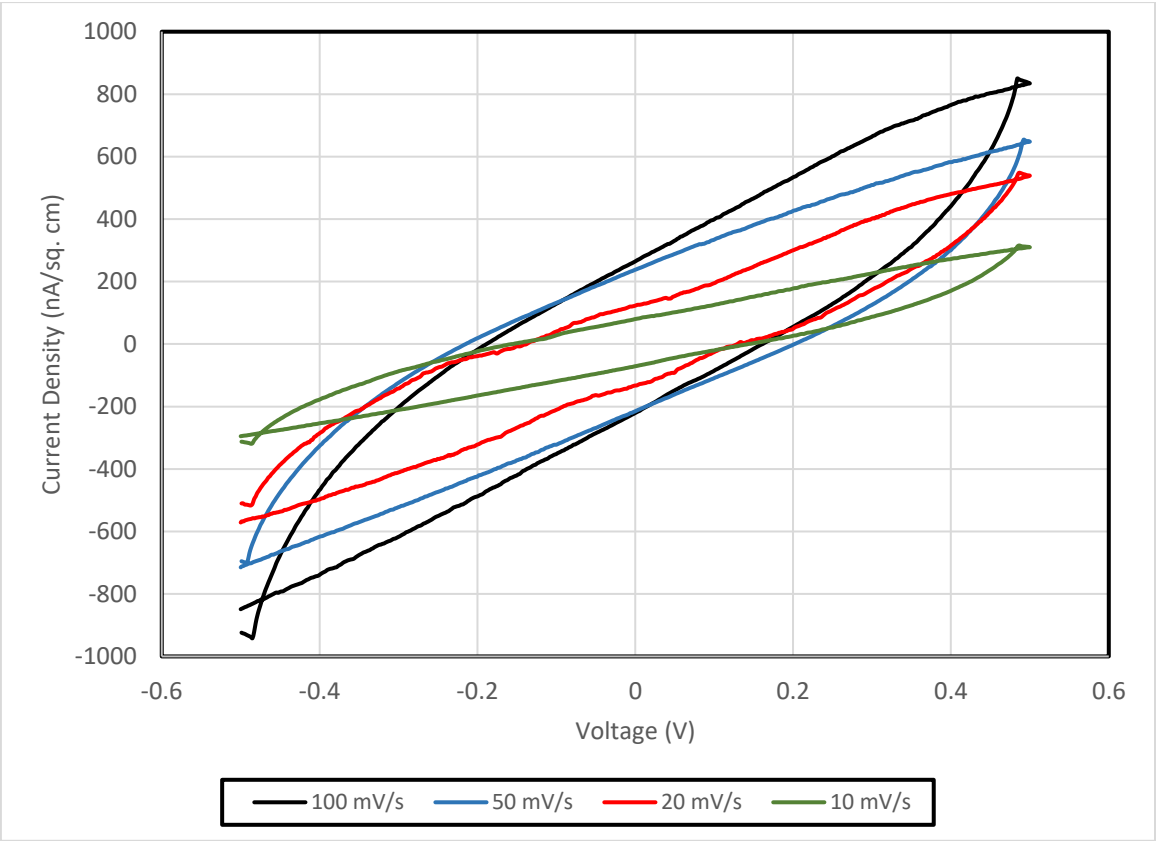

Figure 4.18 Cyclic voltammogram of PEO active layer added with 2.5 ml $LiClO_4$ at different scan rates.

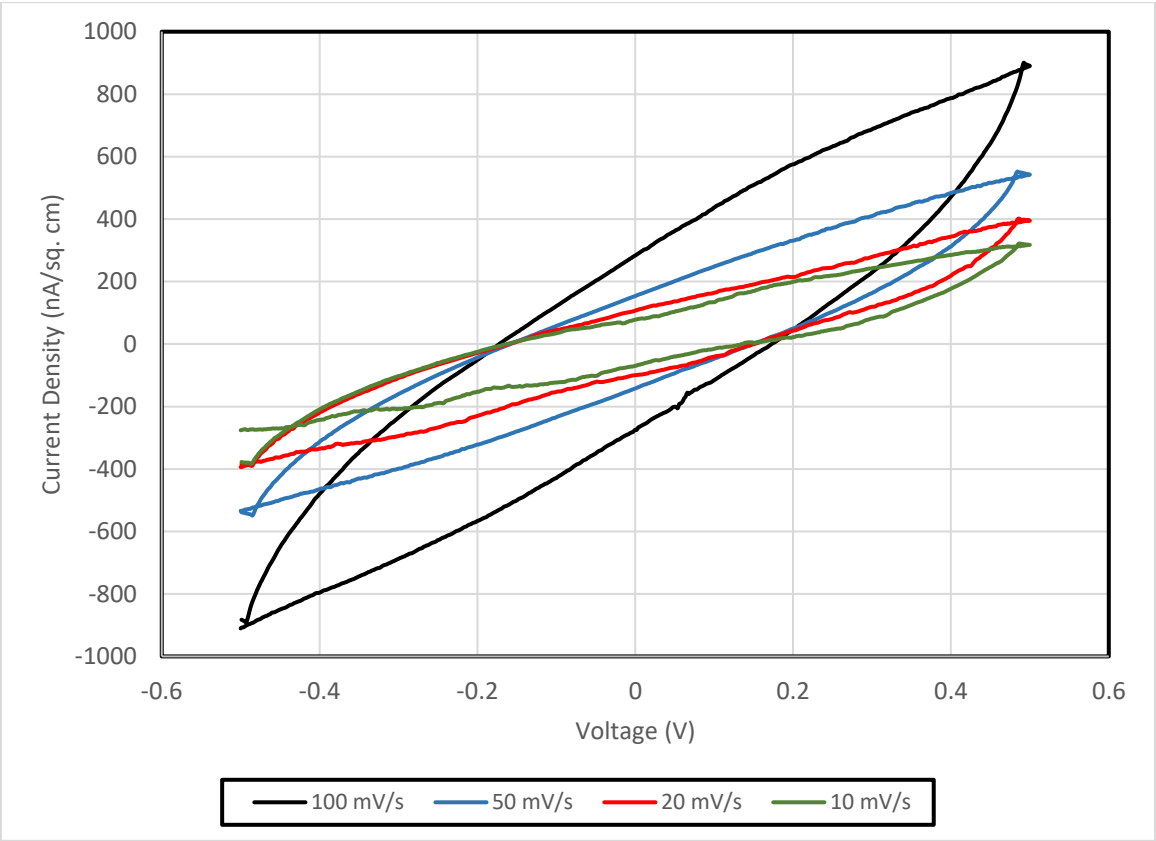

Figure 4.19 Cyclic voltammogram of PEO active layer added with 3.0 ml $LiClO_4$ at different scan rates.

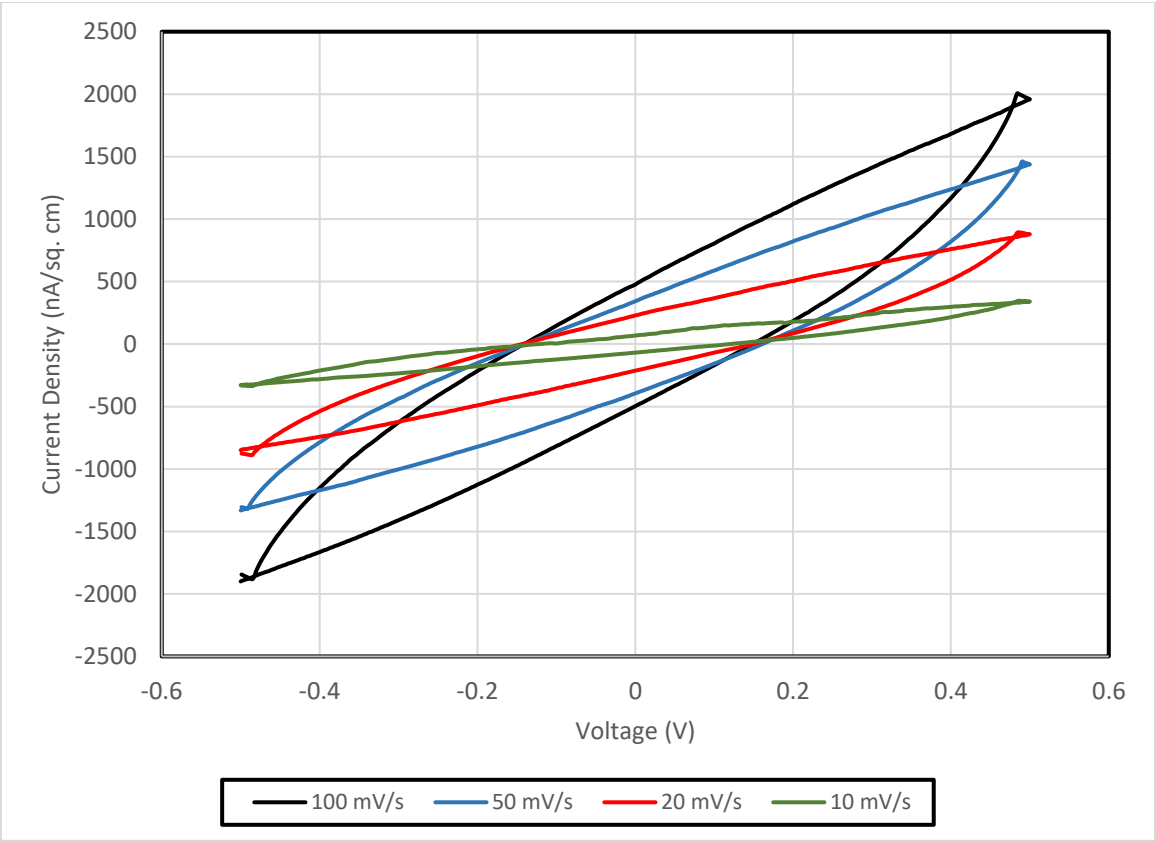

Figure 4.20 Cyclic voltammogram of PEO active layer added with 10.0 ml $LiClO_4$ at different scan rates.

In the experiment, the maximum current density of pure PEO sample at the scan rate of 100 mV/s within ±0.5V is about 177 nA/cm^2. When Li^+ ions are doped into the PEO matrix, the ions increase the charge mobility in the PEO matrix. The maximum current density at the scan rate of 100 mV/s is drastically increased from 243 nA/cm^2 to 1844 nA/cm^2, with Li^+ ions concentration increases from 0.001 to 0.01. The increase of Li^+ ions enhances the current density and hence the charge storage capability by providing sufficient ions to move between different active sites on the branches and backbones of the PEO matrix. The summary of cyclic voltammetry of PEO:Li samples at the scan rate of 100 mV/s is shown in Figure 4.21.

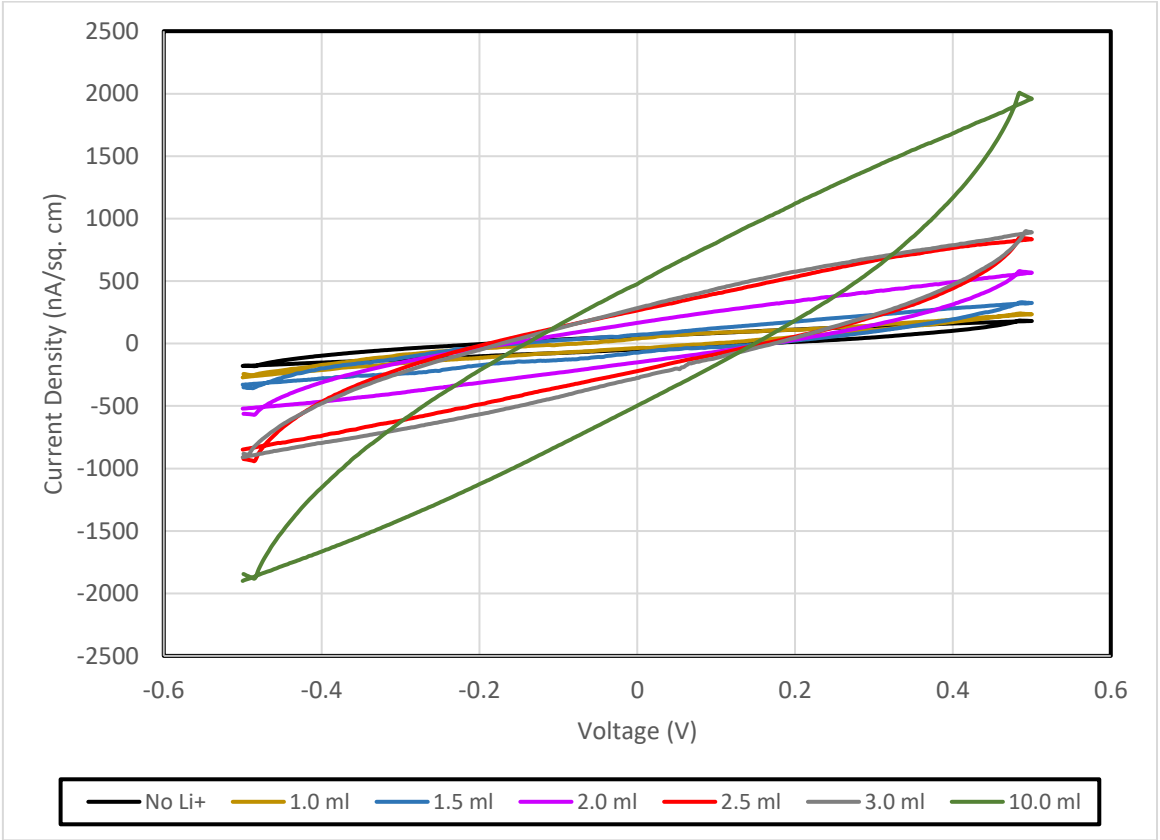

Figure 4.21 Cyclic voltammogram of PEO active layer added with different amount of $LiClO_4$ at a scan rate of 100 mV/s

4.5 Capacitance of PEO-based supercapacitors with different types of nanocarbons

In this study, the electrical properties of the PEO-casted samples doped with different type of nanocarbons in similar density including single-walled carbon nanotube (SW-CNT), double-walled carbon nanotube (DW-CNT), multi-walled carbon nanotube (MW-CNT) and Mesoporous nanocarbons (Mesoporous) are being investigated. The PEO-casted samples are connected to the impedance analyzer to determine their electrical properties in the frequency range between 40 Hz and 110 MHz, including series capacitance (C_s), dissipation factor (D), series resistance (R), series reactance (X), absolute impedance ($|Z|$) and the phase difference between the resistance and reactance (θ).

The specific capacitances of various PEO-nanocarbons supercapacitors are estimated from the series capacitance measured by the impedance analyzer, and their values at 40 Hz, 1 KHz, 100 KHz and 100 MHz are summarized in Table 4.10 and the change of specific capacitance is shown in Figure 4.22.

Table 4.10 Summary of specific capacitance at various frequencies for PEO-based supercapacitors with different types of nanocarbons added.

Sample	@ 40 Hz	@ 1 kHz	@ 100 kHz	@ 100 MHz
PEO with no CNT	1.89 (0%)	0.05	0.02	0.03
PEO + SW-CNT	1.353 (-28.4%)	0.046	0.019	0.030
PEO + DW-CNT	32.798 (+1735.3%)	0.238	0.016	0.020
PEO + MW-CNT	17.806 (+942.1%)	0.206	0.014	0.006
PEO + Mesoporous	8.238 (+435.9%)	0.066	0.009	0.010

*all units are in nF/cm^2

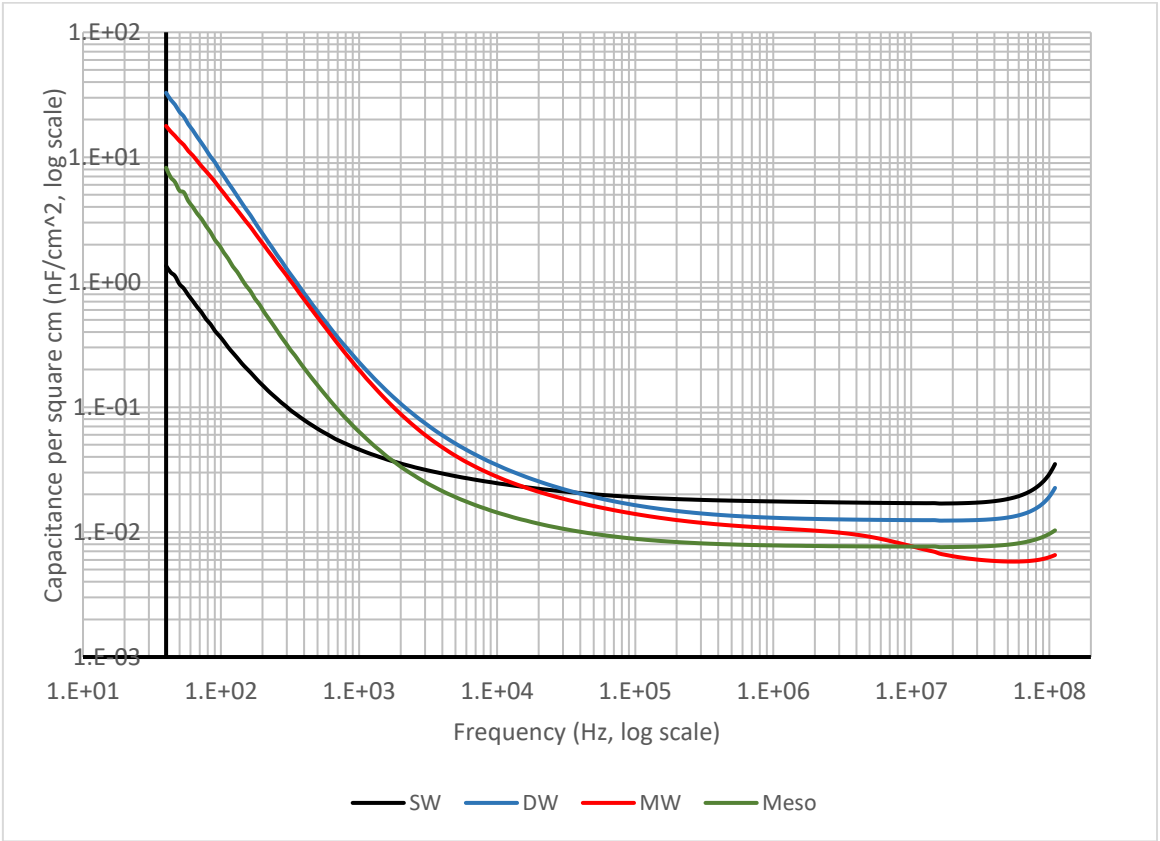

Figure 4.22 The specific capacitances of PEO-based supercapacitors at various frequencies with different types of nanocarbons added.

Generally, all four different types of nanocarbons exhibit the similar trend along the frequency range from 40 Hz to 100 MHz. In low frequency range, the specific capacitance of all PEO:nanocarbons supercapacitors give a higher value than other frequencies.

The best performance among four nanocarbons is DW-CNT, it gives 32.798 nF/cm^2 and then MW-CNT that gives 17.806 nF/cm^2. For Mesoporous and SW-CNT, they give 8.238 nF/cm^2 and 1.353 nF/cm^2 respectively. Once the testing frequency has been raised to intermediate range at 10 kHz, the specific capacitance dramatically decreases and reaches the minimum. It flattens in the range of 0.009 nF/cm^2 to 0.019 nF/cm^2 until the frequency has been increased to higher range at 100 MHz, the specific capacitance increases again to the range of 0.010 nF/cm^2 to 0.030 nF/cm^2.

For Dissipation factor (D), the values for four different types of samples at 40 Hz, 1 KHz, 100 KHz and 100 MHz are listed in Table 4.11, and the change of dissipation factor along the change of frequency is shown in Figure 4.23.

All PEO:nanocarbons supercapacitors give the highest values at 40 Hz with 4.45, 17.75, 11.70 and 14.06 for SW-CNT, DW-CNT, MW-CNT and mesoporous respectively. The dissipation factor then drops in the intermediate range of frequency and reaches the minimum after 1 MHz with value averagely below 0.20. When the frequency continuously increases to 100 MHz, D increases to 1.71, 0.46, 0.46 and 0.21 for samples doped with SW-CNT, DW-CNT, MW-CNT and mesoporous nanocarbons respectively.

When nanocarbons are doped into the PEO matrix, the charge accumulation in the electrochemical system will be largely increased, since they provide a large surface area to capture free charges in the system. In the experiment, DW-CNT gives the highest value of specific capacitance. Structurally, DW-CNT is a simple type of MW-CNT, which consists of two concentric SW-CNTs (inner nanotube and outer nanotube). For each SW-CNT, the electronic configuration of tube wall can be either semiconducting (S) or metallic (M), therefore in DW-CNT, four possible configurations including S@S, S@M, M@S and M@M (inner-nanotube @ outer-nanotube) will occur. All these configurations of DW-CNT can benefit to the electrical conductivity and hence the charge trapping capability in the system. In some experimental studies, DW-CNT with M@M configuration is suggested to behave like a SW-CNT in metallic configuration, which the electrical properties is

comparable to metal, and can provide a better surface for charge trapping in the electrochemical system **[116, 117, 118]**.

Table 4.11 Summary of dissipation factor at various frequencies for PEO-based supercapacitors with different types of nanocarbons added.

Sample	@ 40 Hz	@ 1 kHz	@ 100 kHz	@ 100 MHz
PEO with no CNT	3.87 (0%)	0.52	0.15	0.03
PEO + SW-CNT	4.45 (+115.0%)	0.64	0.10	1.71
PEO + DW-CNT	17.75 (+458.7%)	2.14	0.27	0.46
PEO + MW-CNT	11.70 (+302.3%)	1.87	0.24	0.46
PEO + Mesoporous	14.06 (+363.3%)	1.58	0.17	0.21

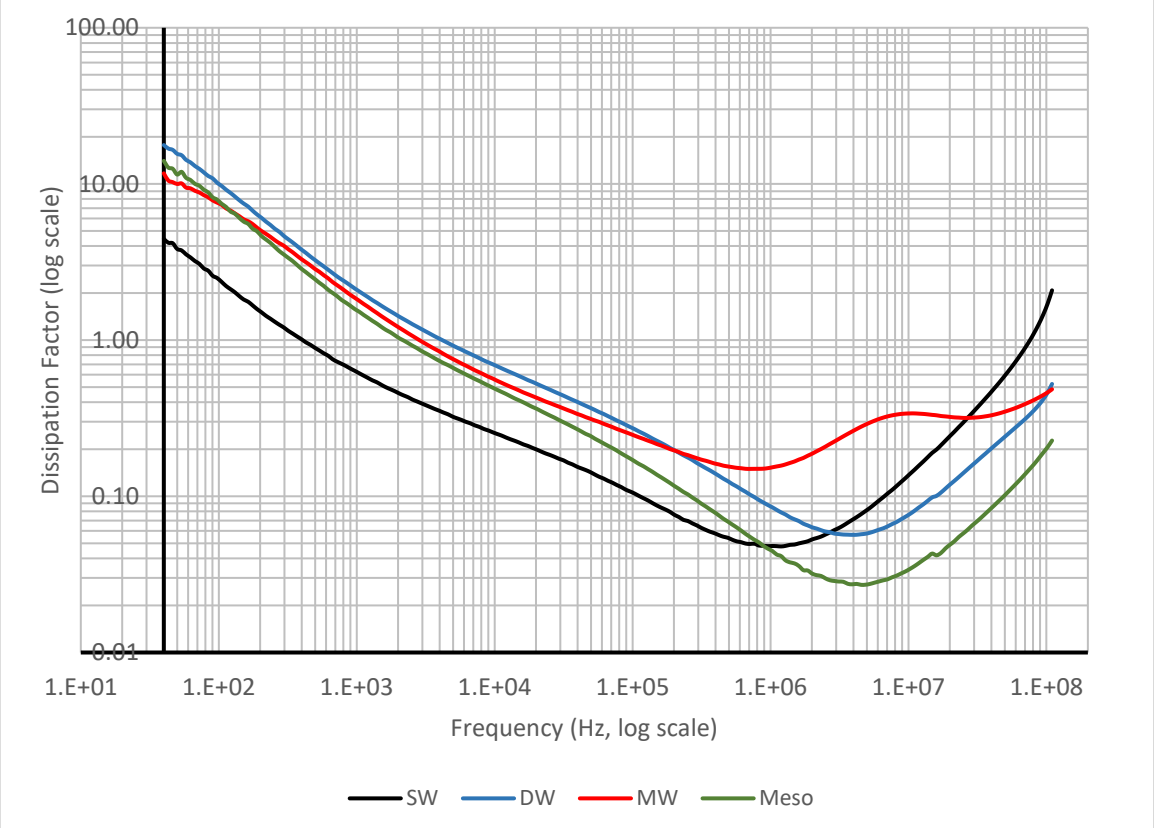

Figure 4.23 The dissipation factor (D) of PEO-based supercapacitors at various frequencies with different types of nanocarbons added.

In the measurement of electrical properties of PEO:nanocarbons supercapacitor, the value of series resistance and reactance measured from various samples at 40 Hz, 1 kHz, 100 kHz and 100 MHz are tabulated in Tables 4.12 and 4.13. Besides, their frequency responds in the frequency range of 40 Hz to 100 MHz are shown in Figures 4.24 and 4.25.

In the experiment, the total impedance measured from the sample consists of two components: the resistive element and reactive element, which are the real part and imaginary part of impedance, respectively. When the frequency increases, the resistance (*R*) of all nanocarbons doped samples decreases from a higher value with the order of MΩ to about tens-to-hundred of Ω when the frequency reaches 100 MHz. For SW-CNT sample, it drops from 23.2 MΩ at 40 Hz to about 160 Ω at 100 MHz. For DW-CNT, the resistance decreases from 4 MΩ at 40 Hz to less than 100 Ω at 100 MHz. For MW-CNT and Mesoporous samples, the decreases are from 22.4 MΩ and 12.1 MΩ at 40 Hz to 230 Ω and 60 Ω at 100 MHz, respectively.

On the side of reactance (*X*), the SW-CNT sample raises from -5.2 MΩ at 40 Hz to -6 MΩ at 1 kHz. Then it sharply drops to about -90 Ω at 100 MHz. For DW-CNT, MW-CNT and mesoporous samples, the reactance increases from -243 kΩ, -2.2 MΩ, and -859 kΩ in low frequency range of 40 Hz to -1.32 MΩ, -7.97 MΩ and -4.45 MΩ at 1 kHz. The reactance drops to -160 Ω, -490 Ω and -280 Ω at 100 MHz for DW-CNT, MW-CNT and mesoporous samples respectively. The negative value of *X* indicates it is mainly influenced by the capacitive element (i.e. capacitive reactance).

Table 4.12 Summary of resistance (R) at various frequencies for PEO-based supercapacitors with different types of nanocarbons added.

Sample	@ 40 Hz	@ 1 kHz	@ 100 kHz	@ 100 MHz
PEO with no CNT	46373.67 (0%)	2712.78	23.18	0.00
PEO + SW-CNT	23241.52 (-49.9%)	4016.48	15.01	0.16
PEO + DW-CNT	4078.95 (-91.2%)	2694.65	46.00	0.08
PEO + MW-CNT	22366.81 (-51.8%)	7258.65	51.32	0.23
PEO + Mesoporous	12060.08 (-74.0%)	7037.73	52.26	0.06

*all units are in kΩ

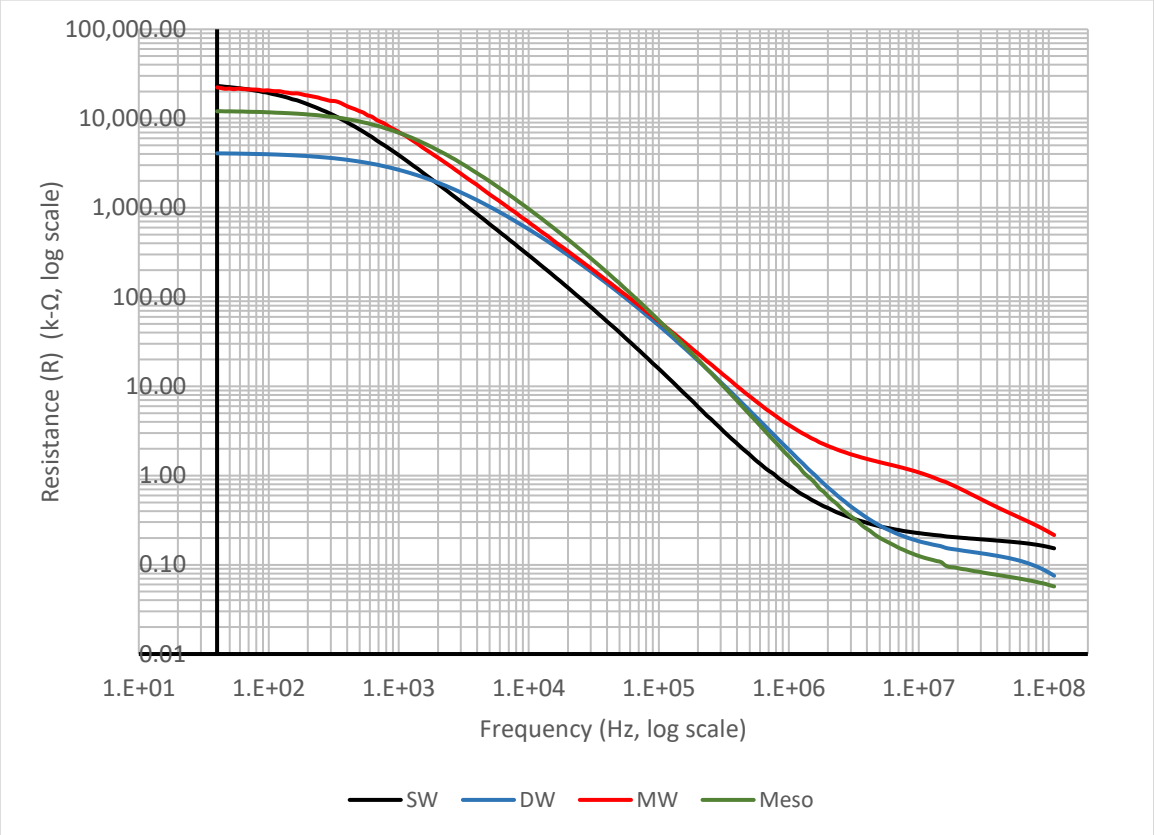

Figure 4.24 The resistance (R) of PEO-based supercapacitors at various frequencies with different types of nanocarbons added.

Table 4.13 Summary of reactance (X) at various frequencies for PEO-based supercapacitors with different types of nanocarbons added. (The negative values represent the capacitive properties of the reactance)

Sample	@ 40 Hz	@ 1 kHz	@ 100 kHz	@ 100 MHz
PEO with no CNT	-31325.38 (0%)	-6471.99	-152.31	-0.11
PEO + SW-CNT	-5239.97 (-83.3%)	-6302.44	-144.30	-0.09
PEO + DW-CNT	-243.79 (-99.2%)	-1315.14	-169.59	-0.16
PEO + MW-CNT	-2228.80 (-92.9%)	-7974.92	-275.94	-0.49
PEO + Mesoporous	-858.95 (-97.3%)	-4453.04	-311.58	-0.28

*all units are in kΩ

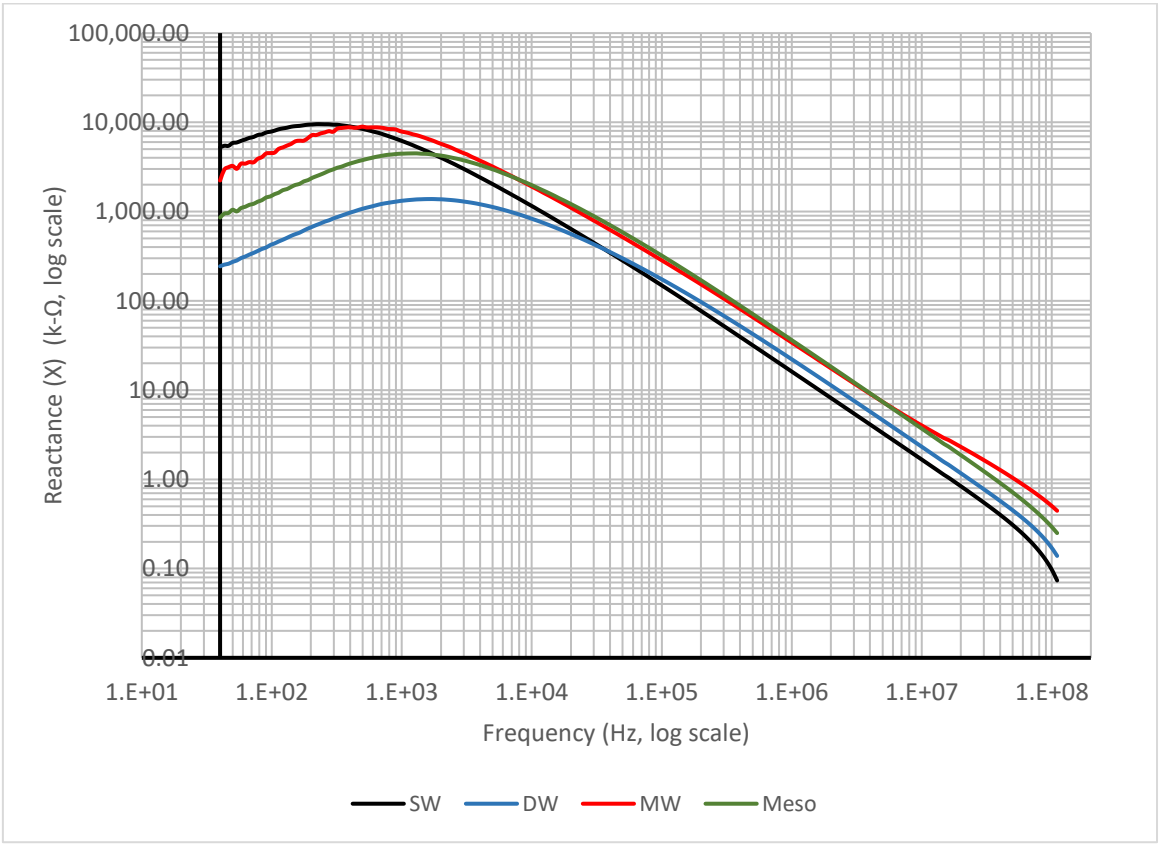

Figure 4.25 The reactance (X) of PEO-based supercapacitors at various frequencies with different types of nanocarbons added.

At low frequency range (e.g. 40 Hz), the magnitude of |*Z*| and *R* for all four different types of PEO:nanocarbons samples are in the same order with similar magnitude, where the magnitude of *X* exhibits negligible effect on that of |*Z*|. Besides, the value of θ in various PEO:nanocarbons samples varies between -3.34° to -12.71°, where the negative value shows the reactance is capacitive. This represents the electrochemical system is mainly dominated by the resistive elements instead of reactive elements. When the frequency increases to 1 kHz, the effect from reactive element becomes significant. The value of |*Z*| is attributed to both *R* and *X*, and the value of phase angle has been raised. After the frequency was increased to 100 kHz, *X* dominates the magnitude of |*Z*|, and the phase angle of four types of samples has been increased to more than -75°, which represents the dominance of capacitive reactance. When the frequency reaches 100 MHz, the effect on *X* becomes different between various samples. For SW-CNT, the magnitude of |*Z*| is mainly affected by *R* and their magnitudes are quite similar, with a smaller phase angle of -30.47°. For DW-CNT, MW-CNT and Mesoporous samples, the magnitude of |*Z*| is still dominated by the reactance *X*, and their phase angle values keep in the range of -65° to -78°. The value of absolute impedance and corresponding phase angle measured from various samples at 40 Hz, 1 kHz, 100 kHz and 100 MHz are tabulated in Tables 4.14 and 4.15. Besides, their frequency responds from of 40 Hz to 100 MHz are shown in Figures 4.26 and 4.27.

Table 4.14 Summary of absolute impedance (|Z|) at various frequencies for PEO-based supercapacitors with different types of nanocarbons added.

Sample	@ 40 Hz	@ 1 kHz	@ 100 kHz	@ 100 MHz
PEO with no CNT	56727.70 (0%)	7149.97	154.26	0.11
PEO + SW-CNT	23826.51 (-58.0%)	7474.36	145.07	0.18
PEO + DW-CNT	4086.41 (-92.8%)	3004.90	175.79	0.18
PEO + MW-CNT	22478.09 (-60.4%)	10944.02	282.84	0.54
PEO + Mesoporous	12090.74 (-78.7%)	8328.22	315.93	0.29

*all units are in kΩ

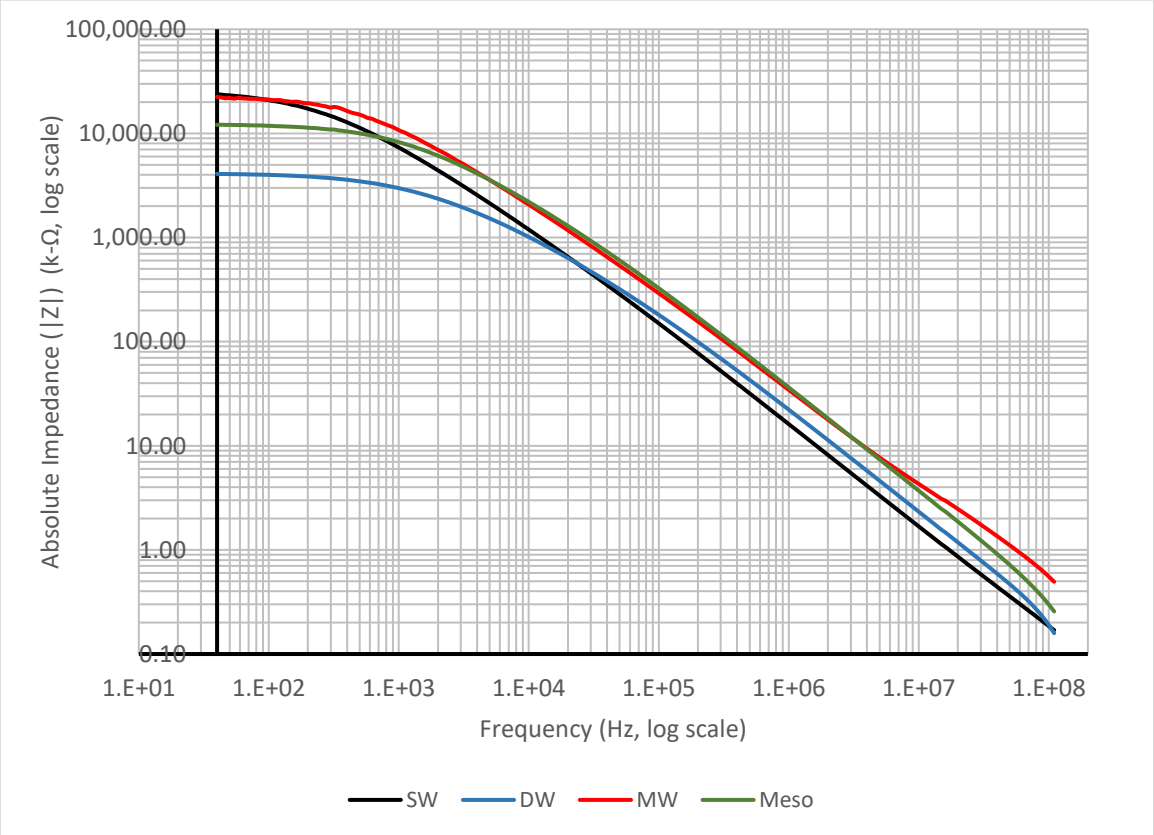

Figure 4.26 The absolute impedance (|Z|) of PEO-based supercapacitors at various frequencies with different types of nanocarbons added.

Table 4.15 Summary of phase angle (θ) between the resistance and capacitive reactance at various frequencies for PEO-based supercapacitors with different types of nanocarbons added.

Sample	@ 40 Hz	@ 1 kHz	@ 100 kHz	@ 100 MHz
PEO with no CNT	-23.11	-63.55	-81.34	-88.06
PEO + SW-CNT	-12.71	-57.56	-84.05	-30.47
PEO + DW-CNT	-3.34	-25.64	-74.94	-65.55
PEO + MW-CNT	-5.00	-34.30	-76.43	-65.23
PEO + Mesoporous	-4.08	-32.32	-80.48	-78.33

*all units are in degree

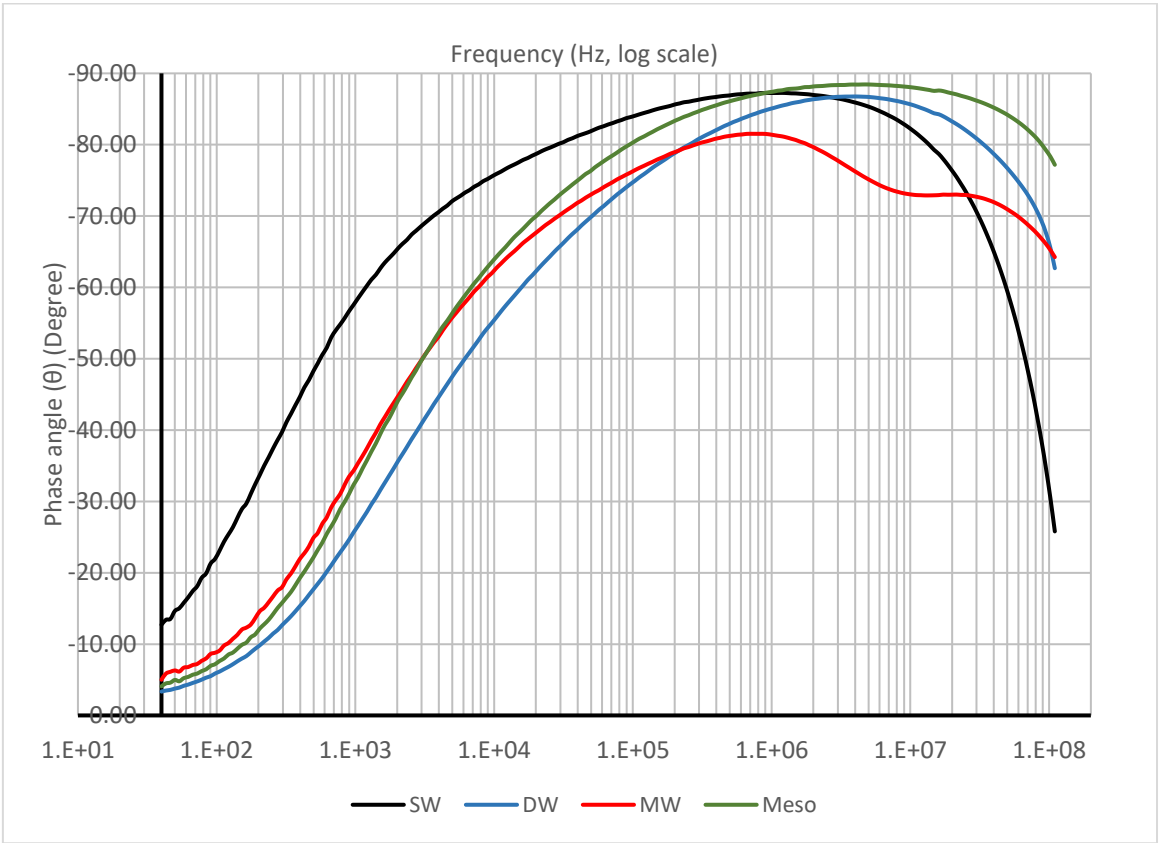

Figure 4.27 The phase angle (θ) between the resistance and capacitive reactance of PEO-based supercapacitors at various frequencies with different types of nanocarbons added.

It can be observed that the values of *R*, *X*, and |*Z*| of PEO:DW-CNT samples are much smaller than that of other three types of PEO:nanocarbons samples. This phenomenon suggests the presence of DW-CNT in PEO matrix would provide a better environment than other three types of nanocarbons for charge mobility in the PEO electrolyte, and manifests the improvement of charge storage capability. Besides, the presence of nanocarbons would introduce a certain effect on reactance at the frequencies around 1 kHz.

4.6 Voltage-current responses of PEO-based supercapacitors with different types of nanocarbons

In this experiment, the maximum current density of different samples at various scan rates are tabulated in Table 4.16.

Table 4.16 Summary of maximum current density measured from PEO-based supercapacitors with different types of nanocarbons added, by cyclic voltammetry between -0.5 V and +0.5 V under different scan rates.

Sample	100 mV/s	50 mV /s	20 mV/s	10 mV/s
PEO with no CNT	0.177 (0%)	0.172	0.087	0.071
PEO + SW-CNT	1.11 (+627.1%)	1.01	0.50	0.41
PEO + DW-CNT	10.51 (+5937.9%)	8.36	6.56	5.30
PEO + MW-CNT	5.56 (+3141.2%)	4.91	2.36	0.99
PEO + Mesoporous	4.68 (+2644.1%)	3.32	1.57	1.32

*all units are in $\mu A/cm^2$

Generally, voltammograms of all PEO:nanocarbons samples exhibit in an olive shape, with maximum values of current density were observed at ±0.5V with the corresponding positive and negative sign. In each sample, the fastest scan rate (100 mV/s) would provide the highest value of current density and the maximum current density will decrease with the decrease of scan rate.

.

In the experiment, the voltage-current responses of four different types of PEO:nanocarbons samples with different scan rates are presented in the form of cyclic voltammetry in Figures 4.28 to 4.31.

The samples doped with DW-CNT exhibits a highest value of current density, at the scan rate of 100 mV/s, the maximum current density within ±0.6V is about 10.51 μA/cm^2. For samples doped with MW-CNT and mesoporous nanocarbons, their maximum current density within ±0.6V is about 5.56 μA/cm^{2}and 4.68 μA/cm^2, respectively. The maximum current density of sample doped with SW-CNT in the same condition is about 1.11 nA/cm^2.

It can be found that DW-CNT can provide better electrical properties than other types of nanocarbons such as better lifetimes and current density under an electric field applied. Therefore, it is no doubt that the current density of sample doped with DW-CNT can show the highest value among the four different types of nanocarbons. The summary of cyclic voltammetry of PEO:nanocarbons samples at scan rate of 100 mV/s is shown in Figure 4.32.

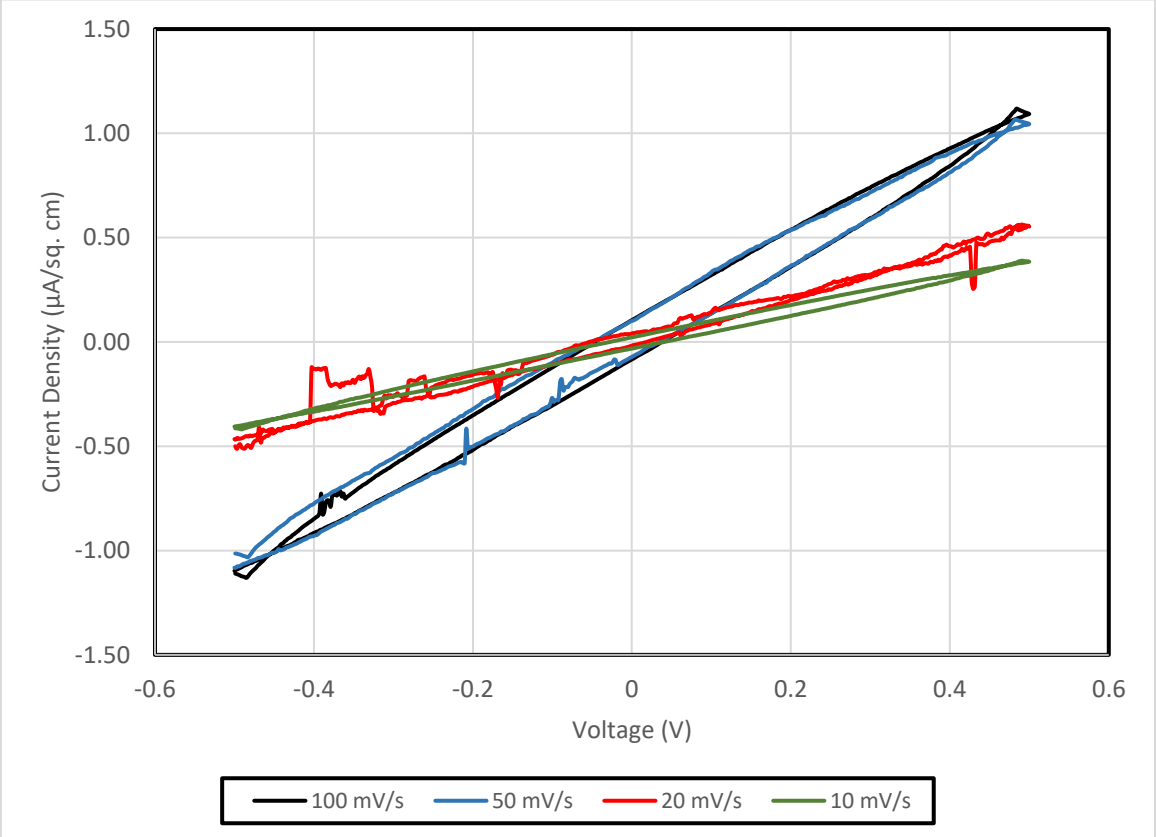

Figure 4.28 Cyclic voltammogram of PEO active layer added with SW-CNT at different scan rates.

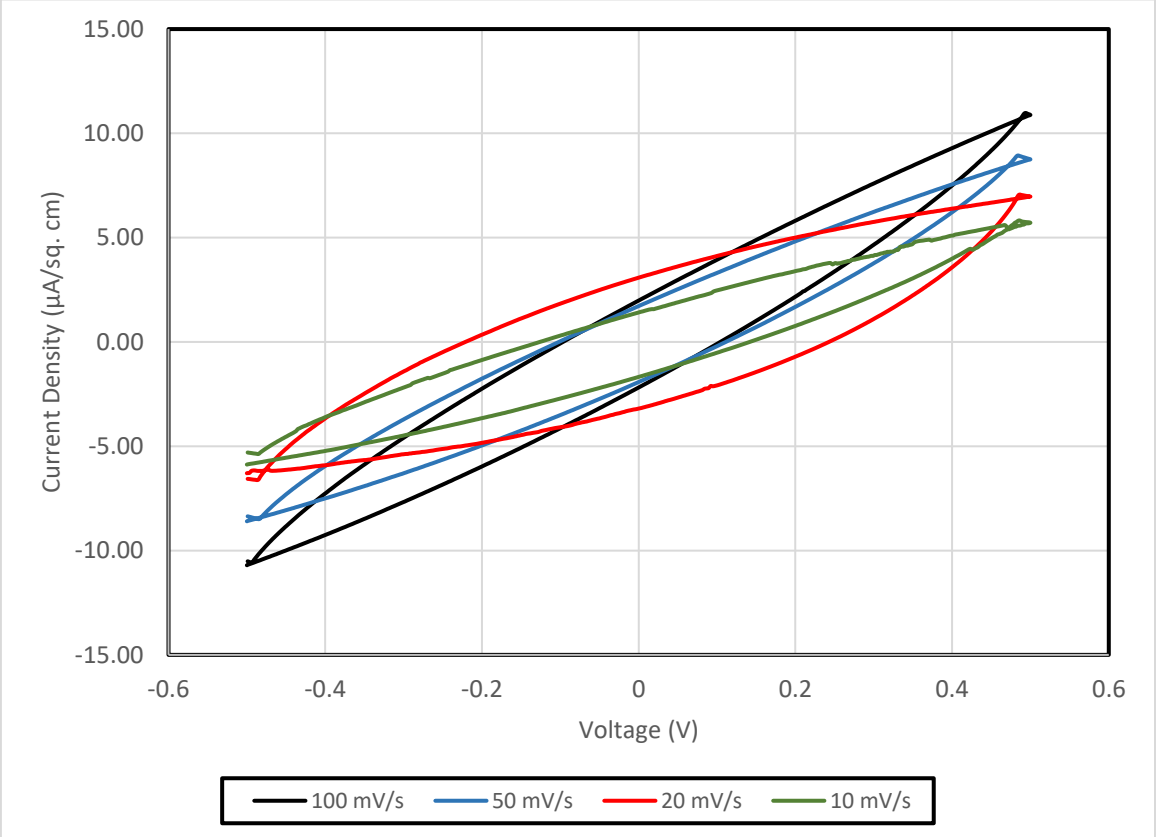

Figure 4.29 Cyclic voltammogram of PEO active layer added with DW-CNT at different scan rates.

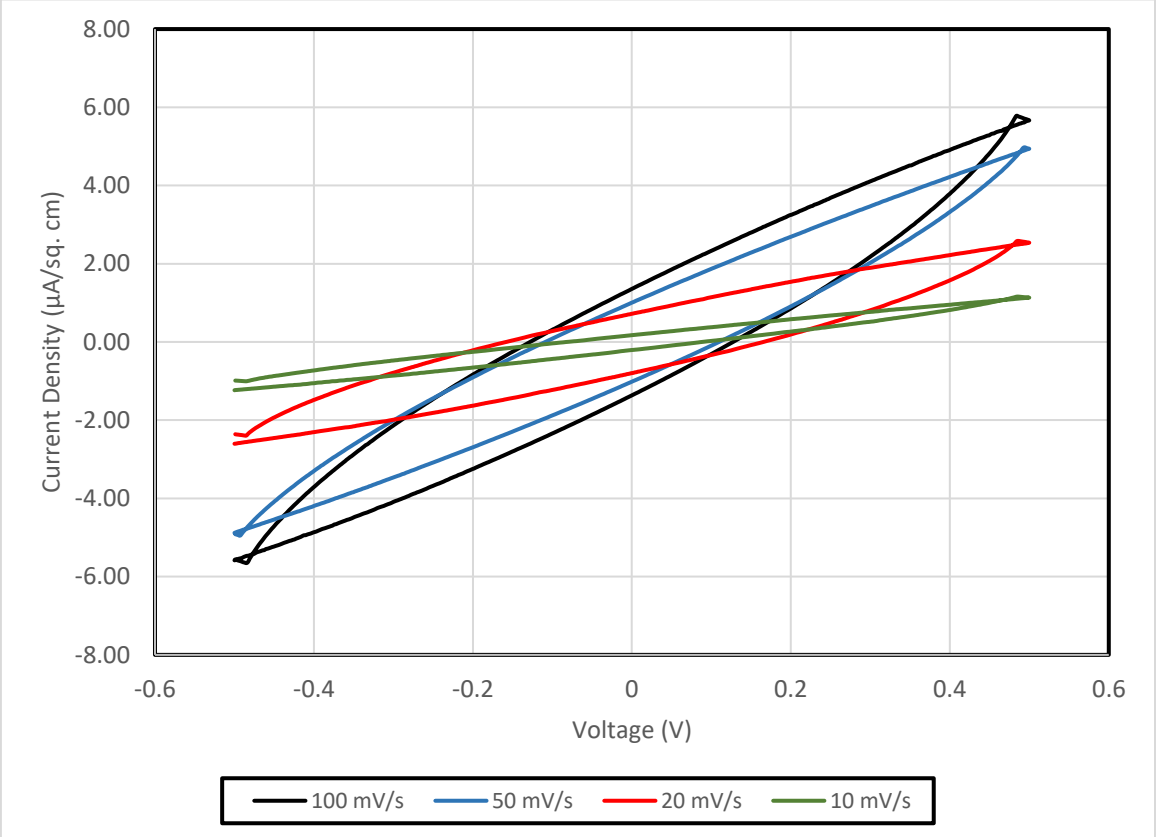

Figure 4.30 Cyclic voltammogram of PEO active layer added with MW-CNT at different scan rates.

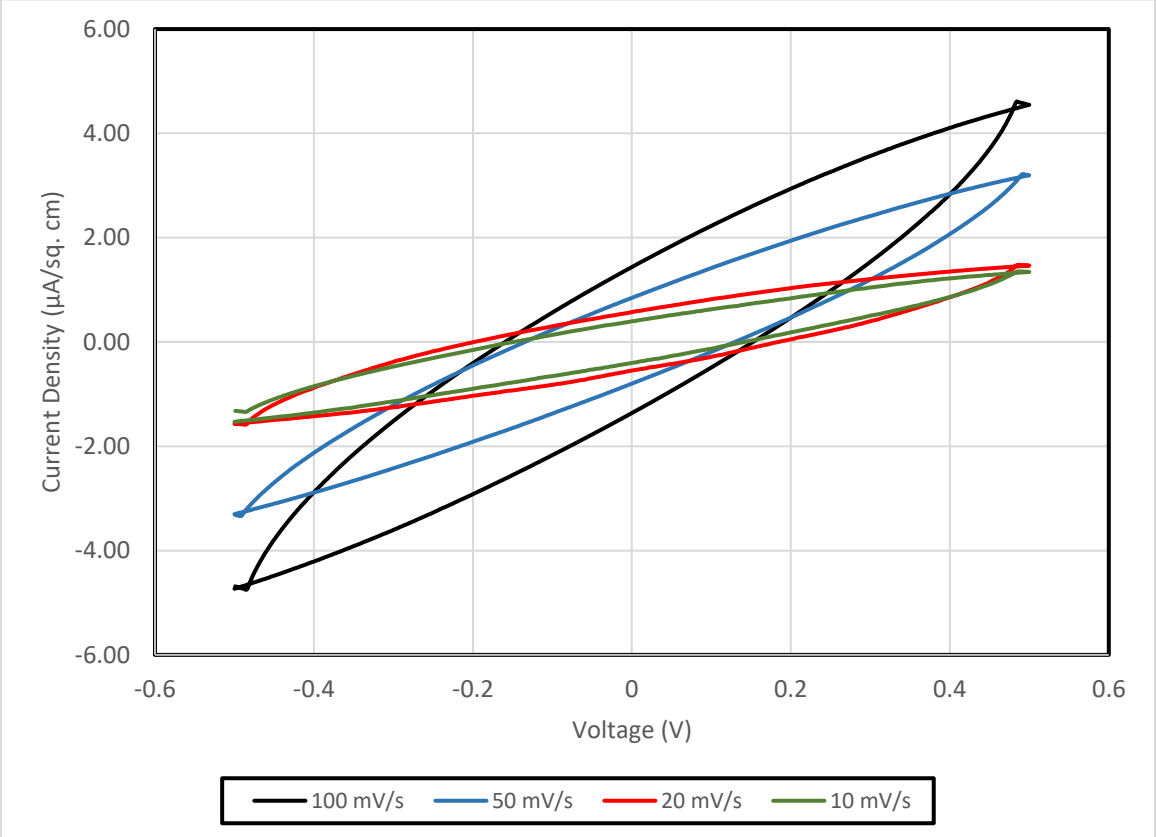

Figure 4.31 Cyclic voltammogram of PEO active layer added with Mesoporous nanocarbons at different scan rates.

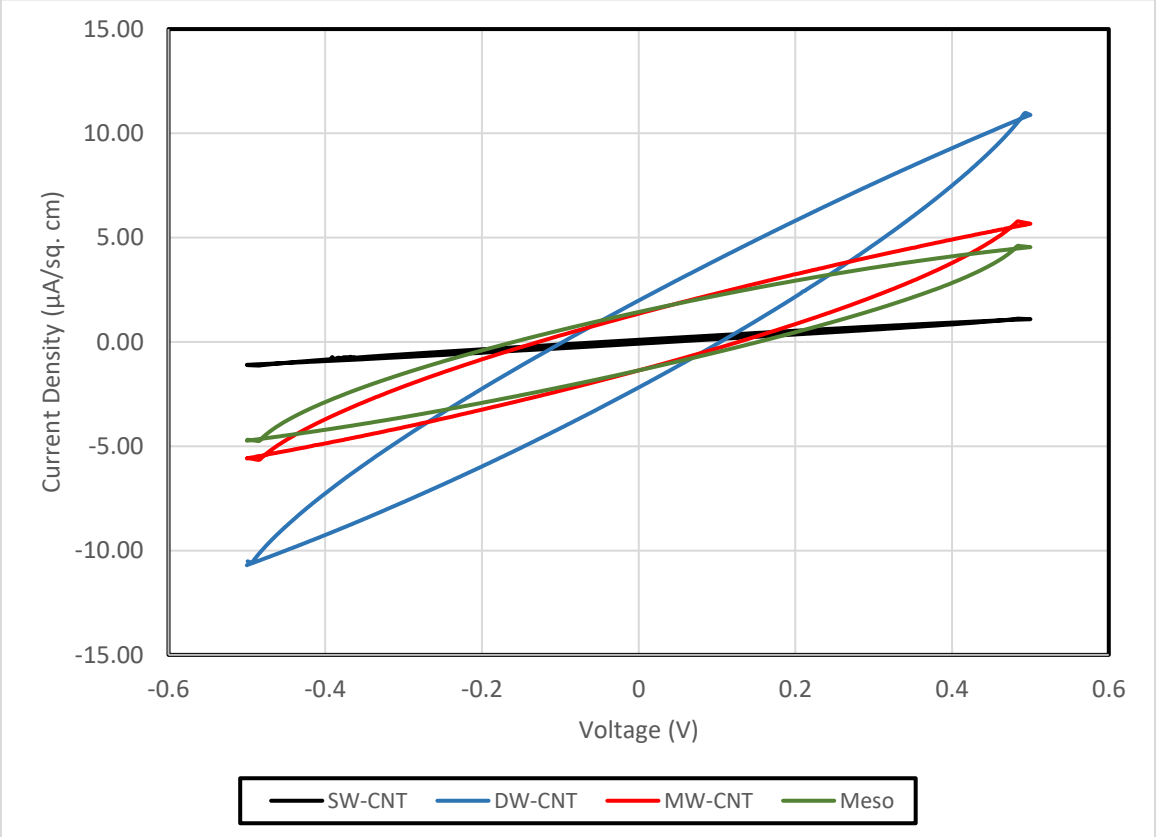

Figure 4.32 Cyclic voltammogram of PEO active layer added with different types of nanocarbons at a scan rate of 100 mV/s

Chapter 5

Effects of Structure on PEO-based Supercapacitors

From the previous chapter, PEO-based supercapacitors doped with different amount of $LiClO_4$ and different types of nanocarbons have been examined, and the candidate with best performance has been indicated. In this chapter, the PEO-based supercapacitors were doped with $LiClO_4$ (with mass ratio of PEO:Li^+ = 100:1) and double-walled carbon nanotubes (DW-CNT) (with mass ratio of PEO:DW-CNT = 5:1), and samples with different combinations on these electrolytic layers were prepared. Four different combinations of electrolytic layers were prepared, the schematic structure of the capacitor layers is shown in Figure 5.1, and the layering details are tabulated in Table 5.1. The electrical properties, electrochemical responses and charge capabilities of these combinations are then studied.

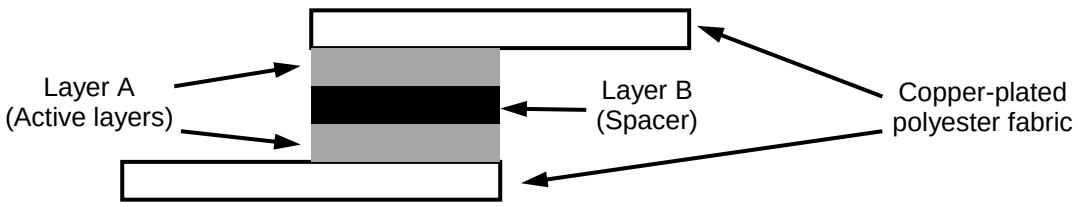

Figure 5.1 The schematic diagram show the combination of active layers and spacers of various PEO-based electrochemical double layer capacitors.

Table 5.1 The combination of active layers and spacers of various PEO-based electrochemical double layer capacitors.

Sample	Layer A (Active layer)	Content in A	Layer B (Spacer)	Content in B
W1F1	W1	PEO + CNT	F1	PEO only
W1Q2	W1	PEO + CNT	Q2	PEO + Li
W2F1	W2	PEO + CNT + Li	F1	PEO only
W2Q2	W2	PEO + CNT + Li	Q2	PEO + Li
Layer	**Content**		**Mass ratio**	
W1	PEO + CNT		PEO:CNT = 5:1	
W2	PEO + CNT + Li		PEO:CNT:Li = 100:20:1	
F1	PEO only		1	
Q2	PEO + Li		PEO:Li = 100:1	

To study the performance and the tolerance of the PEO-based supercapacitors with different layering combinations, galvanostatic charge-discharge measurement was taken place to test for the samples, and the electrical properties of samples were further studied to compare the changes after a long recycling run.

5.1 Capacitance of PEO:CNT:Li supercapacitors with different layering combinations

In this study, the electrical properties of the PEO:CNT:Li supercapacitors with different layering combinations were investigated. The samples were connected to the impedance analyzer to determine their electrical properties in the frequency range between 40 Hz and 110 MHz, including series capacitance (C_S), dissipation factor (D), series resistance (R), series reactance (X), absolute impedance ($|Z|$) and the phase difference between the resistance and reactance (θ).

The specific capacitances of PEO:CNT:Li supercapacitors wee estimated from the series capacitance measured by the impedance analyzer, and their values at 40 Hz, 1 KHz, 100 KHz and 100 MHz are summarized in Table 5.2 and the change of specific capacitance was shown in Figures 5.2. Generally, all four different combinations exhibit the similar trend along the frequency range from 40 Hz to 100 MHz. In low frequency range, the specific capacitance of all PEO:CNT:Li supercapacitors give higher value than other frequencies. The best performance among four types of samples is W1Q2, with PEO:CNT as active layers and PEO:Li, the specific capacitance of this sample is about 10.2 μF/cm^2. For samples W2F1 and W2Q2 with PEO:CNT:Li as active layers, and pure PEO and PEO:Li as spacers, their specific capacitances are 292.88 nF/cm^2 and 238.43 nF/cm^2 respectively. Sample W1F1 as a control, which uses PEO:CNT as active layers and pure PEO as spacers, its specific capacitance is 32.8 nF/cm^2 which is the lowest.

Table 5.2 Summary of specific capacitance at various frequencies for PEO-based supercapacitors with different active layers combination.

Sample	@ 40 Hz	@ 1 kHz	@ 100 kHz	@ 100 MHz
W1F1	32.80 (0%)	0.24	0.02	0.02
W1Q2	10186.66 (+31056.9%)	485.50	0.25	0.11
W2F1	292.88 (+892.9%)	5.19	0.04	0.40
W2Q2	238.43 (+726.9%)	8.05	0.04	0.02

*all units are in nF/cm^2

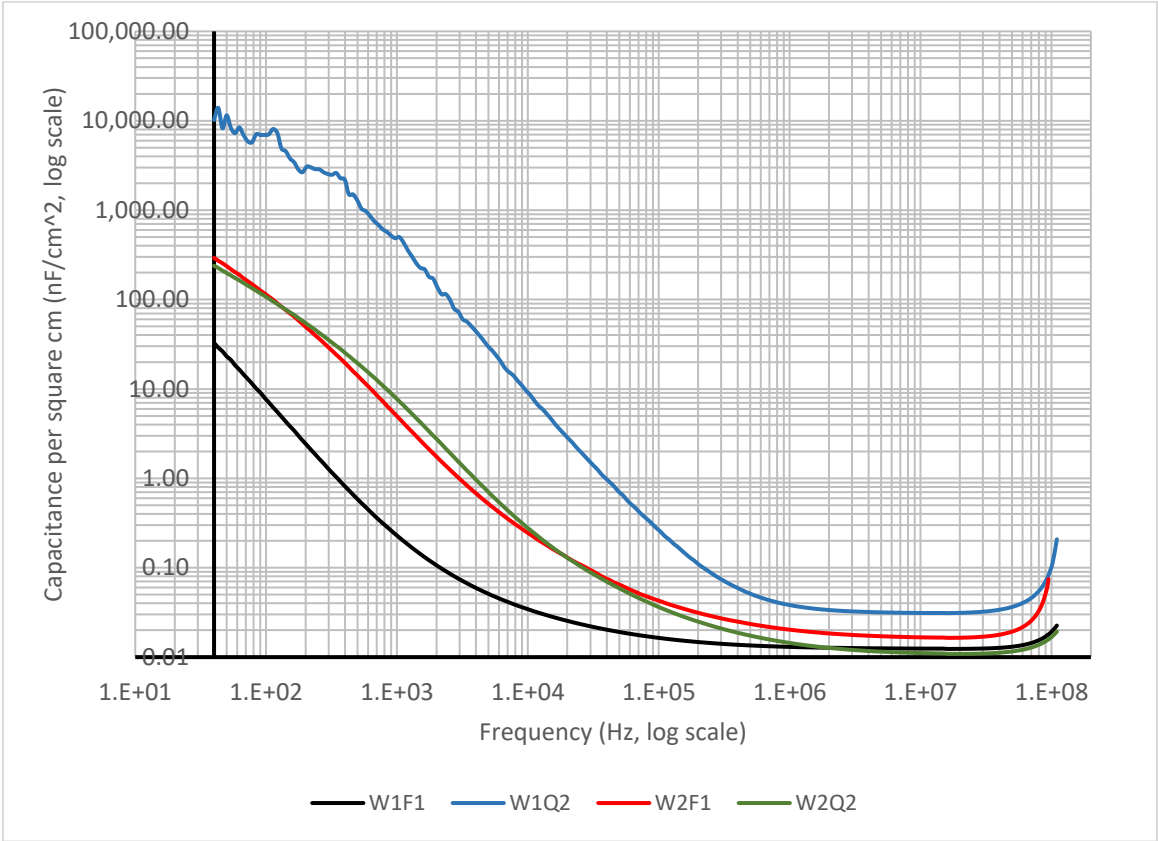

Figure 5.2 The specific capacitances of PEO-based supercapacitors at various frequencies with different layer combinations.

Once the testing frequency has been raised to intermediate range around 100 kHz, the specific capacitance of all four samples with different layering combinations dramatically decreases and reaches the minimum. It flattens in the range of 0.01 nF/cm^2 to 0.10 nF/cm^2 until the frequency has been increased to a higher range at 100 MHz, the specific capacitance increases again in the range of 0.02 nF/cm^2 to 0.40 nF/cm^2.

For Dissipation factor (*D*), the values for the four different types of samples at 40 Hz, 1 KHz, 100 KHz and 100 MHz were listed in Table 5.3 and the change of dissipation factor was shown in Figure 5.3. All PEO:CNT:Li supercapacitors give the highest values at 40 Hz with 17.15, 24.30, 21.05 and 12.96 for sample W1F1, W1Q2, W2F1 and W2Q2 respectively. The dissipation factor then drops in the intermediate range of frequency and reaches the minimum after 1 MHz with value averagely below 0.20. When the continuously increases to 100 MHz, *D* increases to 0.46, 0.81, 1.29 and 0.23 for sample W1F1, W1Q2, W2F1 and W2Q2 respectively.

Table 5.3 Summary of dissipation factor at various frequencies for PEO-based supercapacitors with different active layers combination.

Sample	@ 40 Hz	@ 1 kHz	@ 100 kHz	@ 100 MHz
W1F1	17.75 (0%)	2.14	0.27	0.46
W1Q2	24.30 (+136.9%)	24.65	1.03	0.81
W2F1	21.05 (+118.6%)	7.77	0.74	1.29
W2Q2	12.96 (-27.0%)	6.61	0.83	0.23

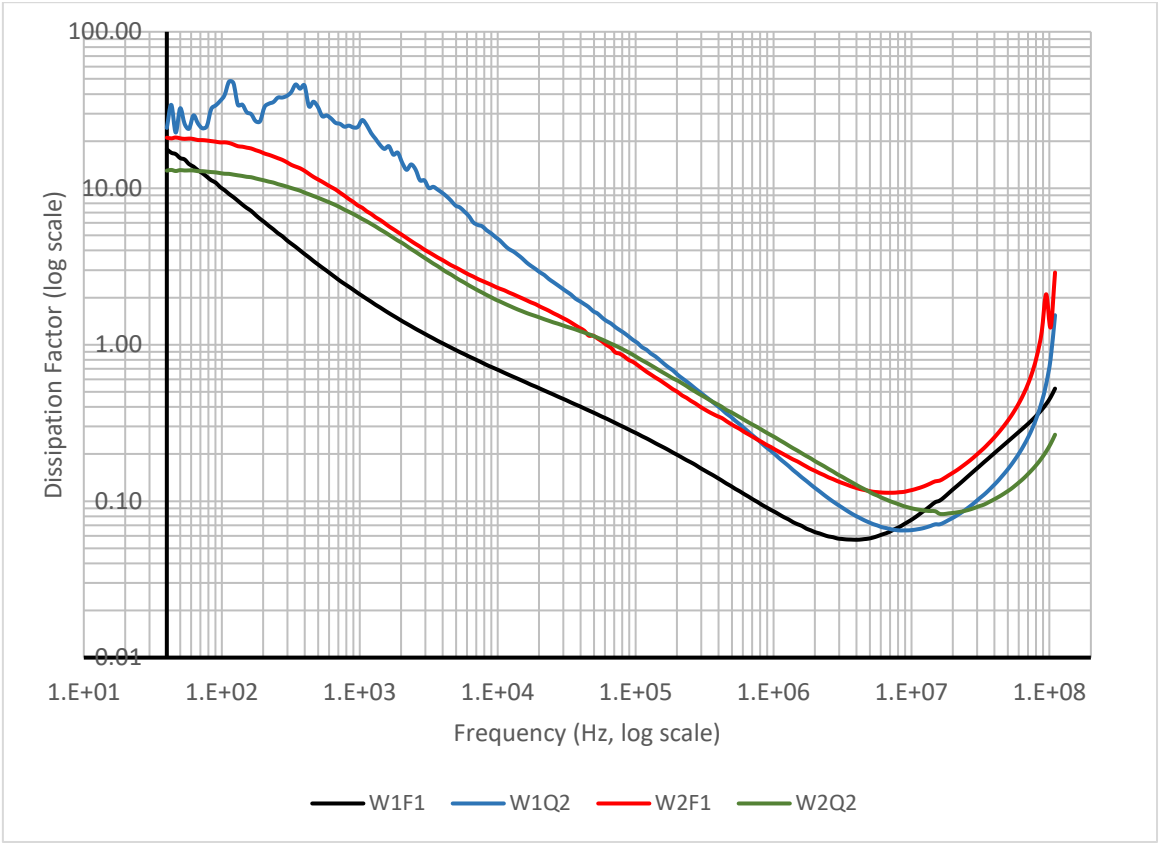

Figure 5.3 The dissipation factor (D) of PEO-based supercapacitors at various frequencies with different layer combinations.

In the measurement of electrical properties of PEO:CNT:Li supercapacitor, the values of series resistance measured from various samples at 40 Hz, 1 kHz, 100 kHz and 100 MHz are tabulated in Table 5.4. Besides, their frequency responds in the frequency range of 40 Hz to 100 MHz are shown in Figure 5.4.

In the experiment, the total impedance measured from the sample consists of two components: the resistive element and reactive element, which are the real part and imaginary part of the impedance, respectively. When the frequency increases, the resistance (*R*) of all PEO:CNT:Li samples decreases from a higher value with the order of MΩ to about few-tens of Ω when the frequency reaches 100 MHz.

For the control sample W1F1, it drops from about 4.08 MΩ at 40 Hz, drastically to about 46.0 kΩ at 100 kHz, then reaches 80 Ω at 100 MHz. For W1Q2, with PEO:CNT as active layers and PEO:Li as spacer, the resistance dramatically decreases from 1.41 MΩ at 40 Hz to 16.68 kΩ at 100 kHz, and reaches 30 Ω at 100 MHz. For samples W2F1 and W2Q2 with PEO:CNT:Li as active layers, and pure PEO and PEO:Li as spacers decrease from 700 kΩ and 1.33 MΩ at 40 Hz gradually to 104.46 kΩ and 120.64 kΩ at 100 kHz respectively, and reaches about 60 Ω for both samples at 100 MHz. With the increase of testing frequency, the electrical properties of the samples become more dependent on the frequency response elements (e.g. capacitive or inductive elements), electric current flowing through the resistive element decreases and the resistance decreases accordingly.

Table 5.4 Summary of resistance (R) at various frequencies for PEO-based supercapacitors with different active layers combination.

Sample	@ 40 Hz	@ 1 kHz	@ 100 kHz	@ 100 MHz
W1F1	4078.95 (0%)	2694.65	46.00	0.08
W1Q2	1405.69 (-65.5%)	677.98	16.68	0.03
W2F1	699.99 (-82.8%)	603.46	104.46	0.06
W2Q2	1328.65 (-67.4%)	1031.02	120.64	0.06

*all units are in kΩ

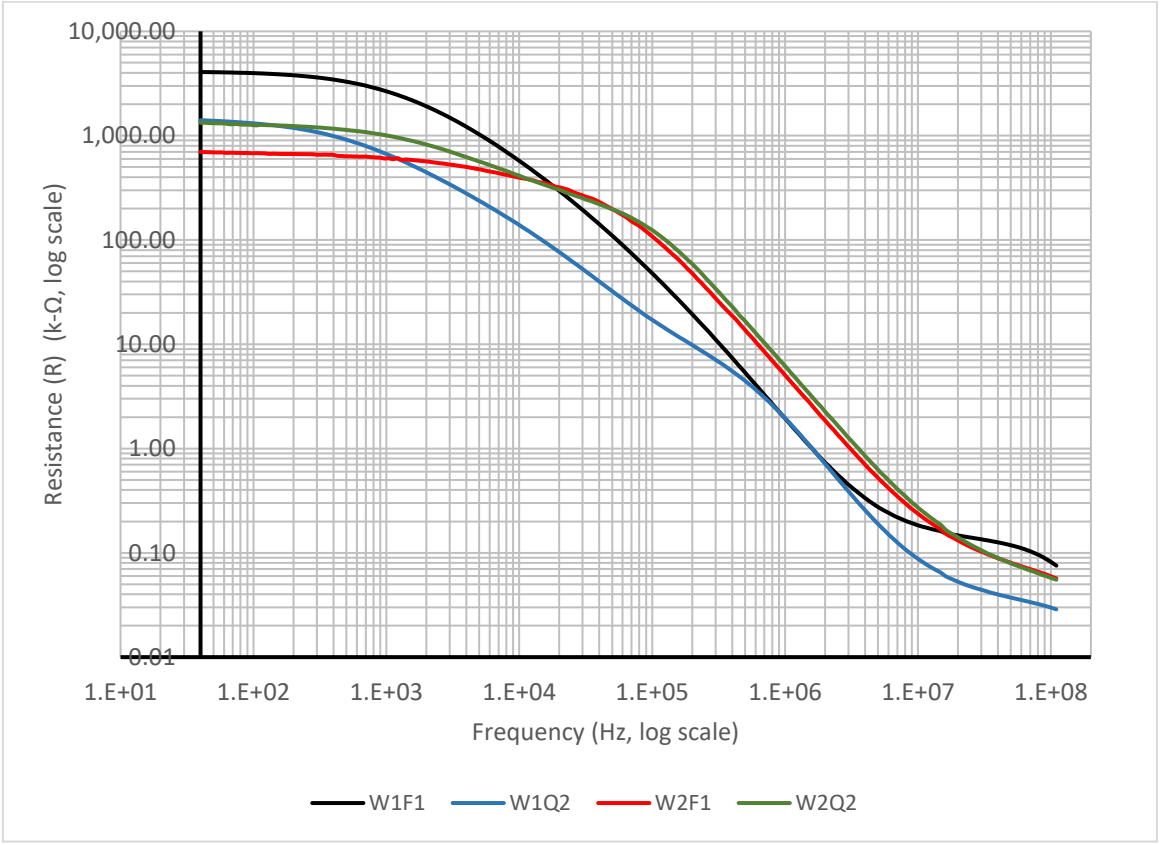

Figure 5.4 The resistance (R) of PEO-based supercapacitors at various frequencies with different layer combinations.

On the side of reactance (*X*), the value measured from various samples at 40 Hz, 1 kHz, 100 kHz and 100 MHz are tabulated in Tables 5.5. Besides, their frequency responds in the frequency range of 40 Hz to 100 MHz are shown in Figure 5.5. The reactance of the control sample W1F1 raises from -243.79 kΩ at 40 Hz to about -1.32 MΩ at 1 kHz, then drops to -160 Ω at 100 MHz. For sample W1Q2, with PEO:CNT as active layers and PEO:Li as spacer, the reactance increases from -150.64 kΩ at 40 Hz to -453.49 kΩ at 1 kHz, then decreases to -20 Ω at 100 MHz. For W2F1 and W2Q2, the reactance increases from -31.40 kΩ and -102.18 kΩ at 40 Hz, to -81.92 and -316.60 kΩ at 1 kHz, respectively. Then the reactance drops to -210 Ω and -270 Ω at 100 MHz. The negative value of *X* indicates it is mainly influenced by the capacitive element (i.e. capacitive reactance).

Table 5.5 Summary of reactance (X) at various frequencies for PEO-based supercapacitors with different active layers combination. (The negative values represent the capacitive properties of the reactance)

Sample	@ 40 Hz	@ 1 kHz	@ 100 kHz	@ 100 MHz
W1F1	-243.79 (0%)	-1315.14	-169.59	-0.16
W1Q2	-150.64 (-38.2%)	-453.49	-41.90	-0.02
W2F1	-31.40 (-87.1%)	-81.92	-145.84	-0.21
W2Q2	-102.18 (-58.1%)	-316.60	-150.13	-0.27

*all units are in kΩ

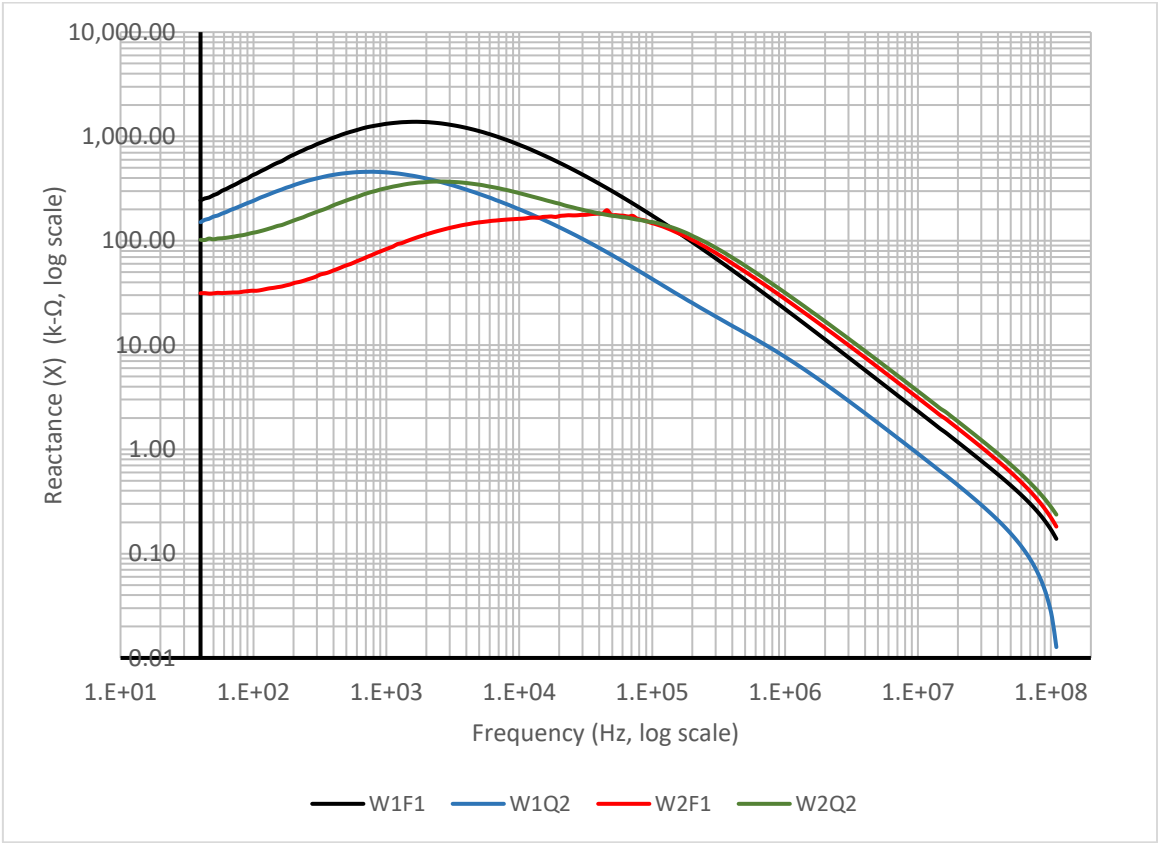

Figure 5.5 The reactance (X) of PEO-based supercapacitors at various frequencies with different layer combinations.

The value of absolute impedance and the corresponding phase angle measured from various samples at 40 Hz, 1 kHz, 100 kHz and 100 MHz are tabulated in Tables 5.6 and 5.7. Besides, their frequency responds in the frequency range of 40 Hz to 100 MHz are shown in Figures 5.6 and 5.7. At low frequency range (e.g. 40 Hz), the magnitude of $|Z|$ and R for all four different combinations of PEO:CNT:Li samples are in the same order with similar magnitude, where the magnitude of X exhibits negligible effect on that of $|Z|$. Besides, the value of θ in various PEO:CNT:Li samples are varying between -2.90° to -4.41°, where the negative value shows the reactance is capacitive. This represents the electrochemical system is mainly dominated by the resistive elements instead of reactive element.

When the frequency increases to 1 kHz, the effect from reactive element becomes significant. The value of $|Z|$ is attributed to both R and X, and the value of phase angle has been raised. After the frequency has been increased to 10 MHz, X dominates the magnitude of $|Z|$, and the phase angle of four types of samples has been increased to more than -80°. The reactance of sample W1F1, W1Q2, W2F1 and W2Q2 are decreased to 175.79 kΩ, 48.70 kΩ, 181.26 kΩ and 192.61 kΩ, respectively.

Table 5.6 Summary of absolute impedance (|Z|) at various frequencies for PEO-based supercapacitors with different active layers combination.

Sample	@ 40 Hz	@ 1 kHz	@ 100 kHz	@ 100 MHz
W1F1	4086.41 (0%)	3004.90	175.79	0.18
W1Q2	1413.79 (-65.4%)	817.44	48.70	0.04
W2F1	700.72 (-82.9%)	609.36	181.26	0.24
W2Q2	1332.58 (-67.4%)	1063.56	192.61	0.28

*all units are in kΩ

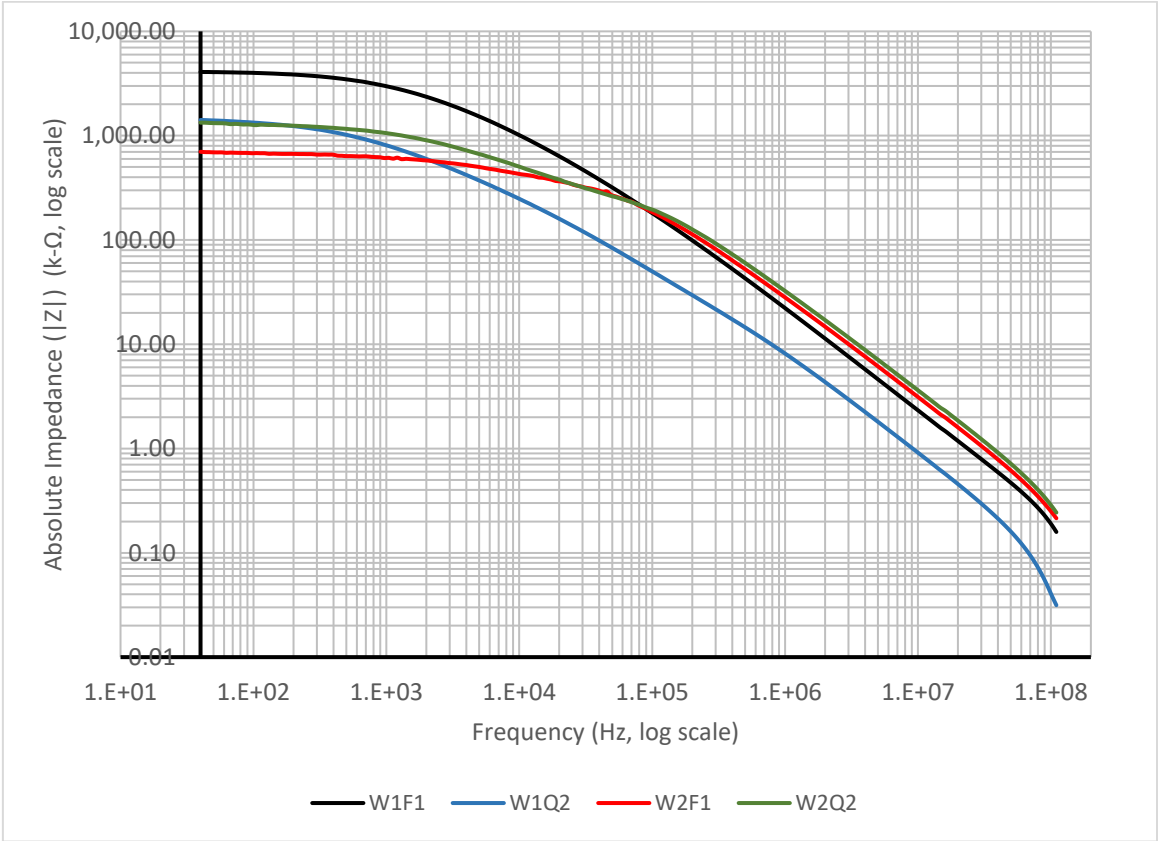

Figure 5.6 The absolute impedance (|Z|) of PEO-based supercapacitors at various frequencies with different layer combinations.

Table 5.7 Summary of phase angle (θ) between the resistance and capacitive reactance at various frequencies for PEO-based supercapacitors with different active layers combination.

Sample	@ 40 Hz	@ 1 kHz	@ 100 kHz	@ 100 MHz
W1F1	-3.34	-25.64	-74.94	-65.55
W1Q2	-3.53	-17.49	-48.59	-39.39
W2F1	-2.90	-8.23	-54.22	-55.04
W2Q2	-4.41	-12.05	-50.46	-76.93

*all units are in degree

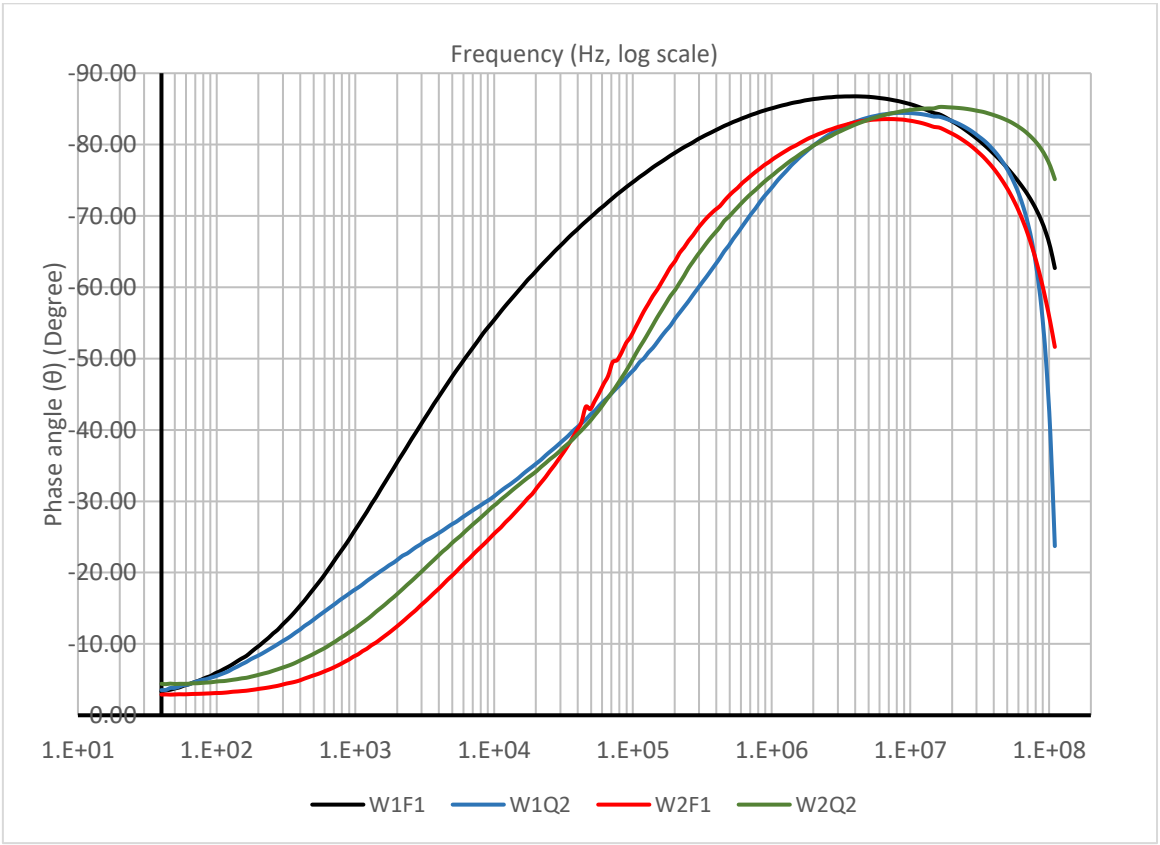

Figure 5.7 The phase angle (θ) between the resistance and capacitive reactance of PEO-based supercapacitors at various frequencies with different layer combinations.

After reaching the maximum, at 100 MHz, the phase angle of control sample with PEO:CNT active layers and PEO:Li spacer (W1F1) has been decreased to -65.55°. For sample W1Q2, it sharply drops to -39.39°, where the phase angle of W2F1 and W2Q2 are decreased to -55.04° and -76.93° respectively.

By comparing the electrical properties of all four samples being tested, the charge storage capability of samples doped with both CNT and Li^+ ions can be enhanced. For the control sample W1F1, which is only doped with CNT, the specific capacitance is 32.80 nF/cm^2. For other samples like W2F1 and W2Q2, their specific capacitances are 292.88 nF/cm^2 and 238.43 nF/cm^2, respectively. For sample W1Q2, it shows a significant improvement that gives 10.19 $\mu F/cm^2$. It can be attributed to the increase of charge storage capability in the PEO:CNT:Li electrochemical system which mainly comes from the presence of Li^+ ions in the PEO matrix.

In the previous chapter, a series experiments show PEO-based supercapacitors doped with either Li^+ ion or CNT could enhance the charge storage capability of the system, but the improvement is limited. In this experiment, we can find that the presence of Li^+ ions and CNT in the same system could largely increase the specific capacitance. The improvement of charge storage capability is not only just adding the benefits of two dopants together, but the enhancement is being amplified.

5.2 Electrochemical properties of PEO:CNT:Li supercapacitors with different layering combinations

In this experiment, each combination of PEO:CNT:Li supercapacitors was examined by cyclic voltammetry (CV), electrochemical impedance spectroscopy (EIS) and cyclic charge-discharge (CCD) measurement. After the samples have been tested by CCD measurement, the tested samples were examined by CV and EIS again, to determine the effect of cyclic charge-discharge process on the electrochemical systems. The maximum current density of various PEO:CNT:Li samples at different scan rates before being tested by CCD measurement are tabulated in Table 5.8, and the summary of cyclic voltammetry of PEO:CNT:Li samples at scan rate of 100 mV/s is shown in Figure 5.8.

Table 5.8 Summary of maximum current density measured from PEO-based supercapacitors with different layer combinations, by cyclic voltammetry between -0.5 V and +0.5 V under different scan rates.

Sample	100 mV/s	50 mV /s	20 mV/s	10 mV/s
W1F1 [Active layer: PEO+CNT Spacer: Pure PEO]	10.51 (0%)	8.36	6.56	5.30
W1Q2 [Active layer: PEO+CNT Spacer: PEO+Li]	29.70 (+282.6%)	25.78	18.15	12.08
W2F1 [Active layer: PEO+CNT+Li Spacer: Pure PEO]	3.87 (-63.2%)	3.76	0.91	0.60
W2Q2 [Active layer: PEO+CNT+Li Spacer: PEO+Li]	49.75 (+473.4%)	39.80	11.83	9.29

*all units are in $\mu A/cm^2$

Generally, voltammograms of all PEO:CNT:Li samples exhibit in an olive shape, with maximum values of current density observed at ±0.5V with the corresponding positive and negative sign. In each sample, the fastest scan rate (100 mV/s) provides the highest value of current density and the maximum current density decreased with the increase of scan rate. By comparing all four types of combination, the maximum current density obtained from sample with PEO:CNT:Li active layers and PEO:Li spacer (W2Q2) is the highest. The performance of these PEO:CNT:Li samples with different layer combinations will be discussed individually in the following parts.

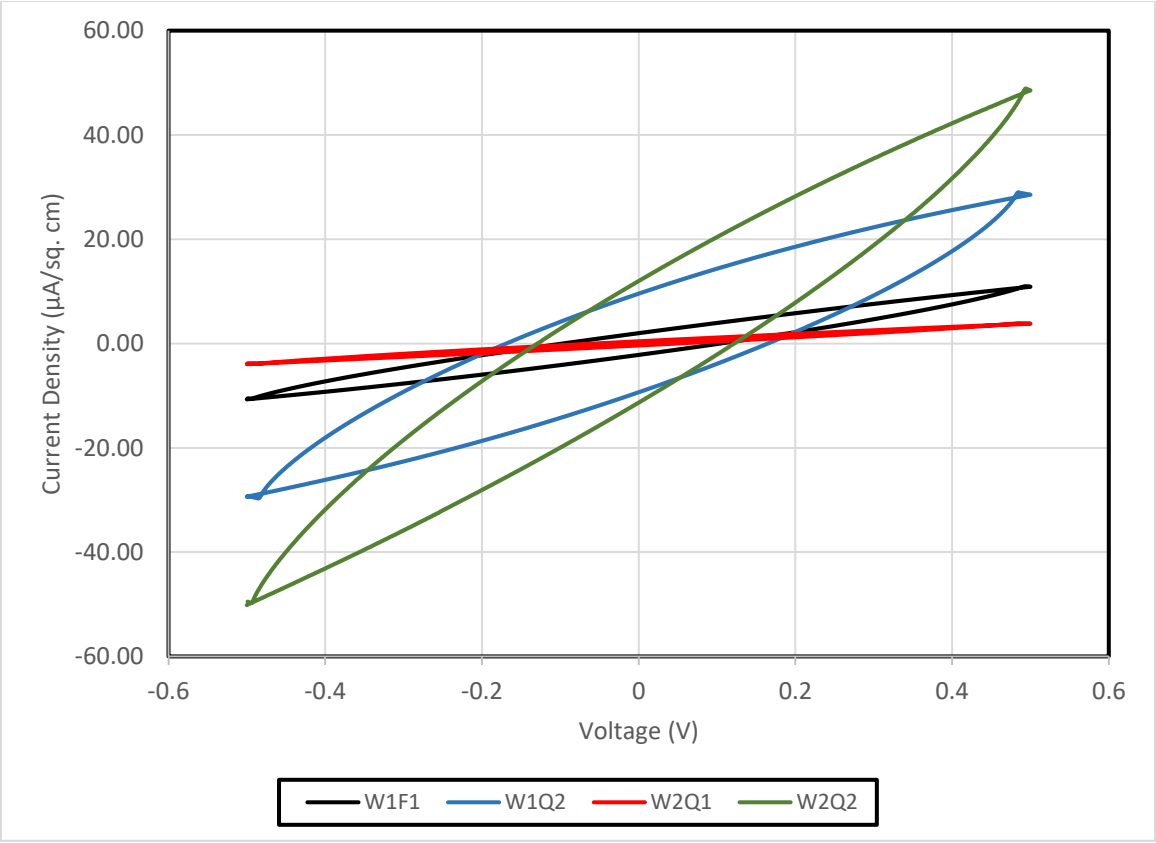

Figure 5.8 Cyclic voltammogram of PEO:CNT:Li supercapacitors with different layer combinations at a scan rate of 100 mV/s

5.2.1 Performance of supercapacitor with PEO:CNT active layers and PEO:Li spacer (W1Q2)

For this sample, a layer of PEO:CNT was casted on the copper-plated polyester fabrics, two pieces of PEO:CNT casted fabrics were then laminated together with a layer of PEO:Li as spacer.

By examining the samples with cyclic voltammetry at various scan rates as shown in Figure 5.9, the maximum current density of W1Q2 at 100 mV/s within ±0.5V is found about 29.70 μA/cm^2. The current density is then dropped with the decrease of scan rate, and gives 12.08 μA/cm^2 at 10 mV/s. Compared to the control sample W1F1, which has PEO:CNT as active layers and pure PEO as spacer, with the maximum current density of 10.51 μA/cm^2, the current density of W1Q2 has been increased nearly three times. It is suggested that the presence of Li^+ ions in spacer can enhance the charge mobility in the electrochemical system. The current passing through the effective laminated area from the electrode (copper-plated polyester fabric) to the PEO:CNT active layers and spacer has been increased. As a result, the specific capacitance of the system is increased, and it implies the increase of charge storage capability.

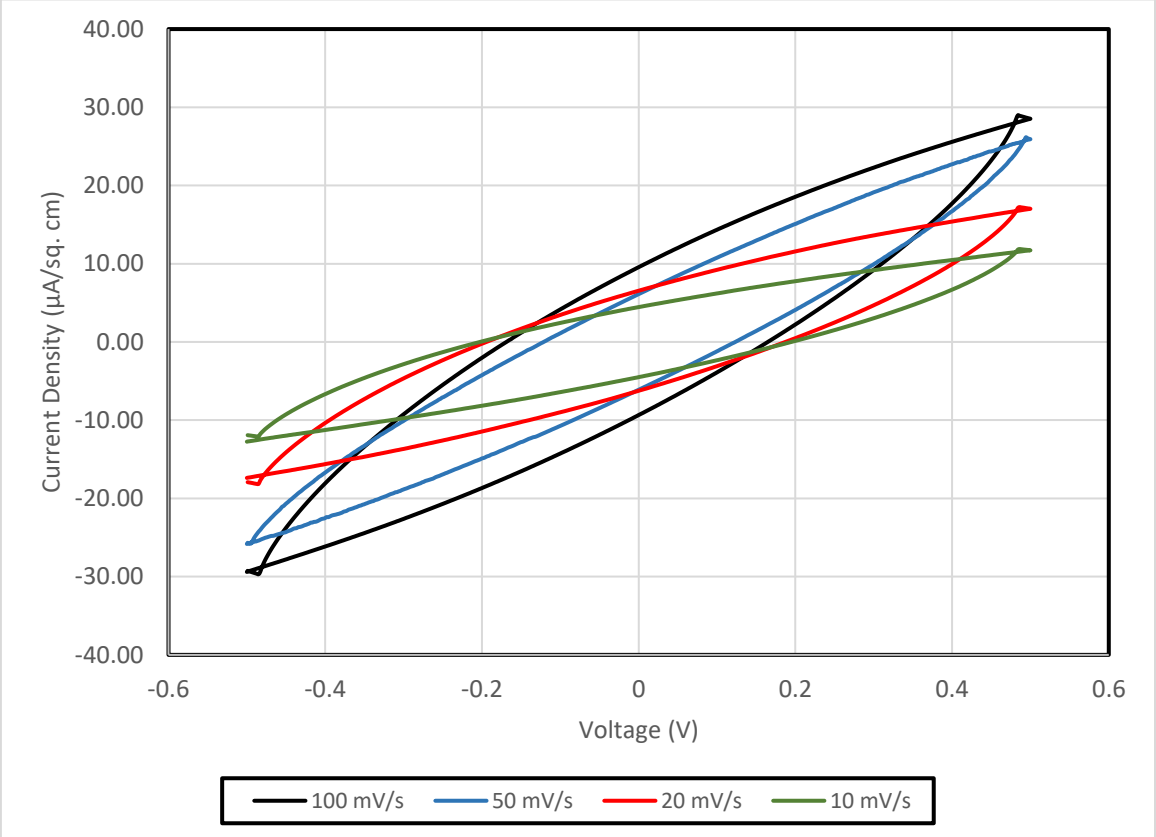

Figure 5.9 Cyclic voltammogram of PEO:CNT:Li supercapacitor with PEO:CNT active layers and PEO:Li spacer (W1Q2) at different scan rates before galvanostatic charge-discharge measurement.

To study the impedance changes of sample with respect to the frequency responses, the sample has been examined by electrochemical impedance spectroscopy (EIS) in the range of 1 mHz to 1 MHz. The change of absolute impedance $|Z|$ of the sample has been illustrated in Figure 5.10. It can be seen that at very low to low frequency range (1 mHz to 1 Hz), the absolute impedance is in a relative high range, since at this frequency range, the impedance is dominated by frequency independent element (resistance) instead of frequency dependent element (reactance). When the frequency has been increased to 1 kHz or even

higher to 1 MHz, the influence from frequency dependent element (reactance) increases, resulting to the decrease of absolute impedance.

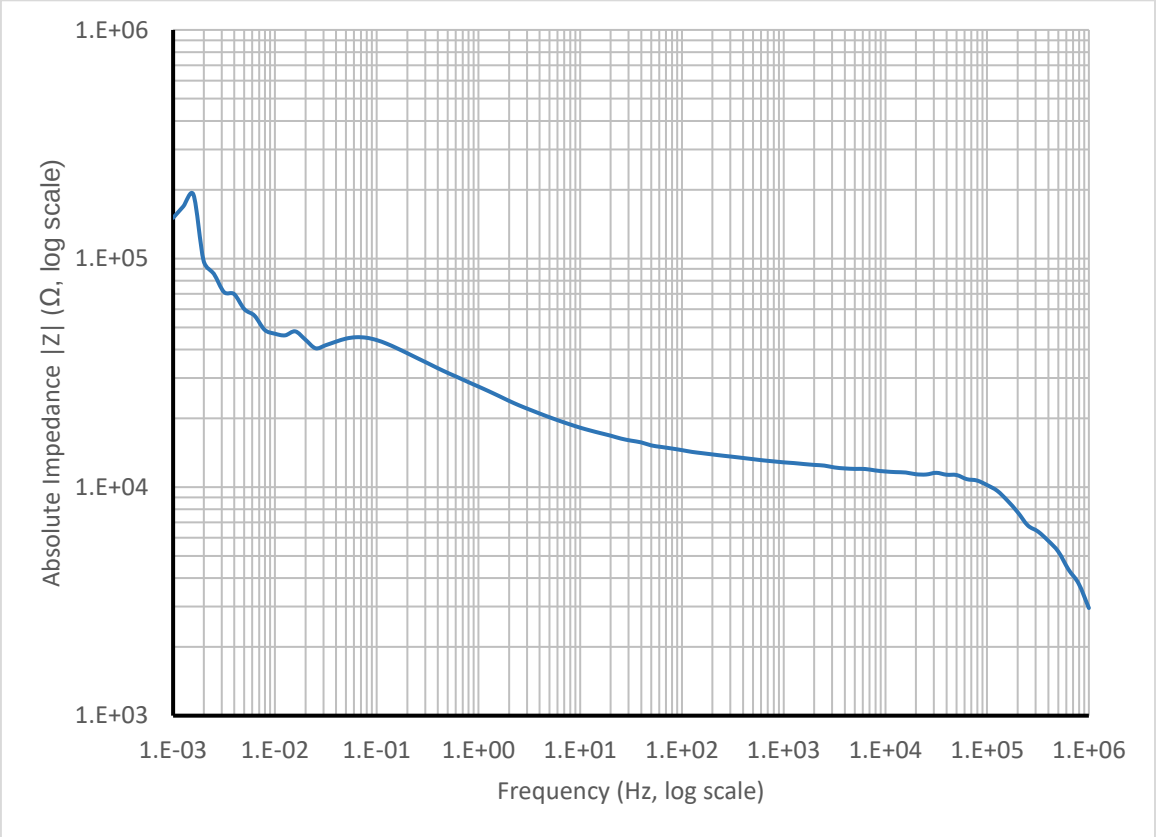

Figure 5.10 The absolute impedance (|Z|) of PEO:CNT:Li supercapacitors with PEO:CNT active layers and PEO:Li spacer (W1Q2) at various frequencies.

After testing the sample with CV and EIS for examining its charge mobility and impedance change with different frequencies, the performance of the electrochemical system is determined by cyclic charge-discharge measurement (CCD). In CCD, the sample has been charged up with a constant current of ±10 μA, which the direction of current will be changed for every 60 s to become a cycle, therefore the charging performance on both poles can be investigated. During charging, the corresponding potential change along the charging time in the supercapacitor is measured. The period for the charging cycle is suggested to be at least 75% of the maximum potential that can be obtained in the initial run. The charge-discharge cycle will continue to run until the potential obtained is exceeded the limit that may destroy the sample (i.e. ±10 V in VersaSTAT3).

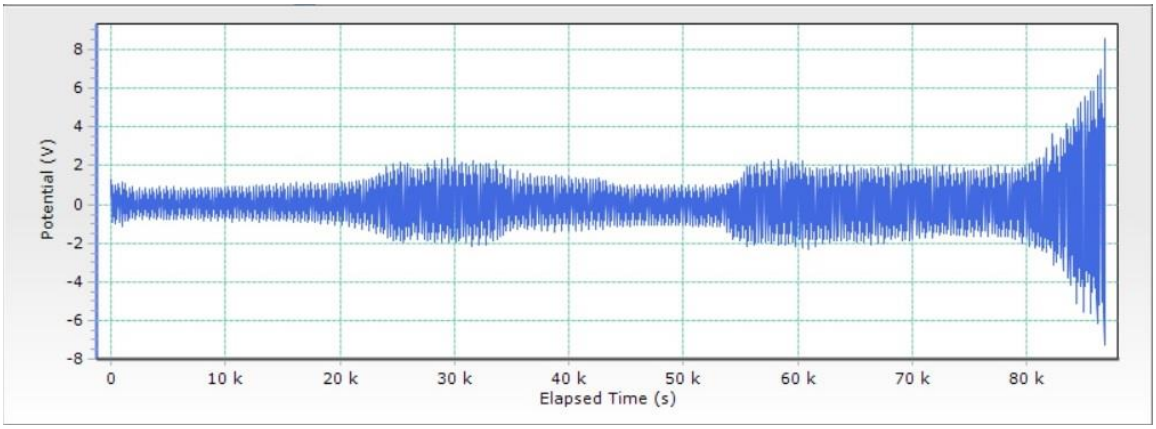

Figure 5.11 The potential change of PEO:CNT:Li supercapacitor with PEO:CNT active layers and PEO:Li spacer (W1Q2) at a constant current of ±10 μA with a charging period of 60 s in each direction under cyclic charge-discharge measurement.

In Figure 5.11, the potential change of sample W1Q2 along the time under cyclic charge-discharge cycles is illustrated. Under a constant supply of current, the

potential of the sample during charging is between ±1.2 V to ±2.0 V with several fluctuations for the 660 cycles. Afterwards the potential rapidly increased and the sample died-out at 723rd cycle.

To investigate the condition of sample after being died-out, the sample is re-examined by CV and EIS to determine its electrochemical properties after cyclic charge-discharge measurement.

The comparison of maximum current density before and after CCD measurement at different scan rates are tabulated in Table 5.9, and the cyclic voltammetry at various scan rates after the sample being run for cyclic charge-discharge measurement is shown in Figure 5.12. The maximum current density of W1Q2 at 100 mV/s after CCD measurement is about 9.46 μA/cm^2. The current density is then dropped with the decrease of scan rate, and gives 5.63 μA/cm^2 at 10 mV/s.

Table 5.9 Comparison of maximum current density measured from PEO:CNT:Li supercapacitor with PEO:CNT active layers and PEO:Li spacer (W1Q2), by cyclic voltammetry between -0.5 V and +0.5 V under different scan rates before and after galvanostatic charge-discharge measurement.

Sample	100 mV/s	50 mV /s	20 mV/s	10 mV/s
Before charge-discharge	29.70 (0%)	25.78	18.15	12.08
After charge-discharge	9.46 (-68.1%)	8.22	7.98	5.63

*all units are in μA/cm^2

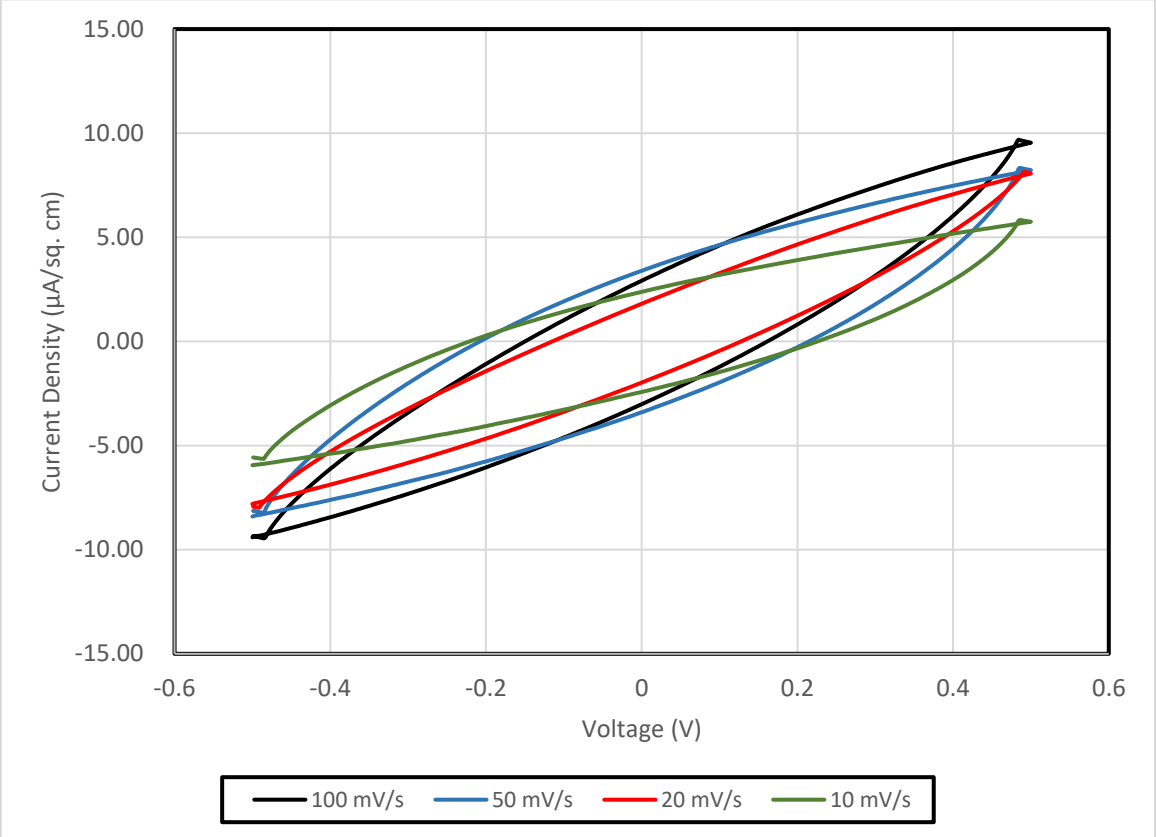

Figure 5.12 Cyclic voltammogram of PEO:CNT:Li supercapacitor with PEO:CNT active layers and PEO:Li spacer (W1Q2) at different scan rates after galvanostatic charge-discharge measurement.

Besides CV, the sample has been examined by EIS to investigate the impedance change along the frequency after CCD measurement being taken place. The comparison of absolute impedance of the sample before and after cyclic charge-discharge measurement are tabulated in Table 5.10 and illustrated in Figure 5.13.

Table 5.10 Comparison of absolute impedance of PEO:CNT:Li supercapacitor with PEO:CNT active layers and PEO:Li spacer (W1Q2), by electrochemical impedance spectroscopy at different frequencies before and after galvanostatic charge-discharge measurement.

Sample	1 mHz	1 Hz	1 kHz	1 MHz
Before charge-discharge				
Absolute Impedance (|Z|)	150.57 kΩ	27.53 kΩ	12.83 kΩ	2.96 kΩ
Resistance (R)	123.15 kΩ	26.38 kΩ	12.81 kΩ	2.84 kΩ
Reactance (X)	-86.64 kΩ	-7.88 kΩ	-628.65 Ω	834.92 Ω
After charge-discharge				
Absolute Impedance (|Z|)	10.84 MΩ (+7199.3%)	56.69 MΩ	10.67 MΩ	7.49 kΩ
Resistance (R)	10.84 MΩ (+8802.3%)	55.64 MΩ	8.17 MΩ	7.45 kΩ
Reactance (X)	455.24 Ω (-99.5%, properties change)	-10.84 MΩ	-6.87 MΩ	-741.12 Ω

It can be observed that after CCD measurement and the sample died-out, the absolute impedance of the sample has been increased for 2-3 order of magnitudes in the frequency range below 1 kHz, and more than two times at 1 MHz. This increase of impedance can be suggested as an establishment of depletion layer in the PEO-matrix. When the sample is repeatedly charged-up for hundreds of cycles, some of the oxygen atoms in the PEO matrix will be oxidized and the efficiency for these atoms to form complexation site with Li^+ ions will be decreased (see Chapter

4 for the mechanism). As the oxidation of PEO increases the material impedance, and the yield of forming complexation is decreased, the mobility of Li^+ ions in the PEO matrix will be weakened and less current can pass through the electrochemical system. As a result, the charge storage capability of the system is being decreased.

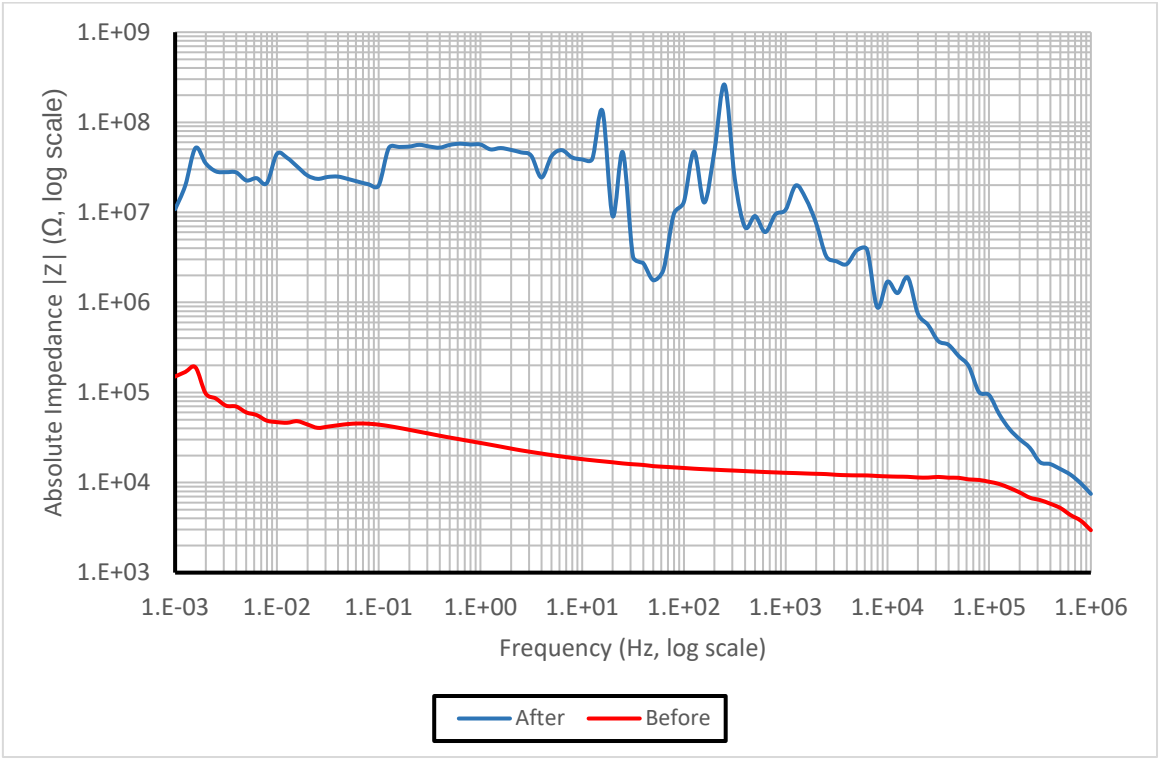

Figure 5.13 The comparison of absolute impedance (|Z|) of PEO:CNT:Li supercapacitors with PEO:CNT active layers and PEO:Li spacer (W1Q2) at various frequencies before and after galvanostatic charge-discharge measurement.

5.2.2 Performance of supercapacitor with PEO:CNT:Li active layers and pure PEO spacer (W2F1)

For this sample, a layer of PEO:CNT:Li was casted on the copper-plated polyester fabrics, two pieces of PEO:CNT:Li casted fabrics were then laminated together with a layer of pure PEO as spacer.

By examining the sample with cyclic voltammetry at various scan rates as shown in Figure 5.14, the maximum current density of W2F1 at 100 mV/s within ±0.5V is found about 3.87 μA/cm^2. The current density is then dropped with the decrease of scan rate, and gives 0.60 μA/cm^2 at 10 mV/s. Compared to the control sample W1F1, which has PEO:CNT as active layers and pure PEO as spacer, with the maximum current density of 10.51 μA/cm^2, the current density of W2F1 is about 1/3 of the control sample. It is suggested that the presence of Li^+ ions in active layers cannot enhance the charge mobility in the electrochemical system. The current passing through the effective laminated area from the electrode (copper-plated polyester fabric) to the PEO:CNT active layers and spacer has not been increased. However, the specific capacitance of the W2F1 (292.88 nF/cm^2) is nearly ten times more than that of W1F1 (32.80 nF/cm^2), it seems that the increase of charge storage capability is due to the combination of PEO:CNT:Li in the active layers.

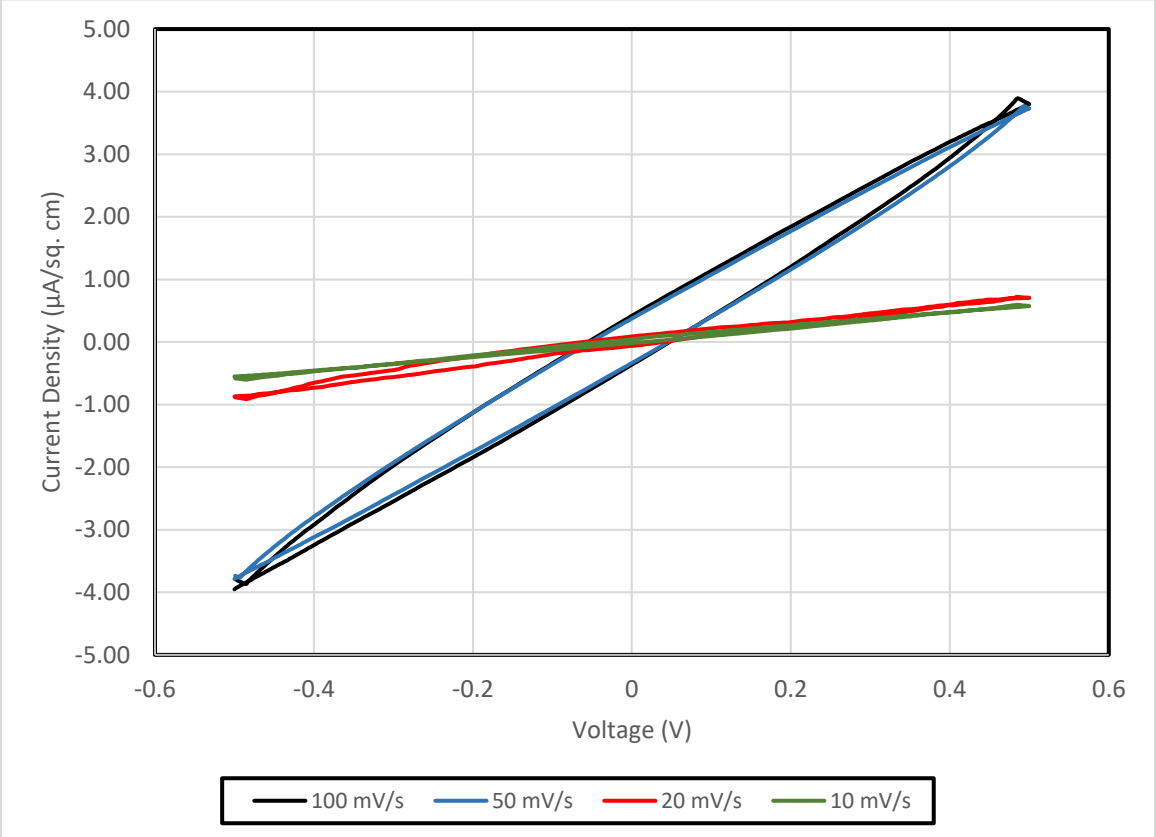

Figure 5.14 Cyclic voltammogram of PEO:CNT:Li supercapacitor with PEO:CNT:Li active layers and pure PEO spacer (W2F1) at different scan rates before galvanostatic charge-discharge measurement.

To study the impedance changes of sample with respect to the frequency responses, the sample has been examined by electrochemical impedance spectroscopy (EIS) in the range of 1 mHz to 1 MHz. The change of absolute impedance |*Z*| of the sample has been illustrated in Figure 5.15. It can be seen that at very low to low frequency range (1 mHz to 1 Hz), the absolute impedance is in a relative high range, since at this frequency range, the impedance is dominated by frequency independent element (resistance) instead of frequency dependent element (reactance). When the frequency has been increased from 1 Hz to 10 kHz, the absolute impedance keeps at a steady level until it increases to 100 kHz, the

influence from frequency dependent element (reactance) becomes significant, resulting to the decrease of absolute impedance.

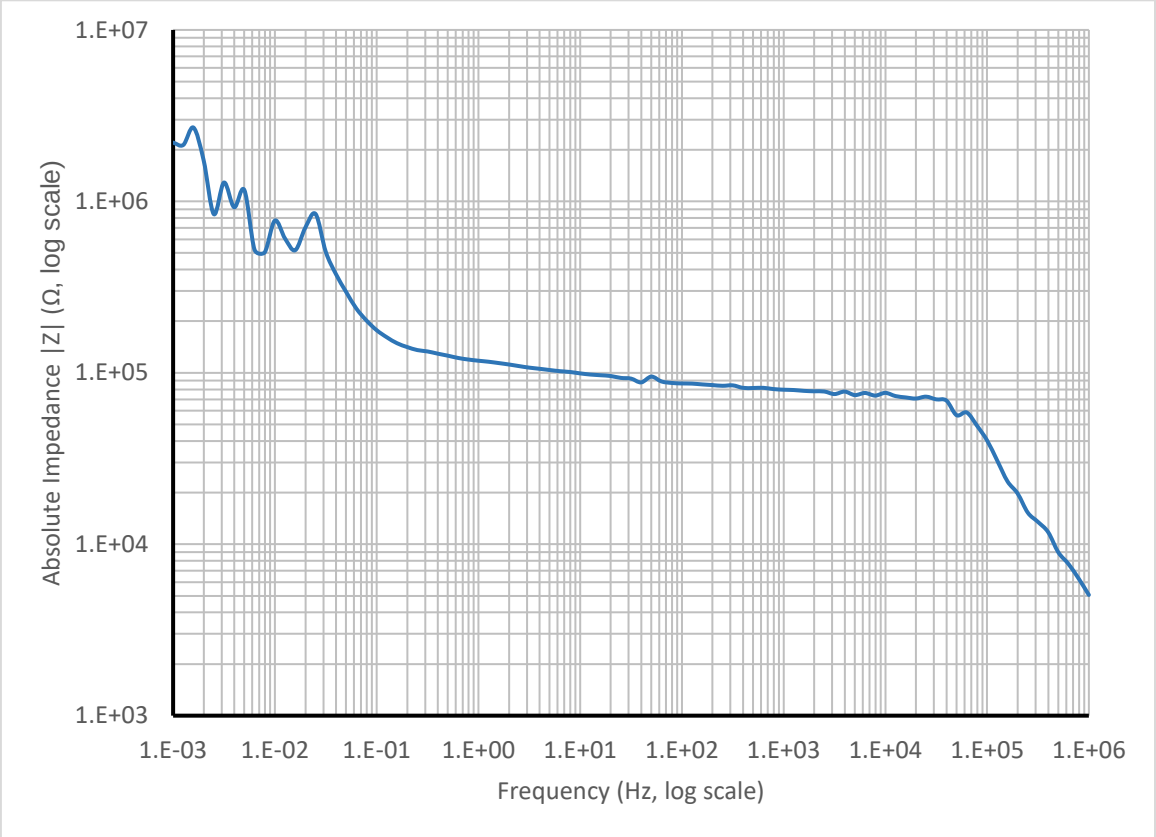

Figure 5.15 The absolute impedance (|Z|) of PEO:CNT:Li supercapacitors with PEO:CNT:Li active layers and pure PEO spacer (W2F1) at various frequencies.

After testing the sample with CV and EIS for examining its charge mobility and impedance change with different frequencies, the performance of the electrochemical system is then determined by cyclic charge-discharge measurement (CCD). In CCD, the sample has been charged up with a constant current of ±10 μA, which the direction of current will be changed for every 60 s to become a cycle, therefore the charging performance on both poles can be investigated.

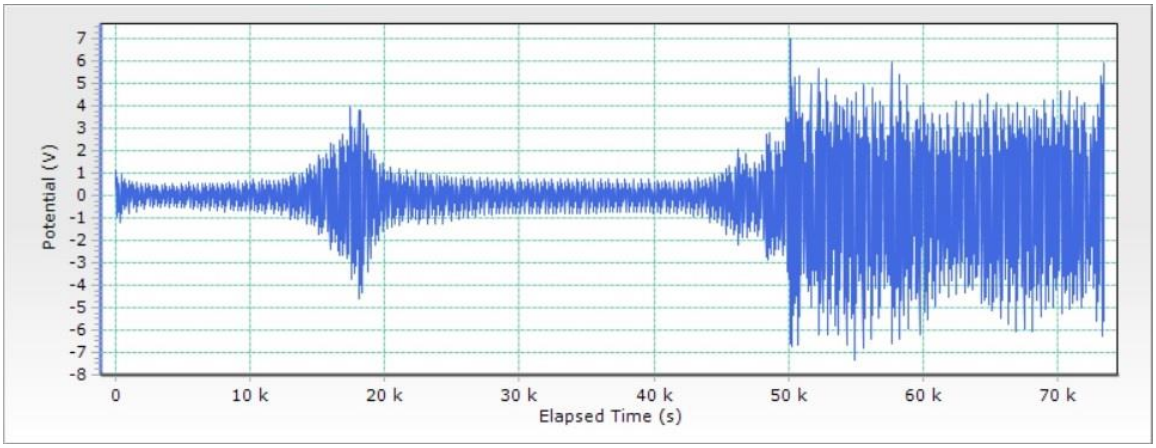

Figure 5.16 The potential change of PEO:CNT:Li supercapacitor with PEO:CNT:Li active layers and pure PEO spacer (W2F1) at a constant current of ±10 μA with a charging period of 60 s in each direction under cyclic charge-discharge measurement.

In Figure 5.16, the potential change of sample W2F1 along the time under cyclic charge-discharge cycles is illustrated. Under a constant supply of current, the potential of the sample during charging is about ±0.8 V from the beginning to 117th cycle. Then the potential increases until it reaches the peak at 153th cycle with ±4.0 V, then the potential decreases back to ±0.8 V after 225th cycle. The potential

increases again after 370th cycle and fluctuates with ±6.0 V. Afterwards the potential rapidly increased at 605th cycle and the sample died-out at 612th cycle.

To investigate the condition of sample after being died-out, the sample is re-examined by CV and EIS to determine its electrochemical properties after cyclic charge-discharge measurement.

Figure 5.17 shows the cyclic voltammetry at various scan rates after the sample has been run for cyclic charge-discharge measurement. The comparison of maximum current density before and after the CCD measurement at different scan rates is tabulated in Table 5.11. The maximum current density of W2F1 at 100 mV/s after CCD measurement is about 0.16 μA/cm^2. The current density is then dropped with the decrease of scan rate, and gives 0.12 μA/cm^2 at 10 mV/s.

Table 5.11 Comparison of maximum current density measured from PEO:CNT:Li supercapacitor with PEO:CNT:Li active layers and pure PEO spacer (W2F1), by cyclic voltammetry between -0.5 V and +0.5 V under different scan rates before and after galvanostatic charge-discharge measurement.

Sample	100 mV/s	50 mV /s	20 mV/s	10 mV/s
Before charge-discharge	3.87 (0%)	3.76	0.91	0.60
After charge-discharge	0.16 (-95.9%)	0.13	0.12	0.12

*all units are in μA/cm^2

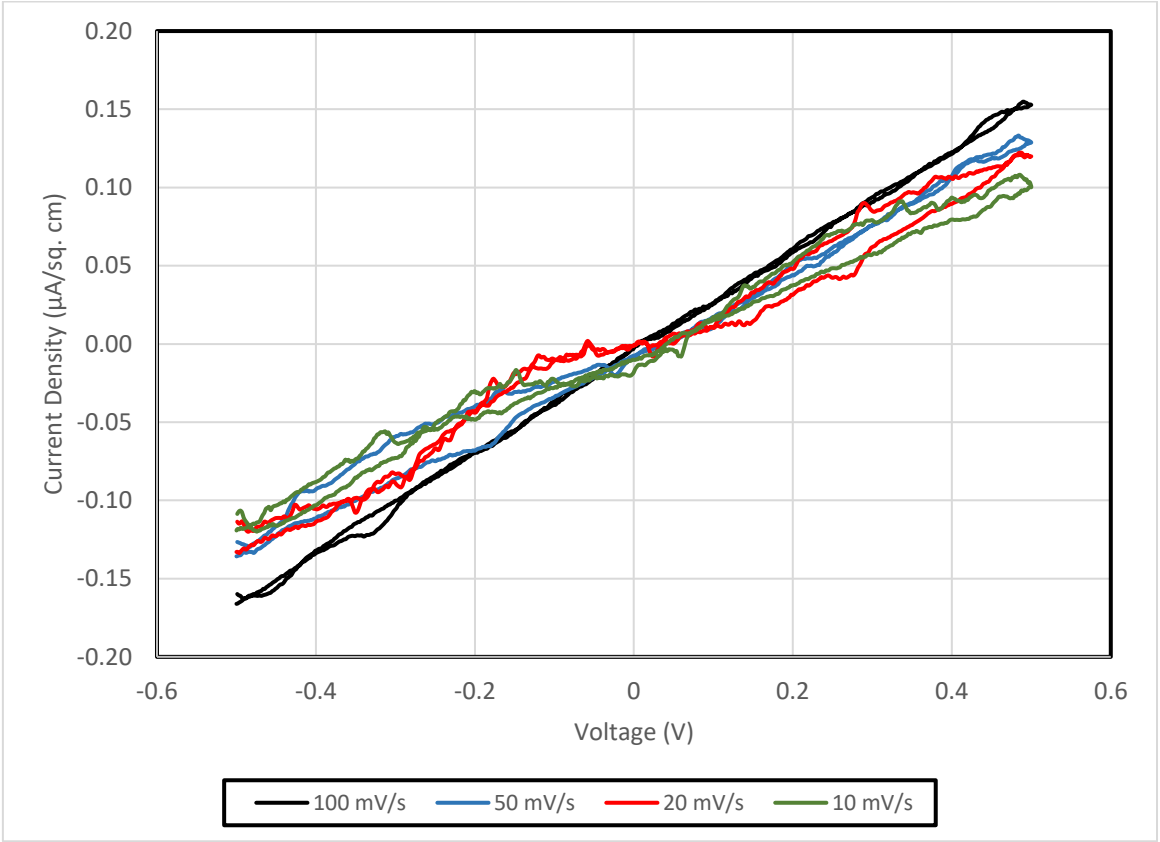

Figure 5.17 Cyclic voltammogram of PEO:CNT:Li supercapacitor with PEO:CNT:Li active layers and pure PEO spacer (W2F1) at different scan rates after galvanostatic charge-discharge measurement.

Besides CV, the sample has been examined by EIS to investigate the impedance change along the frequency after CCD measurement taken place. The comparison of absolute impedance of the sample before and after cyclic charge-discharge measurement is tabulated in Table 5.12 and illustrated in Figure 5.18. it can be observed that after CCD measurement and the sample died-out, the absolute impedance of the sample at 1 mHz has been decreased for 50%, and become double in the frequency range of 1 Hz to 10 kHz, and more or less the same after 100 kHz. The increase of impedance after 1 Hz can be suggested as an establishment of depletion layer in the PEO-matrix. As the oxidation of PEO will increase the material impedance, and the yield of forming complexation has been decreased, Li^+ ions mobility in the PEO matrix will be weaken and less current can pass through the electrochemical system. Therefore, the charge storage capability of the system will be decreased.

Table 5.12 Comparison of absolute impedance of PEO:CNT:Li supercapacitor with PEO:CNT:Li active layers and pure PEO spacer (W2F1), by electrochemical impedance spectroscopy at different frequencies before and after galvanostatic charge-discharge measurement.

Sample	1 mHz	1 Hz	1 kHz	1 MHz
Before charge-discharge				
Absolute Impedance (|Z|)	2.20 MΩ	117.59 kΩ	79.66 kΩ	5.06 kΩ
Resistance (R)	2.14 MΩ	116.63 kΩ	79.66 kΩ	5.05 kΩ
Reactance (X)	-528.00 kΩ	-15.00 kΩ	-377.70 Ω	250.75 Ω
After charge-discharge				
Absolute Impedance (|Z|)	1.11 MΩ (-49.5%)	232.93 kΩ	199.96 kΩ	5.51 kΩ
Resistance (R)	1.05 MΩ (-50.9%)	231.83 kΩ	199.95 kΩ	5.50 kΩ
Reactance (X)	-381.39 kΩ (-27.8%)	-22.67 kΩ	-1.98 kΩ	-316.51 Ω

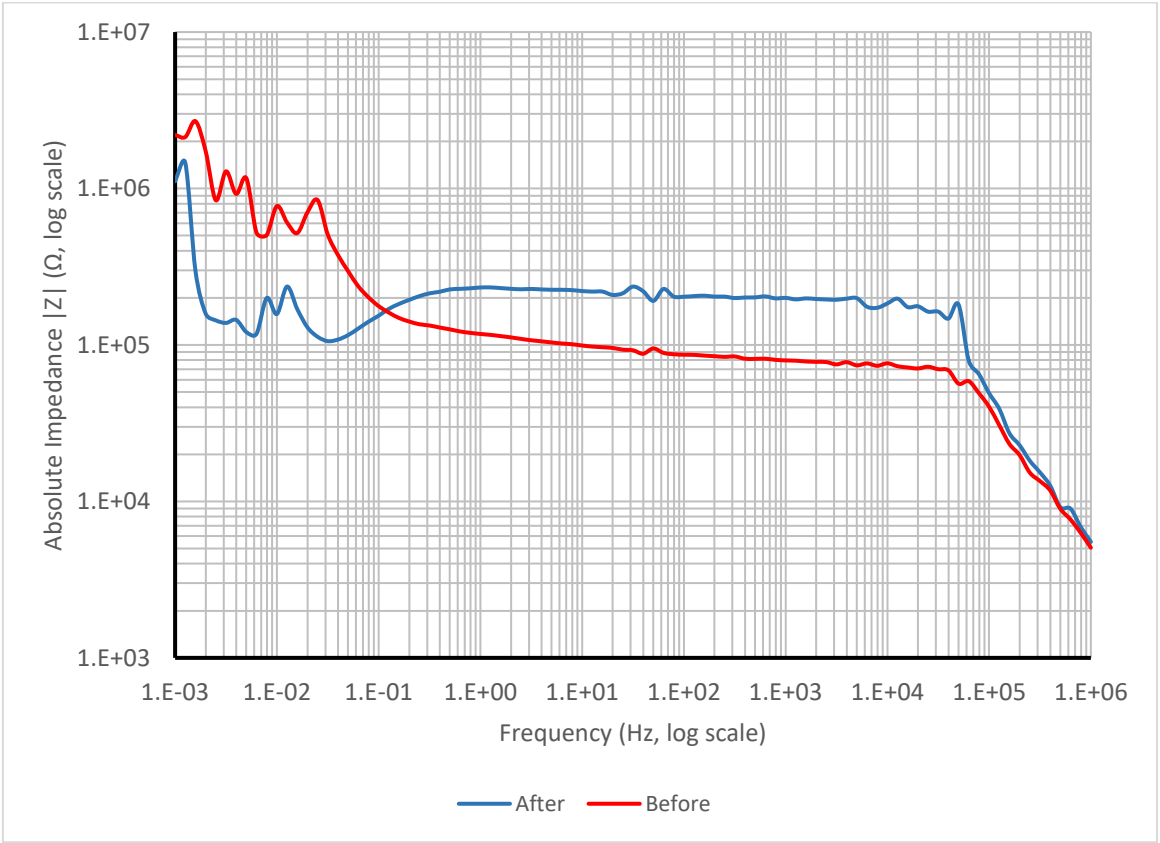

Figure 5.18 The comparison of absolute impedance (|Z|) of PEO:CNT:Li supercapacitors with PEO:CNT:Li active layers and pure PEO spacer (W2F1) at various frequencies before and after galvanostatic charge-discharge measurement.

5.2.3 Performance of supercapacitor with PEO:CNT:Li active layers and PEO:Li spacer (W2Q2)

For this sample, a layer of PEO:CNT:Li was casted on the copper-plated polyester fabrics, two pieces of PEO:CNT:Li casted fabrics were then laminated together with a layer of PEO:Li as spacer.

By examining the sample with cyclic voltammetry at various scan rates as shown in Figure 5.19, the maximum current density of W2Q2 at 100 mV/s within ±0.6V is about 49.75 μA/cm^2. The current density is then dropped with the decrease of scan rate, and gives 9.29 μA/cm^2 at 10 mV/s. Compared to sample W1Q2, which has PEO:CNT as active layers and PEO:Li as spacer, with the maximum current density of 29.70 μA/cm^2, the current density of W2Q2 is about 70% more than that of W1Q2. On the other hand, by comparing with sample W1F1 and W2F1, which are using pure PEO as spacer, the current density of samples using PEO:Li as spacer much higher than that pure PEO one. Therefore, it is suggested that the presence of Li^+ ions in spacer can enhance the charge mobility in the electrochemical system. The current passing through the effective laminated area from the electrode (copper-plated polyester fabric) to the PEO:CNT active layers and spacer has been increased. As a result, the specific capacitance of the system is increased, and it implies the increase of charge storage capability.

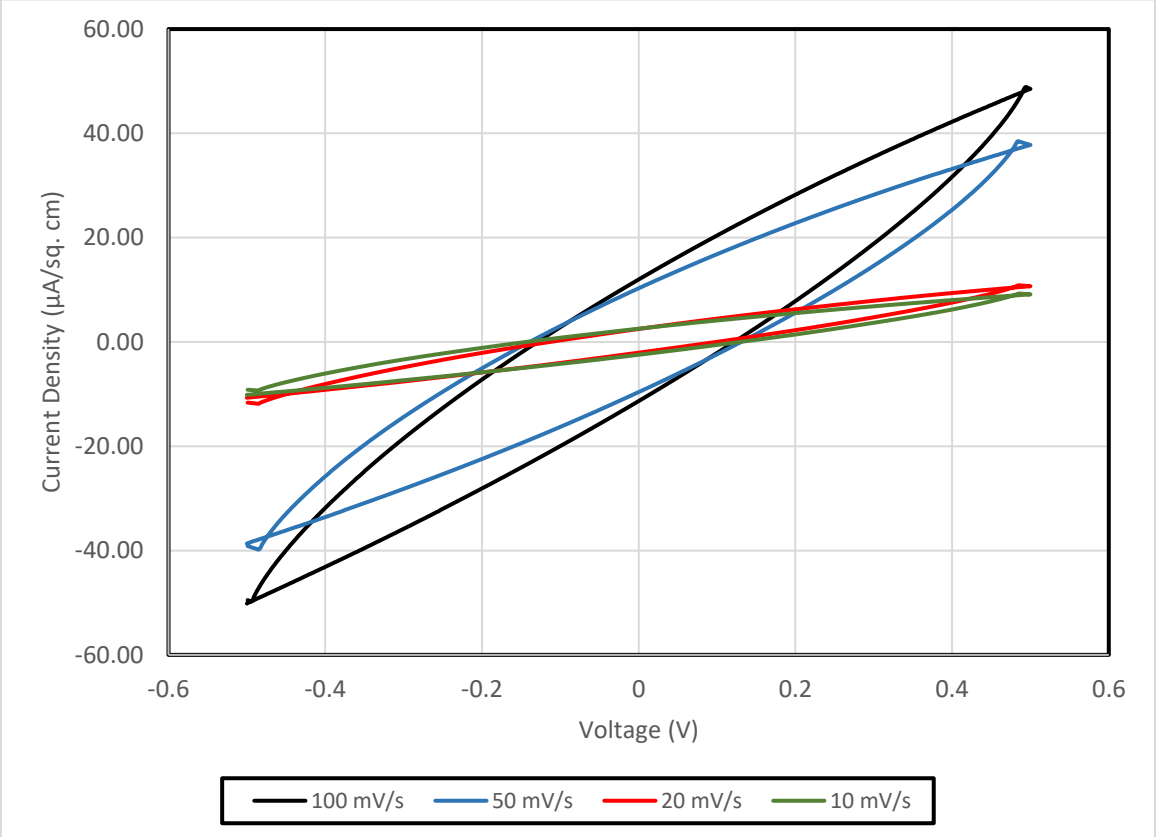

Figure 5.19 Cyclic voltammogram of PEO:CNT:Li supercapacitor with PEO:CNT:Li active layers and PEO:Li spacer (W2Q2) at different scan rates before galvanostatic charge-discharge measurement.

To study the impedance changes of sample with respect to the frequency responses, the sample has been examined by electrochemical impedance spectroscopy (EIS) in the range of 1 mHz to 1 MHz. The change of absolute impedance |*Z*| of the sample has been illustrated in Figure 5.20.

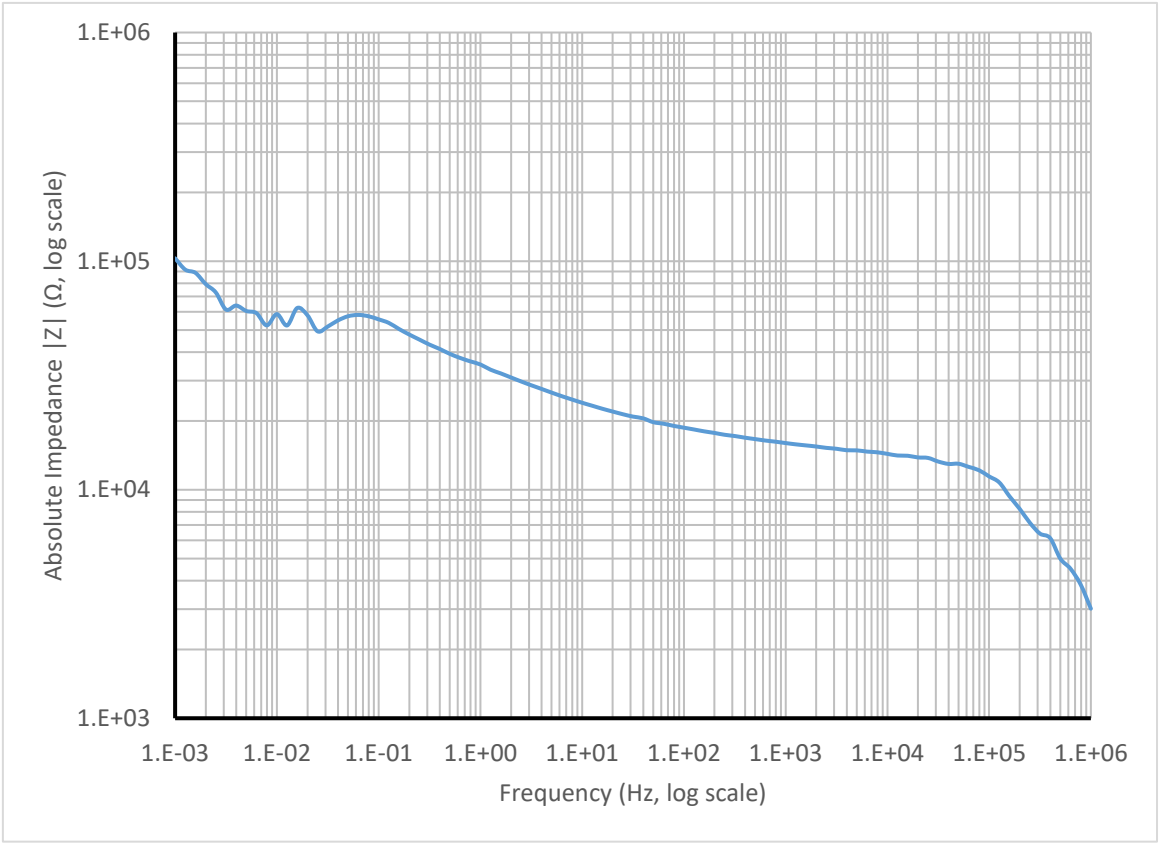

Figure 5.20 The absolute impedance (|Z|) of PEO:CNT:Li supercapacitors with PEO:CNT:Li active layers and PEO:Li spacer (W2Q2) at various frequencies.

It can be seen that at very low frequency range (1 mHz to 100 mHz), the absolute impedance is in a relative high range, since at this frequency range, the impedance is dominated by frequency independent element (resistance) instead of frequency dependent element (reactance). When the frequency has been increased to 1 Hz or even higher to 100 kHz, the influence from frequency dependent element (reactance) increases, resulting to the gradually decrease of absolute impedance.

Once the frequency increases towards 100 kHz, the absolute impedance rapidly drops.

After testing the sample with CV and EIS for examining its charge mobility and impedance change with different frequencies, the performance of the electrochemical system is then determined by cyclic charge-discharge measurement (CCD). In CCD, the sample has been charged up with a constant current of ±10 μA, which the direction of current will be changed for every 60 s to become a cycle, therefore the charging performance on both poles can be investigated.

In Figure 5.21, the potential change of sample W2Q2 along the time under cyclic charge-discharge cycles is illustrated. Under a constant supply of current, the potential of the sample during charging becomes steady at ±1.8 V after 13th cycle. Until 63rd cycle, the potential rapidly increased and the sample died-out at 76th cycle.

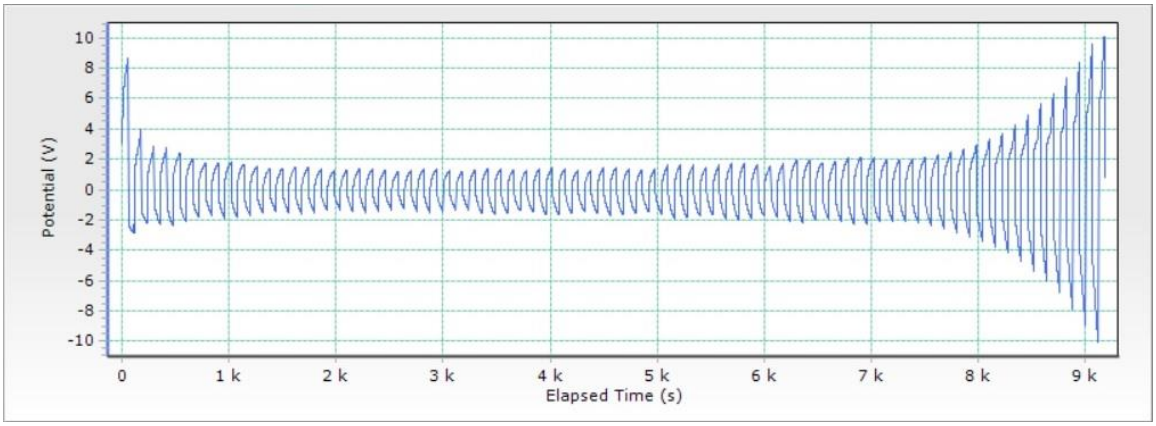

Figure 5.21 The potential change of PEO:CNT:Li supercapacitor with PEO:CNT:Li active layers and PEO:Li spacer (W2Q2) at a constant current of ±10 μA with a charging period of 60 s in each direction under cyclic charge-discharge measurement.

To investigate the condition of sample after died-out, the sample is re-examined by CV and EIS to determine its electrochemical properties after cyclic charge-discharge measurement.

Figure 5.22 shows the cyclic voltammetry at various scan rates after the sample has been run for cyclic charge-discharge measurement. The comparison of maximum current density before and after the CCD measurement at different scan rates is tabulated in Table 5.13. The maximum current density of W2Q2 at 100

mV/s after CCD measurement is about 0.56 μA/cm^2. The current density is then dropped with the decrease of scan rate, and gives 0.26 μA/cm^2 at 10 mV/s.

Table 5.13 Comparison of maximum current density measured from PEO:CNT:Li supercapacitor with PEO:CNT:Li active layers and PEO:Li spacer (W2Q2), by cyclic voltammetry between -0.5 V and +0.5 V under different scan rates before and after galvanostatic charge-discharge measurement.

Sample	100 mV/s	50 mV /s	20 mV/s	10 mV/s
Before charge-discharge	49.75 (0%)	39.80	11.83	9.29
After charge-discharge	0.56 (-98.9%)	0.55	0.28	0.26

*all units are in μA/cm^2

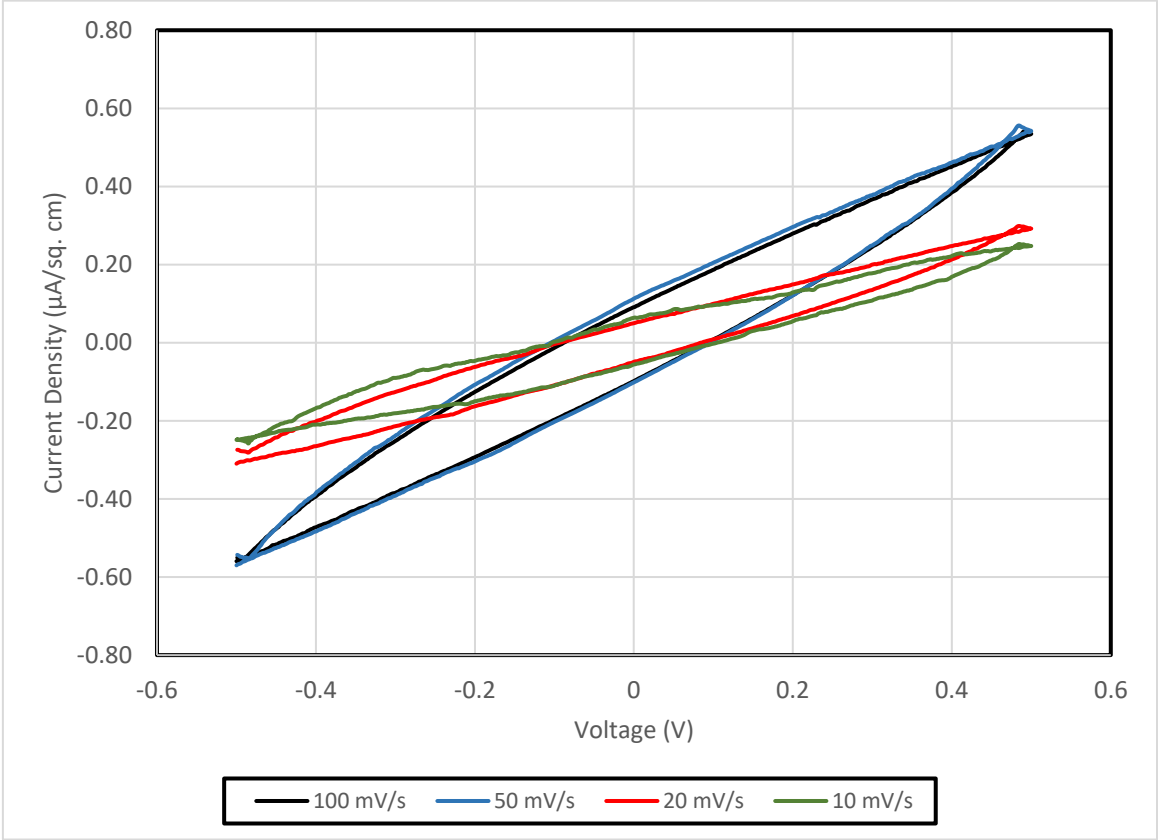

Figure 5.22 Cyclic voltammogram of PEO:CNT:Li supercapacitor with PEO:CNT:Li active layers and PEO:Li spacer (W2Q2) at different scan rates after galvanostatic charge-discharge measurement.

Besides CV, the sample has been examined by EIS to investigate the impedance change along the frequency after CCD measurement taken place. The comparison of absolute impedance of the sample before and after cyclic charge-discharge measurement is tabulated in Table 5.14 and illustrated in Figure 5.23. It can be observed that after CCD measurement and the sample died-out, the absolute impedance of the sample has been increased for two order of magnitudes in the frequency range below 10 kHz. After10 kHz, the difference will be decreased to one order of magnitude. This increase of impedance can be suggested as an establishment of depletion layer in the PEO-matrix.

Table 5.14 Comparison of absolute impedance of PEO:CNT:Li supercapacitor with PEO:CNT:Li active layers and PEO:Li spacer (W2Q2), by electrochemical impedance spectroscopy at different frequencies before and after galvanostatic charge-discharge measurement.

Sample	1 mHz	1 Hz	1 kHz	1 MHz
Before charge-discharge				
Absolute Impedance (|Z|)	102.83 kΩ	35.29 kΩ	15.99 kΩ	3.02 kΩ
Resistance (R)	77.62 kΩ	34.30 kΩ	15.95 kΩ	2.93 kΩ
Reactance (X)	-67.45 kΩ	-8.32 kΩ	-1.14 kΩ	733.33 Ω
After charge-discharge				
Absolute Impedance (|Z|)	7.24 MΩ (+7040.7%)	1.79 MΩ	1.50 MΩ	6.64 kΩ
Resistance (R)	6.40 MΩ (+8245.3%)	1.79 MΩ	1.50 MΩ	6.60 kΩ
Reactance (X)	-3.39 MΩ (+5025.9%)	-153.68 kΩ	-32.69 kΩ	-645.53 Ω

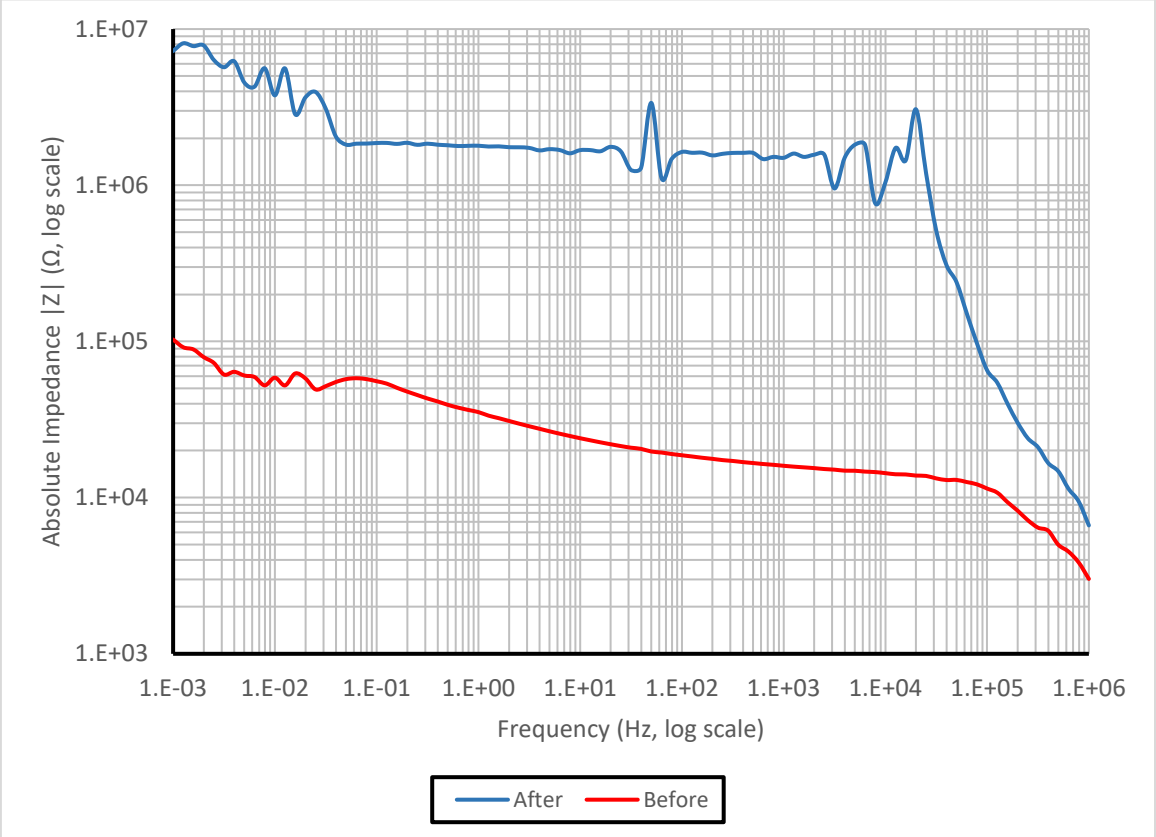

Figure 5.23 The comparison of absolute impedance (|Z|) of PEO:CNT:Li supercapacitors with PEO:CNT:Li active layers and PEO:Li spacer (W2Q2) at various frequencies before and after galvanostatic charge-discharge measurement.

5.3 Performance comparison of PEO-based supercapacitors with different dopants and layering combinations

In this study, PEO-based supercapacitors with different types of dopants and layering combinations were fabricated and examined. The specific capacitance and absolute impedance measured at 40 Hz, and the maximum current density obtained from scan rate of 100 mV/s are tabulated in Table 5.15.

Table 5.15 Performance comparison of PEO-based supercapacitors with different dopants and layering combinations.

Sample	C_{sp}	|Z|	J_{max}
Pure PEO	1.89 nF/cm^2 (0%)	56.73 MΩ (0%)	177 nA/cm^2 (0%)
PEO:Li (mass ratio 100:1)	33.56 nF/cm^2 (+1775.7%)	7.12 MΩ (-87.4%)	1.84 μA/cm^2 (+1039.5%)
PEO:DW-CNT (same as W1F1)	32.80 nF/cm^2 (+1735.4%)	4.09 MΩ (-92.8%)	10.51 μA/cm^2 (+5937.9%)
PEO:CNT active layers and PEO:Li spacer (W1Q2)	10.19 μF/cm^2 (+5391.53%)	1.41 MΩ (-97.5%)	29.70 μA/cm^2 (+16779.7%)
PEO:CNT:Li active layers and Pure PEO spacer (W2F1)	292.88 nF/cm^2 (+15496.3%)	700.72 kΩ (-98.8%)	3.87 μA/cm^2 (+2186.4%)
PEO:CNT:Li active layers and PEO:Li spacer (W2Q2)	238.43 nF/cm^2 (+12615.3%)	1.33 MΩ (-97.7%)	49.75 μA/cm^2 (+28107.3%)
C_{sp}: Specific Capacitance at 40 Hz |Z|: Absolute Impedance at 40 Hz J_{max}: Maximum current density at scan rate of 100 mV/s			

Compared to the samples prepared in the previous chapter, it is no doubt that CNT and Li^+ ions can enhance the charge storage capability of the electrochemical system, and improve the efficiency of current passing through the PEO matrix. Besides, it can be found that the charge storage capability of PEO-based supercapacitors doped with both CNT and Li^+ ions are better than those samples have only doped either CNT or Li^+ ions.

By comparing sample W2F1 and W2Q2, though the presence of Li^+ ions in the spacer could increase the current density of the sample, the sample tolerance was sacrificed and the charging cycle was deduced from more than 600 cycles to less than 100 cycles.

Compared to sample W2Q2, the active layers in sample W1Q2 only consist of PEO and DW-CNT, which gave a lower value of current density. However, the charge storage capability of W1Q2 is the highest in all of the PEO-based supercapacitors, and the sample tolerance is higher than that of W2Q2, which can charge for more than 700 cycles. It is suggested that the electrochemical system with PEO-based material can be enhanced by doping Li^+ ions and DW-CNT separately to achieve a better performance instead of mixing both dopants together.

Chapter 6

Conclusions & Recommendations

6.1 Conclusions

In this study, polyester fabrics were metalized by electroless nickel plating and cyanide-free electroless copper plating to become flexible metalized fabrics. PEO-based electrolytic materials doped with different amount of lithium salt and different types of nanocarbons were solution casted on the fabric surface to form an electrolytic active layer. Two casted fabrics were laminated together with PEO-based spacer to form a supercapacitor. The surface morphology, electrochemical properties and electrical performance of these electrochemical systems were studied by various characterization techniques.

In the experiment of PEO-based supercapacitors doped with different amount of lithium salt, the copper-plated polyester fabrics were solution casted with pure PEO solution, and PEO solution doped with 1 g/L of $LiClO_4$ in different PEO:Li ratio (1000:1, 667:1, 500:1, 400:1, 333:1 and 100:1). By the impedance analyzer, it can be found that the specific capacitance of the sample casted with PEO:Li ratio of 100:1 exhibited the highest value under a low range frequency at 40 Hz, which is nearly 18 times higher than that of the sample casted with pure PEO. Besides, by cyclic voltammetry, the maximum current density of the sample casted with PEO:Li ratio of 100:1 obtained under the scan rate of 100 mV/s also gave the highest value

in all 7 samples, which was 10 times more than that of the sample casted with pure PEO. It was suggested that the presence of Li^+ ions in PEO matrix could provide an enhancement of charge mobility in the electrolyte by providing sufficient ions to move between different active sites on the branches and backbones of the PEO matrix. Hence, the improvement of charge storage capability was then manifested.

In the experiment of PEO-based supercapacitors doped with different types of nanocarbons, the copper-plated polyester fabrics were solution casted with four types of nanocarbons. When nanocarbons were doped into the samples, the charge storage capability of the electrochemical system will be largely increased, since nanocarbons provided a large surface area to capture free charges in the system. In the experiment, DW-CNT gave the highest value of specific capacitance, which was 17 times more than that of the sample casted with only pure PEO. On the side of maximum current density, sample doped with DW-CNT showed a large enhancement of nearly 60 times higher than that of sample with only pure PEO at 40 Hz. DW-CNT can provide better electrical properties than other type of nanocarbons such better lifetimes and current density under an electric field applied.

For the experiment of various layer combinations, PEO-based supercapacitors doped with DW-CNT and Li^+ ions under different layering combinations were fabricated and examined. Compared to the sample casted with pure PEO, the specific capacitance of PEO:CNT:Li supercapacitors have been increased for 126 times (sample W2Q2) to 5390 times (sample W1Q2) more than that of the pure

PEO sample. On the other hand, the maximum current density of PEO:CNT:Li supercapacitors has been improved for 22 times (sample W2F1) to 281 times (sample W2Q2) than that of the pure PEO sample.

Comparing to the samples doped with single dopant, it is no doubt that CNT and Li^+ ions can enhance the charge storage capability of the electrochemical system, and improve the efficiency of current passing through the PEO matrix. Besides, it can be found that the charge storage capability of PEO-based supercapacitors doped with both CNT and Li^+ ions are better than those samples have only doped either CNT or Li^+ ions.

Comparing the performance of sample W2F1 and W2Q2, though the presence of Li^+ ions in the spacer could increase the current density of the sample in W2Q2, the sample tolerance was sacrificed and the charging cycle was deduced from more than 600 cycles to less than 100 cycles.

Compared to sample W2Q2, the active layers in sample W1Q2 only consisted of PEO and DW-CNT, which gave a lower value of current density. However, the charge storage capability of W1Q2 is the highest in all of the PEO-based supercapacitors, and the sample tolerance is higher than that of W2Q2, which can charge for more than 700 cycles. It is suggested that the electrochemical system with PEO-based material can be enhanced by doping Li^+ ions and DW-CNT separately to achieve a better performance instead of mixing both dopants together.

6.2 Recommendations

In this study, the PEO-based supercapacitors doped with different amount of $LiClO_3$ and different types of nanocarbons were prepared to examine the performance of charge storage capability. Compared to other researches and reports, the PEO-based electrolyte prepared in this study was only consisted of deionized water, PEO and dopants, but no extra solvents have been used in experiment. This act can ensure all the electrochemical responses are attributed to PEO and dopants instead of other solvents involved. Therefore, in-depth studies on different combinations of water-soluble polymers with various types of alkaline metal salts can be done.

Besides, in the experiment, double-walled carbon nanotube (DW-CNT) was found to give a better performance in charge accumulation at the electrode and hence the charge storage capability has been enhanced. For further study in this phenomenon, PEO-base electrolyte doped with different concentration of DW-CNT can be prepared to investigate the effect of DW-CNT to the charge storage performance.

Once the study on different combinations of water-soluble polymers with various types of alkaline metal salts have been done, and the optimum amount of DW-CNT has been obtained from the experiments suggested above, different layering combinations with polymeric electrolyte, salts and DW-CNT can be studies and the effects on these ingredients can be investigated.

Besides the study on various materials and the investigation of structural combinations, the physical performances of these supercapacitors such as wearability, flexibility, tolerance of materials after wash can be taken place, since if these supercapacitors are being commercialized as wearable smart clothes, the durability and reliability of products will be the crucial factors for consumers to concern.

Reference

[1] **Liu, C.G., Yu, Z.N., Neff, D., Zhamu, A. and Jang, B. Z.** "Graphene-based supercapacitor with an ultrahigh energy density", *Nano Letter*, Vol.10, pp.4863-4868 (2010)

[2] **Balducci, A., Dugas, R., Taberna, P., Simon, P., Plee, D., Mastragostino, M. and Passerini, S.** "High temperature carbon-carbon supercapacitor using ionic liquid as electrolyte", *Journal of Power Sources*, Vol.165, pp.922-927 (2007)

[3] **Mastragostino, M., Arbizzani, C. and Soavi, F.** "Polymer-based supercapacitors", *Journal of Power Sources*, Vol.97-98, pp.812-815 (2001)

[4] **Zhang, L.L. and Zhao, X.S.** "Carbon-based materials as supercapacitor electrodes", *Chemical Society Reviews*, Vol.38, pp.2520-2531 (2009)

[5] **Frackowiak, E., Khomenko, V., Jurewicz, K., Lota, K. and Beguin, F.** "Supercapacitors based on conducting polymers/nanotubes composites", *Journal of Power Sources*, Vol.153, pp.413-418 (2006)

[6] **Lee, S.W., Kim, B.S., Chen, S., Yang, S.H. and Hammond, P.T.** "Layer-by-layer assembly of all carbon nanotube ultrathin films for electrochemical applications", *Journal of the American Chemical Society*, Vol.131, pp.671-679 (2009)

[7] **Gan, X.P., Wu, Y.T., Liu, L., Shen, B. and Hu, W.B.** "Electroless copper plating on PET fabrics using hypophosphite as reducing agent", *Surface & Coatings Technology*, Vol.201, pp.7018-7023 (2007)

[8] **Jayalakshmi, M. and Balasubramanian K.** "Simple capacitors to supercapacitors – An Overview", *International Journal of Electrochemical Science*, Vol.3, pp.1196-1217 (2008)

[9] **Snook, G.A., Kao P. and Best A.S.** "Conducting-polymer-based supercapacitor devices and electrodes", *Journal of Power Sources*, Vol.196, pp.1-12 (2011)

[10] **Peng, C., Zhang, S., Jewell, D. and Chen, G.Z.** "Carbon nanotube and conducting polymer composites for supercapacitors", *Progress in Natural Science*, Vol.18, pp.777-788 (2008)

[11] **Sharma, P. and Bhatti, T.S.** "A review on electrochemical double-layer capacitors", *Energy Conversion and Management*, Vol.51, Issue 12, pp.2901-2912 (2010)

[12] **Pandolfo, A.G. and Hollenkamp, A.F.** "Carbon properties and their role in supercapacitors", *Journal of Power Sources*, Vol.157, pp.11-27 (2006)

[13] **Inagaki, M., Konno, H. and Tanaike, O.** "Carbon materials for electrochemical capacitors", *Journal of Power Sources*, Vol.195, pp.7880-7903 (2010)

[14] **Lee, T., Ooi, C.H., Othman, R. and Yeoh F.Y.** "Activated carbon fiber – The hybrid of carbon fiber and activated carbon", *Reviews on Advanced Materials Science*, Vol.36, Issue 2, pp.118-136 (2014)

[15] **Cazorla-Amorós, D., Alcañiz-Monge, J. and Linares-Solano, A.** "Characterization of activated carbon fibers by CO_2 adsorption", *Langmuir*, Vol.12, pp.2820-2824 (1996)

[16] **Trasatti, S. and Buzzanca, G.** "Rutenium dioxide: a new interesting electrode material. Solid state structure and electrochemical behaviour", *Journal of Electroanalytical Chemistry and Interfacial Chemistry*, Vol.29, Issue 2, pp.A1-A5 (1971)

[17] **Sugimoto, W., Yokoshima, K., Murakami, Y. and Takasu, Y.** "Charge storage mechanism of nanostructured anhydrous and hydrous ruthenium-based oxides", *Electrochimica Acta*, Vol.52, Issue 4, pp.1742-1748 (2006)

[18] **Trasatti, S. and Kurzweil, P.** "Electrochemical supercapacitors as versatile energy stores", *Platinum Metal Review*, Vol.38, Issue 2, pp.46-56 (1994)

[19] **Srinivasan, V. and Weidner, J.W.** "Capacitance studies of cobalt oxide films formed via electrochemical precipitation", *Journal of Power Sources*, Vol.108, Issue 1–2, pp.15-20 (2002)

[20] **Shinde, V.R., Mahadik, S.B., Gujar, T.P., Lokhande, C.D.** "Supercapacitive cobalt oxide (Co_3O_4) thin films by spray pyrolysis", *Applied Surface Science*, Vol.252, Issue 20, pp.7487-7492 (2006)

[21] **Ganesha, V., Pitchumanib, S. and Lakshminarayanana, V.** "New symmetric and asymmetric supercapacitors based on high surface area porous nickel and activated carbon", *Journal of Power Sources*, Vol.158, Issue 2, pp.1523-1532 (2006)

[22] **Zheng, Y.Z. and Zhang, M.L.** "Preparation and electrochemical properties of nickel oxide by molten-salt synthesis ", *Materials Letters*, Vol.61, Issue 18, pp.3967-3969 (2007)

[23] **Lee, H.Y. and Goodenough, J.B.** "Supercapacitor Behavior with KCl Electrolyte", *Journal of Solid State Chemistry*, Vol.144, Issue 1, pp.220-223 (1999)

[24] **Hu, C.C. and Tsou, T.W.** "Ideal capacitive behavior of hydrous manganese oxide prepared by anodic deposition", *Electrochemistry Communications*, Vol.4, Issue 2, pp.105-109 (2002)

[25] **Gupta, V. and Miura, N.** "High performance electrochemical supercapacitor from electrochemically synthesized nanostructured polyaniline", *Materials Letters*, Vol.60, Issue 12, pp.1466-1469 (2006)

[26] **Fan, L.Z. and Maier, J.** "High-performance polypyrrole electrode materials for redox supercapacitors", *Electrochemistry Communications*, Vol.8, Issue 6, pp.937-940 (2006)

[27] **Xu, Y., Wang, J., Sun, W. and Wang, S.** "Capacitance properties of poly(3,4-ethylenedioxythiophene) / polypyrrole composites", *Journal of Power Sources*, Vol.159, Issue 1, pp.370-373 (2006)

[28] **Ryu, K.S., Kim, K.M., Park, Y.J., Park, N.G., Kang, M.G. and Chang, S.H.** "Redox supercapacitor using polyaniline doped with Li salt as electrode", *Solid State Ionics*, Vol.152-153, pp.861-866 (2002)

[29] **Villers, D., Jobin, D., Soucy, C., Cossement, D., Chahine, R., Breau, L. and Bélanger, D.** "The Influence of the Range of Electroactivity and Capacitance of Conducting Polymers on the Performance of Carbon Conducting Polymer Hybrid Supercapacitor", *Journal of The Electrochemical Society*, Vol.150, Issue 6, pp.A747-A752 (2003)

[30] **Hashmi, S.A. and Upadhyaya, H.M.** "Polypyrrole and poly(3-methyl thiophene)-based solid state redox supercapacitors using ion conducting polymer electrolyte", *Solid State Ionics*, Vol.152-153, pp.883-889 (2002)

[31] **Vol'fkovich, Y.M. and Serdyuk, T.M.** "Electrochemical Capacitors", *Russian Journal of Electrochemistry*, Vol.38, Issue 9, pp.935-959 (2002)

[32] **Arbizzani, C., Mastragostino, M., Meneghello, L. and Paraventi, R.** "Electronically conducting polymers and activated carbon: Electrode materials in supercapacitor technology", *Advanced Materials*, Vol.8, Issue 4, pp.331-334 (1996)

[33] **Wu, M.Q., Snook, G.A., Gupta, V., Shaffer, M., Fray, D.J. and Chen, G.Z.** "Electrochemical fabrication and capacitance of composite films of carbon nanotubes and polyaniline", *Journal of Materials Chemistry*, Vol.15, pp.2297-2303 (2005)

[34] **Ryu, K.S., Kim, K.M., Park, N.G., Park, Y.J. and Chang, S.H.** "Symmetric redox supercapacitor with conducting polyaniline electrodes", *Journal of Power Sources*, Vol.103, Issue 2, pp.305-309 (2002)

[35] **Park, J.H. and Park, O.O.** "Hybrid electrochemical capacitors based on polyaniline and activated carbon electrodes", *Journal of Power Sources*, Vol.111, Issue 1, pp.185-190 (2002)

[36] **Snook, G.A., Peng, C., Fray, D.J. and Chen, G.Z.** "Achieving high electrode specific capacitance with materials of low mass specific capacitance: Potentiostatically grown thick micro-nanoporous PEDOT films", *Electrochemistry Communications*, Vol.9, Issue 1, pp.83-88 (2007)

[37] **Suematsu, S., Oura, Y., Tsujimoto, H., Kanno, H. and Naoi, K.** "Conducting polymer films of cross-linked structure and their QCM analysis", *Electrochimica Acta*, Vol.45, Issue 22-23, pp.3813-3821 (2000)

[38] **Hashmi, S.A., Latham, R.J., Linford, R.G. and Schlindwein, W.S.** "Conducting polymer-based electrochemical redox supercapacitors using proton and lithium ion conducting polymer electrolytes", *Polymer International*, Vol.47, Issue 1, pp.28-33 (1998)

[39] **Skompska, M., Mieczkowski, J., Holze, R. and Heinze, J.** "In situ conductance studies of p- and n-doping of poly(3,4-dialkoxythiophenes)", *Journal of Electroanalytical Chemistry*, Vol.577, Issue 1, pp.9-17 (2005)

[40] **Levi, M.D., Gofer, Y., Aurbach, D., Lapkowski, M., Vieilc, E. and Serose, J.** "Simultaneous Voltammetric and In Situ Conductivity Studies of n‐Doping of Polythiophene Films with Tetraalkylammonium, Alkali, and Alkaline–Earth Cations", *Journal of Electrochemical Society*, Vol.147, Issue 3, pp.1096-1104 (2000)

[41] **Laforgue, A., Simon, P., Fauvarque, J.F., Mastragostino, M., Soavi, F., Sarrau, J.F., Lailler, P., Conte, M., Rossi, E. and Saguattie, S.** "Activated Carbon/Conducting Polymer Hybrid Supercapacitors", *Journal of Electrochemical Society*, Vol.150, Issue 5, pp.A645-A65 (2003)

[42] **Ryu, K.S., Lee, Y.G., Hong, Y.S., Park, Y.J., Wu, X.L., Kim, K.M., Kang, M.G., Park, N.G. and Chang, S.H.** "Poly(ethylenedioxythiophene) (PEDOT) as polymer electrode in redox supercapacitor", *Electrochimica Acta*, Vol.50, Issue 2-3, pp.843-847 (2004)

[43] **Arbizzani, C., Catellani, M., Mastragostino, M. and Mingazzini, C.** "N- and P-doped Polydithieno [3,4-B:3',4'-D] thiophene: A narrow band gap polymer for redox supercapacitors", *Electrochimica Acta*, Vol.40, Issue 12, pp.1871-1876 (1995)

[44] **Lota, K., Khomenko, V. and Frackowiak, E.** "Capacitance properties of poly(3,4-ethylenedioxythiophene)/carbon nanotubes composites", *Journal of Physics and Chemistry of Solids*, Vol.65, Issue 2-3, pp.295-301 (2004)

[45] **Arbizzani, C., Mastragostino, M. and Meneghello, L.** "Characterization by impedance spectroscopy of a polymer-based supercapacitor", *Electrochimica Acta*, Vol.40, Issue 13-14, pp.2223-2228 (1995)

[46] **Snook, G.A. and Chen, G.Z.** "The measurement of specific capacitances of conducting polymers using the quartz crystal microbalance", *Journal of Electroanalytical Chemistry*, Vol.612, Issue 1, pp.140-146 (2008)

[47] **Stenger-Smith, J.D., Webber, C.K., Anderson, N., Chafin, A.P., Zong, K.K. and Reynolds, J.R.,** "Poly(3,4-alkylenedioxythiophene)-Based Supercapacitors Using Ionic Liquids as Supporting Electrolytes", *Journal of Electrochemical Society*, Vol.149, Issue 8, ppA973-A977 (2002)

[48] **Hong, J.I., Yeo, I.H. and Paik, W.K.** "Conducting Polymer with Metal Oxide for Electrochemical Capacitor: Poly(3,4-ethylenedioxythiophene) RuOx Electrode", *Journal of Electrochemical Society*, Vol.148, Issue 2, pp.A156-A163 (2001)

[49] **Ghosh, S. and Inganäs, O.** "Networks of Electron-Conducting Polymer in Matrices of Ion - Conducting Polymers Applications to Fast Electrodes" , *Electrochemical and Solid-State Letters*, Vol.3, Issue 5, pp.213-215 (2000)

[50] **Arulepp, M., Permann, L., Leis, J., Perkson, A., Rumma, K., Jänes, A. and Lust, E.** "Influence of the solvent properties on the characteristics of a double layer capacitor", *Journal of Power Sources*, Vol.133, Issue 2, pp.320-328 (2004)

[51] **Morita, M., Kaigaishi, T., Yoshimoto, N., Egashira, M. and Aida, T.** "Effects of the Electrolyte Composition on the Electric Double-Layer Capacitance at Carbon Electrodes", *Electrochemical and Solid-State Letters*, Vol.9, Issue 8, pp.A386-A389 (2006)

[52] **Lust, E., Nurk, G., Jänes, A., Arulepp, M., Nigu, P., Möller, P., Kallip, S. and Sammelselg, V.** "Electrochemical properties of nanoporous carbon electrodes in various nonaqueous electrolytes", *Journal of Solid State Electrochemistry*, Vol.7, Issue 2, pp.91-105 (2003)

[53] **Lazzari, M., Mastragostino, M. and Soavi, F.** "Capacitance response of carbons in solvent-free ionic liquid electrolytes", *Electrochemistry Communications*, Vol.9, Issue 7, pp.1567-1572 (2007)

[54] **Mastragostino, M. and Soavi, F.** "Strategies for high-performance supercapacitors for HEV", *Journal of Power Sources*, Vol.174, Issue 1, pp.89-93 (2007)

[55] **Liu, X.J. and Osaka, T.** " All - Solid - State Electric Double - Layer Capacitor with Isotropic High - Density Graphite Electrode and Polyethylene Oxide/ LiClO4 Polymer Electrolyte " , *Journal of Electrochemical Society*, Vol.143, Issue 12, pp.3982-3986 (1996)

[56] **Liu, X.J. and Osaka, T.** " Properties of Electric Double - Layer Capacitors with Various Polymer Gel Electrolytes " , *Journal of Electrochemical Society*, Vol.144, Issue 9, pp.3066-3071 (1997)

[57] **Arbizzani, C., Mastragostino, M. and Meneghello, L.** "Polymer-based redox supercapacitors: A comparative study", *Electrochimica Acta*, Vol.41, Issue 1, pp.21-26 (1996)

[58] **Rudge, A., Davey, J., Raistrick, I., Gottesfeld, S. and Ferraris, J.P.** "Conducting polymers as active materials in electrochemical capacitors", *Journal of Power Sources*, Vol.47, Issue 1-2, pp.89-107 (1994)

[59] **Rudge, A., Raistrick, I., Gottesfeld, S. and. Ferraris, J.P.** "A study of the electrochemical properties of conducting polymers for application in electrochemical capacitors", *Electrochimica Acta*, Vol.39, Issue 2, pp.273-287 (1994)

[60] **Hashmi, S.A., Latham, R.J., Linford, R.G. and Schlindwein, W.S.** "Studies on all solid state electric double layer capacitors using proton and lithium ion conducting polymer electrolytes", *Journal of the Chemical Society, Faraday Transactions*, Vol.93, Issue 23, pp.4177-4182 (1997)

[61] **Clemente, A., Panero, S., Spila, E. and Scrosati, B.** "Solid-state, polymer-based, redox capacitors", *Solid State Ionics*, Vol.85, Issue 1-4, pp.273-277 (1996)

[62] **Carlberg, J.C. and Inganäs, O.** "Poly(3,4‐ethylenedioxythiophene) as Electrode Material in Electrochemical Capacitors", *Journal of Electrochemical Society*, Vol.144, Issue 4, pp.L61-L64 (1997)

[63] **Aziz, S.B., Woo, T.J., Kadir, M. and Ahmed, H.M.** "A conceptual review on polymer electrolytes and ion transport models", *Journal of Science: Advanced Materials and Devices*, Vol.3, Issue 1, pp.1-17 (2018)

[64] **Fergus, J.W.** "Ceramic and polymeric solid electrolytes for lithium-ion batteries", *Journal of Power Sources*, Vol.195, Issue 15, pp.4554-4569 (2010)

[65] **Mindemark, J., Lacey, M.J., Bowden, T. and Brandell, D.** "Beyond PEO—Alternative host materials for Li+-conducting solid polymer electrolytes", *Progress in Polymer Science*, Vol.81, pp.114-143 (2018)

[66] **Yue, L.P., Ma, J., Zhang, J.J., Zhao, J.W., Dong, S.M., Liu, Z.H., Cui, G.L. and Chen, L.Q.** "All solid-state polymer electrolytes for high-performance lithium ion batteries", *Energy Storage Materials*, Vol.5, pp.139-164 (2016)

[67] **Meyer, W.H.** "Polymer Electrolytes for Lithium-Ion Batteries", *Advanced Materials*, Vol.10, Issue 6, pp.439-448 (1998)

[68] **Marcinek, M., Syzdek, J., Marczewski, M., Piszcz, M., Niedzicki, L., Kalita, M., Plewa-Marczewska, A., Bitner, A., Wieczorek, P., Trzeciak, T., Kasprzyk, M., Łężak, P., Zukowska, Z., Zalewska, A. and Wieczorek, W.** "Electrolytes for Li-ion transport – Review", *Solid State Ionics*, Vol.276, pp.107-126 (2015)

[69] **Mohapatra, S.R., Thakur, A.K. and Choudhary, R.N.P.** "Effect of nanoscopic confinement on improvement in ion conduction and stability properties of an intercalated polymer nanocomposite electrolyte for energy storage applications", *Journal of Power Sources*, Vol.191, Issue 2, pp.601-613 (2009)

[70] **Dubal, D.P., Kim, J.G., Kim, Y., Holze, R., Lokhande, C.D. and Kim, W.B.** "Supercapacitors based on flexible substrates: An overview", *Energy Technology*, Vol.2, Issue 4, pp.325-341 (2014)

[71] **Wang, Y.S., Li, S.M., Hsiao, S.T., Liao, W.H., Chen, P.H., Yang, S.Y., Tien H.W., Ma, C.C.M. and Hu, C.C.** "Integration of tailored reduced graphene oxide nanosheets and electrospun polyamide-66 nanofabrics for a flexible supercapacitor with high-volume- and high-area-specific capacitance", *Carbon*, Vol.73, pp.87-98 (2014)

[72] **Jost, K., Perez, C.R., McDonough, J.K., Presser, V., Heon, M., Dion, G. and Gogotsi, Y.** "Carbon coated textiles for flexible energy storage", *Energy & Environmental Science*, Vol.4, pp.5060-5067 (2011)

[73] **Gan, X.P., Wu, Y.T., Liu, L., Shen, B. and Hu, W.B.** "Electroless plating of Cu-Ni-P alloy on PET fabrics and effect of plating parameters on the properties of conductive fabrics", *Journal of Alloys and Compounds*, Vol.455, pp.308-313 (2008)

[74] **Han, E.G., Kim, E.A. and Oh, K.W.** "Electromagnetic interference shielding effectiveness of electroless Cu-plated PET fabrics", *Synthetic Metals*, Vol.123, pp.469-476 (2001)

[75] **Gasana, E., Westbroek, P., Hakuzimana, J., De Clerck, K., Priniotakis, G., Kiekens, P. and Tseles, D.** "Electroconductive texile structures through electroless deposition of polypyrrole and copper at polyaramide surfaces", *Surface & Coatings Technology*, Vol.201, pp.3547-3551 (2006)

[76] **Park, N.W., Kim, I.W. and Kim, J.Y.** "Copper Metallization of Poly(ethylene terephthalate) Fabrics via Intermediate Polyaniline Layers", *Fibres and Polymers*, Vol.10, pp.310-314 (2009)

[77] **Shoji, E., Takagi, S. and Araie, H.** "Novel conducting fabric polymer composites as stretchable electrodes: one-step fabrication of chemical actuators", *Polymers Advanced Technologies*, Vol.20, pp.423-426 (2009)

[78] **Kofod, G., Stoyanov, H. and Gerhard, R.** "Multilayer coaxial fibre dielectric elastomers for actuation and sensing", *Applied Physics A*, Vol.102, pp.577-581 (2011)

[79] **Jost, K., Stenger, D., Perez, C.R., McDonough, J.K., Lian, K., Gogotsi, Y. and Dion, G.** "Knitted and screen printed carbon-fiber supercapacitors for applications in wearable electronics", *Energy & Environmental Science*, Vol.6, pp.2698-2705 (2013)

[80] **Dong, L., Xu, C., Li, Y., Huang, Z.H., Kang, F., Yang, Q.H. and Zhao, X.** "Flexible electrodes and supercapacitors for wearable energy storage: a review by category", *Journal of Materials Chemistry A*, Vol.4, pp.4659-4685 (2016)

[81] **Yong, S., Owen, J.R., Tudor, M.J. and Beeby, S.P.** "Fabric based supercapacitor", *Journal of Physics: Conference Series*, Vol.476, 012114 (2013)

[82] **Lu, X., Yu, M., Wang, G., Tong, Y. and Li, Y.** "Flexible solid-state supercapacitors: design, fabrication and applications", *Energy & Environmental Science*, Vol.7, pp.2160-2181 (2014)

[83] **Ding, Y., Invernale M.A. and Sotzing, G.A.** "Conductivity trends of PEDOT-PSS impregnated fabric and the effect of conductivity on electrochromic textile", *ACS Applied Materials & Interfaces*, Vol.2, No.6, pp.1588-1593 (2010)

[84] **Le, V.T., Kim, H., Ghosh, A., Kim, J., Chang, J., Vu, Q.A., Pham, D.T., Lee, J.H., Kim, S.W. and Lee, Y.H.** "Coaxial fiber supercapacitor using all-carbon material electrodes", *ACS Nano*, Vol.77, pp.5940-5947 (2013)

[85] **Dong, L., Xu, C., Yang, Q., Fang, J., Li, Y. and Kang, F.** "High-performance compressible supercapacitors based on functionally synergic multiscale carbon composite textiles", *Journal of Materials Chemistry A*, Vol.3, pp.4729-4737 (2015)

[86] **Meng, Y., Zhao, Y., Hu, C., Cheng, H., Hu, Y., Zhang, Z., Shi, G. and Qu, L.** "All-graphene core-sheath microfibers for all-solid-state, stretchable fibriform supercapacitors and wearable electronic textiles", *Advanced Materials*, Vol.25, Issue16, pp.2326-2331 (2013)

[87] **Lyu, X., Su, F. and Miao, M.** "Two-ply yarn supercapacitor based on carbon nanotube/stainless steel core-sheath yarn electrodes and ionic liquid electrolyte", *Journal of Power Sources*, Vol.307, pp.489-495 (2016)

[88] **Gu, L., Wang, Y., Fang, Y., Lu, R. and Sha, J.** "Performance characteristics of supercapacitor electrodes made of silicon carbide nanowires grown on carbon fabric", *Journal of Power Sources*, Vol.243, pp.648-653 (2013)

[89] **Yun, T.G., Oh, M., Hu, L., Hyun, S. and Han, S.M.** "Enhancement of electrochemical performance of textile based supercapacitor using mechanical pre-straining", *Journal of Power Sources*, Vol.244, pp.783-791 (2013)

[90] **Kissinger, P.T. and Heineman, W.R.** "Cyclic Voltammetry", *Journal of Chemical Education*, Vol.60, Issue 9, pp.702-706 (1983)

[91] **Heinze, J.** “Cyclic Voltammetry – Electrochemical Spectroscopy”, *Angewandte Chemie International Edition in English*, Vol.23, Issue 11, pp.831-847 (1984)

[92] **Homolka, D., Hung, L.Q., Hofmanova, A., Khalil, M.W., Koryta, J., Marecek, V., Samec, Z., Sen, S.K., Vanysek, P., Weber, J. and Brezina, M.** “Faradaic ion transfer across the interface of two immiscible electrolyte solutions: chronopotentiometry and cyclic voltammetry”, *Analytical Chemistry*, Vol.52, Issue 11, pp.1606–1610 (1980)

[93] **Macdonald, D.D.** “Reflections on the history of electrochemical impedance spectroscopy”, *Electrochimica Acta*, Vol.51, Issue 8–9, pp.1376-1388 (2006)

[94] **Huang, V.M.W., Wu, S., Orazem M.E., Pébère, N., Tribollet, B. and Vivier, V.** “Local electrochemical impedance spectroscopy: A review and some recent developments”, *Electrochimica Acta*, Vol.56, Issue 23, pp.8048-8057 (2011)

[95] **Ates M.** “Review study of electrochemical impedance spectroscopy and equivalent electrical circuits of conducting polymers on carbon surfaces”, *Progress in Organic Coatings*, Vol. 71, Issue 1, pp.1-10 (2011)

[96] **Sacco, A.** “Electrochemical impedance spectroscopy: Fundamentals and application in dye-sensitized solar cells”, *Renewable and Sustainable Energy Reviews*, Vol.79, pp.814-829 (2017)

[97] **Harrington, D.A. and van den Driessche, P.** “Mechanism and equivalent circuits in electrochemical impedance spectroscopy”, *Electrochimica Acta*, Vol.56, Issue 23, pp.8005-8013 (2011)

[98] **Pajkossy, T. and Jurczakowski, R.** “Electrochemical impedance spectroscopy in interfacial studies”, *Current Opinion in Electrochemistry*, Vol.1, Issue 1, pp.53-58 (2017)

[99] **Gueshi, T., Tokuda, K. and Matsuda, H.** "Voltammetry at partially covered electrodes: Part I. Chronopotentiometry and chronoamperometry at model electrodes", *Journal of Electroanalytical Chemistry and Interfacial Electrochemistry*, Vol.89, Issue 2, pp.247-260 (1978)

[100] **Ivanishchev, A.V., Churikov, A.V. and Ushakov, A.V.** "Lithium transport processes in electrodes on the basis of $Li_3V_2(PO_4)_3$ by constant current chronopotentiometry, cyclic voltammetry and pulse chronoamperometry", *Electrochimica Acta*, Vol.122, pp.187-196 (2014)

[101] **Li, J., Murphy, E., Winnick, J. and Kohl, P.A.** "Studies on the cycle life of commercial lithium ion batteries during rapid charge–discharge cycling" *Journal of Power Sources*, Vol.102, Issue 1–2, pp.294-301 (2001)

[102] **Prosini, P.P., Zane, D. and Pasquali, M.** "Improved electrochemical performance of a $LiFePO_4$-based composite cathode", *Electrochimica Acta*, Vol.46, Issue 23, pp.3517-3523 (2001)

[103] **Lingane, P.J**. "Chronopotentiometry and Chronoamperometry with Unshielded Planar Electrodes", *Analytical Chemistry*, Vol.36, Issue 9, pp.1723-1726 (1964)

[104] **Pyun, S.I., Shin, H.C., Lee, J.W. and Go, J.Y.** "Electrochemistry of Insertion Materials for Hydrogen and Lithium; Chapter 2: Electrochemical Methods", *Springer-Verlag Berlin Heidelberg*, pp.11-32 (2012)

[105] **Lu, Y.X., Xue, L.L. and Li, F.** "Silver nanoparticle catalyst for electroless Ni deposition and the promotion of its adsorption onto PET substrate", *Surface & Coatings Technology*, Vol.205, pp.519-524 (2010)

[106] **Zheng, Z.R., Gu, Z.Y., Huo, R.T. and Ye, Y.H.** "Superhydrophobicity of polyvinylidene fluoride membrane fabricated by chemical vapour deposition from solution", *Applied Surface Science*, Vol.255, pp.7263-7267 (2009)

[107] **Das R.N., Rosser S.G., Papathomas, K.I., Poliks, M.D., Lauffer, J.M. and Markovich, V.R.** "Resin coated copper capacitive (RC3) nanocomposites for multilayer embedded capacitors", *IEEE 2008 Electronic Components and Technology Conference*, pp.729-735 (2008)

[108] **Das R.N., Rosser S.G., Papathomas, K.I., Antesberger, T. and Markovich, V.R.** "Resin coated copper capacitive (RC3) nanocomposites for multilayer embedded capacitors: towards system in a package (SiP)", *Circuit World*, Vol.35, pp.31-39 (2009)

[109] **Sun, Y.Y., Li, X., Gandhi, J., Luo, S.J. and Jiang, T.** "Adhesion improvement for polymer dielectric to electrolytic-plated copper", *IEEE 2010 Electronic Components and Technology Conference*, pp.1106-1111 (2010)

[110] **Armand, M.** "Polymers with ionic conductivity", *Advanced Materials*, Vol.2, Issue 6-7, pp.278-286 (1990)

[111] **Xi, J., Qiu, X., Zhu, W. and Tang, X.** "Enhanced electrochemical properties of poly(ethylene oxide)-based composite polymer electrolyte with ordered mesoporous materials for lithium polymer battery", *Microporous and Mesoporous Materials*, Vol.88, Issues 1–3, pp. 1-7 (2006)

[112] **Gadjourova, Z., Andreev, Y.G., Tunstall, D.P. and Bruce, P.G.** "Ionic conductivity in crystalline polymer electrolytes", *Nature*, Vol.412, pp.520-523 (2001)

[113] **Edman, L., Ferry, A. and Doeff, M.M.** "Slow recrystallization in the polymer electrolyte system poly(ethylene oxide)$_n$ – LiN(CF_3SO_2)$_2$", *Journal of Materials Research*, Vol.15, Issue 9, pp.1950–1954 (2000)

[114] **Strawhecker, K.E. and Manias, E.** "Crystallization behavior of poly(ethylene oxide) in the presence of Na^+ montmorillonite fillers", *Chemistry of Materials*, Vol.15, Issue 4, pp.844-849 (2003)

[115] **Frackowiak E. and Béguin F.** "Carbon materials for the electrochemical storage of energy in capacitors", *Carbon*, Vol.39, pp.937–950 (2001)

[116] **Moradian, R., Azadi, S. and Refii-tabar, H.** "When double-wall carbon nanotubes can become metallic or semiconducting", *Journal of Physics: Condensed Matter*, Vol.19, No.17, 176209 (2007)

[117] **Villalpando-Paez, F., Son, H., Nezich, D., Hsieh, Y.P., Kong, J., Kim, Y.A., Shimamoto, D., Muramatsu, H., Hayashi, T., Endo, M., Terrones, M. and Dresselhaus, M.S.** "Raman spectroscopy study of isolated double-walled carbon nanotubes with different metallic and semiconducting configurations", *Nano Letters*, Vol.8, No.11, pp.3879-3886 (2008)

[118] **Shen, C., Brozena, A.H. and Wang, Y.H**. "Double-walled carbon nanotubes: Challenges and opportunities", *Nanoscale*, Vol.3, pp.503-518 (2011)